THE UNIVERSITY
of EDINBURGH

ON THE DETECTION OF VULNERABLE PLAQUES IN HUMAN CORONARY ATHEROSCLEROSIS

Alastair James Moss

MA (Cantab) MRCP (UK) MRCP (London)

A Thesis Presented for the Degree of Doctor of Philosophy

The University of Edinburgh

2020

When, namely, the anatomists of the last century applied the name of atheroma to a definite change in the coats of arteries, they of course had in their minds a condition similar to that of the skin, to which ever since the days of ancient Greece, the name of atheroma, grit-follicle (Grützbalg) has been assigned…

At all times there have moreover been observers who regarded the ossification of vessels as a change belonging to the same category as atheroma. Haller and Crell believed that the ossification proceeded from the atheromatous matter, and that this was a juice which like that exuding under the periosteum of bone, was capable of generating plates of bone out of itself.

Rudolf Virchow, Lecture XVI - A more precise account of fatty metamorphosis. Cellular Pathology as based upon physiological and pathological histology. 1858

To Reshma

CONTENTS

INDEX OF TABLES

INDEX OF FIGURES

DECLARATION

This thesis represents research undertaken at the Centre for Cardiovascular Science, University of Edinburgh, Royal Infirmary of Edinburgh, United Kingdom.

The SCOT-HEART trial substudy presented in Chapter 3 was funded by the Chief Scientist Office of the Scottish Government Health and Social Care Directorates (CZH/4/588) with supplementary awards from Edinburgh and Lothian's Health Foundation Trust and the Heart Diseases Research Fund.

The PRE^{18}FFIR and DIAMOND studies presented in Chapters 4, 5 & 6 were funded by a Wellcome Trust Senior Investigator Award (WT103782AIA). The DIAMOND study received additional funding in the form of an unrestricted educational grant from AstraZeneca. DIAMOND was an investigator-initiated double blind randomised parallel-group placebo-controlled trial conducted at a single centre at the Royal Infirmary of Edinburgh, UK. It was performed in accordance with regulations governing controlled trials of an investigational medicinal product. In accordance with these regulations, a dedicated clinical trials unit in Edinburgh approved of all study protocols and authorised all statistical analysis plans for the DIAMOND study. AstraZeneca was not involved in the study design or analysis.

Sample processing, immunohistochemistry and Raman spectroscopy of post-mortem coronary artery specimens were undertaken in collaboration with the EaStCHEM School of Chemistry, University of Edinburgh and the Department of Pathology, St. Paul's Hospital, University of British Columbia.

I was the primary investigator for the PRE^{18}FFIR study and directly responsible for the study design, patient recruitment, patient visits and coronary positron emission tomography analysis. I was a co-investigator for the DIAMOND study and worked collaboratively with Dr. Philip Adamson who was the primary investigator on this study. Professor David Newby was the chief investigator of all studies presented in this thesis. All studies involving human participants were approved by the local institutional review board, the Scottish Research Ethics Committee, Medicines and Healthcare products Regulatory Agency, and the United Kingdom (UK) Administration of Radiation Substances Advisory Committee and in accordance with the Declaration of Helsinki.

This thesis has not been accepted in any previous applications for a degree and all sources of information have been acknowledged.

Alastair James Moss 20th March 2020

ACKNOWLEDGEMENTS

This research was performed under the direct supervision of Professor David Newby (British Heart Foundation Duke of Edinburgh Chair of Cardiology) and Dr. Marc Dweck (British Heart Foundation Senior Lecturer in Cardiology) at the University of Edinburgh, to whom I owe a huge debt of gratitude in providing me with a unique opportunity to take part in cutting edge clinical research in an academic centre of research excellence.

I would like to acknowledge the support I received from the Wellcome Trust and the British Heart Foundation during my doctoral studies. I am very grateful to the dedicated staff at the Wellcome Trust Clinical Research Facility, Edinburgh Imaging and the Edinburgh Clinical Trials Unit, all of whom played an integral role in the successful delivery of the studies presented in this thesis. In particular, I would like to acknowledge the contributions of Dr. Laura Forsyth who has provided wise counsel in navigating the minefield that is an international controlled trial of an investigational medicinal product.

The success of the Edinburgh cardiovascular research network has its foundations built around the many talented fellows and lecturers that find pleasure in the pursuit of scientific inquiry. I feel privileged to have worked alongside so many exceptional clinical scientists and have made so many close friendships along the way. The 'Barn' has given me a lot of fond memories and I only hope it continues to nurture and enthuse future clinical investigators, as much as it has done for me.

Finally, the relocation to the Athens of the North would not have been possible without the love and support of my family and especially my wife, Reshma. It is to you whom I devote this body of work as it has occupied as much of your life as it has mine. Your patience,

understanding and compassion are virtues I treasure and hold dear to my heart. May the next journey be as exciting as our last.

ABSTRACT

BACKGROUND

Coronary atherosclerosis is a chronic inflammatory disease which progresses to luminal stenosis and plaque rupture events. Recent developments in non-invasive cardiovascular imaging have enabled the identification of coronary plaques with an increased propensity to rupture. Coronary computed tomography angiography allows visualisation of the arterial wall to discern regions of high-risk plaque in patients with non-obstructive and obstructive coronary artery disease. The anatomical assessment afforded by coronary computed tomography angiography can be combined with hybrid positron emission tomography computed tomography to provide a measure of disease activity. Using novel radiotracers targeted at specific cellular pathways in atherosclerosis, it is now possible to observe plaque activity with 18F-sodium fluoride in vivo.

The principal aims of this thesis were to evaluate the prognostic impact of adverse plaque features using standard coronary computed tomography angiography, to perform reproducibility and histological validation studies of a novel non-invasive imaging technique for detecting high-risk plaque with coronary 18F-fluoride imaging and assess whether coronary 18F-fluoride could be used to select high-risk individuals as part a phase 3 clinical trial of an investigational medicinal product.

ADVERSE CORONARY ARTERY PLAQUE CHARACTERISTICS IN PATIENTS WITH CORONARY ARTERY DISEASE

In a prognostic substudy of the SCOT-HEART trial, adverse plaque features were associated with a three-fold increase in coronary heart disease death or non-fatal myocardial infarction (hazard ratio 3.01 [95% confidence intervals 1.61 to 5.63]; p=0.001). Patients with both

obstructive disease and adverse plaque had the highest event rate with a greater than 10-fold increase in events (hazard ratio 11.50 [95% confidence interval 3.39 to 39.04]; p<0.001). However, these associations were dependent coronary artery calcium score, a surrogate measure of coronary plaque burden.

MOLECULAR CORONARY PLAQUE IMAGING USING 18F-FLUORIDE

To explore whether a novel non-invasive imaging technique could accurately detect regions of coronary microcalcification in patients with coronary artery disease, a scan-rescan reproducibility study of 30 patients was undertaken. Using a standardised metric (coronary to atrial blood pool ratio, TBR_{MAX}), 18F-fluoride activity could be precisely and reproducibly measured within the coronary vasculature. The analytical performance of coronary 18F-fluoride activity was sufficient to determine whether this radiotracer could be used as a non-invasive imaging marker of plaque vulnerability in clinical trials.

EX VIVO 18F-FLUORIDE UPTAKE IN HUMAN CORONARY ATHEROSCLEROSIS

Ex vivo validation of coronary artery specimens using 18F-fluoride demonstrated highly selectivity for hydroxyapatite deposition in atherosclerotic coronary plaque. Specifically, coronary 18F-fluoride binding has a high signal to noise ratio compared with surrounding myocardium that makes it feasible to identify coronary mineralisation activity. Areas of 18F-fluoride binding are associated with osteopontin, an inflammatory-stimulated glycophosphoprotein that increases tissue mineralisation. These results suggest that 18F-fluoride is a non-invasive imaging biomarker of active coronary atherosclerotic mineralisation.

TICAGRELOR TO REDUCE MYOCARDIAL INJURY IN PATIENTS WITH HIGH-RISK CORONARY ARTERY PLAQUE

In a double-blind randomised placebo-controlled trial, 191 patients with multivessel coronary artery disease underwent 18F-fluoride positron emission tomography and computed tomography coronary angiography. In patients with high-risk plaque defined by 18F-fluoride uptake in at least one coronary plaque (n=120/191), there was no evidence that dual antiplatelet therapy with ticagrelor affected 30-day plasma troponin concentrations (ratio of geometric means 1.11 [95% confidence interval 0.90-1.36], p=0.32).

CONCLUSION

These observations suggest that high-risk plaque detection identifies individuals at increased risk of cardiovascular events. Coronary 18F-fluoride can be utilised in the setting of randomised controlled trials as a precise biomarker of plaque activity. Further projects to assess whether coronary 18F-fluoride can predict plaque rupture events are ongoing.

LAY SUMMARY OF THESIS

Coronary artery disease is a leading cause of global mortality and morbidity due to the consequences that stem from a heart attack. The cellular processes that underlie coronary artery disease may be noted as early as the second decade of life, however these processes often remain silent until a patient presents with symptoms in middle age or later in life. Trying to identify patients at the highest risk of heart attacks from amongst the general population remains an ongoing challenge, especially as over half of patients presenting with their first heart attack lack prior warning symptoms. To provide a more 'personalised' approach to the treatment of coronary artery disease, new medical imaging scanners have been developed to assess different disease states. These medical advances allow researchers to detect the cellular processes in the wall of heart arteries that may determine whether a patient is at risk of a heart attack. This thesis set out to investigate how these new medical imaging scanners can be used in patients to provide a more detailed understanding of coronary artery disease activity and whether these imaging tests can help direct doctors to use different types of treatment.

Coronary computed tomography angiography is an imaging test that can assess the narrowing of blood vessels coronary arteries and the composition of the wall of the artery. To identify whether different components in the wall of the artery contribute to the risk of a future heart attack, CT scans obtained from the SCOT-HEART study were analysed and classified according to whether the heart arteries contained high-risk features or not. If high-risk features were present in the wall of the artery, these patients were three times more likely to have a heart attack compared to those who did not. However, patients with high-risk features also had a higher burden of coronary artery disease which may have accounted for this finding.

A new type of imaging test using a radioactive tracer, 18F-sodium fluoride, was investigated to see whether it provided accurate measurements of disease activity in heart arteries. Thirty patients, including patients with stable heart artery disease and patients with a recent heart attack, were scanned using this new imaging test and results were compared to assess whether there were any major differences between them. 18F-Sodium fluoride imaging of the heart arteries had good repeatability when performed within a two-week window. This is an important finding as an imaging test should be assessed in this way before it can be used in clinical practice. In order to establish which specific cellular processes are detected using 18F-sodium fluoride imaging, a study using samples of human heart arteries was performed. In regions that had a high signal of 18F-sodium fluoride, cellular processes that control how tissue retains calcium were present. The cellular processes in arteries with 18F-sodium fluoride binding are similar to the mineralisation processes found in bone metabolism.

Finally, a 'gold standard' research trial (double-blind randomised placebo-controlled trial) was performed to assess whether this imaging test could guide the use of additional anti-platelet therapy in patients with high-risk features identified using a high signal of 18F-sodium fluoride. Measures of a sensitive heart enzyme did not change at one month or one year when using this imaging test to guide treatment. This suggests that further research is needed before this imaging test should be used in a clinical setting.

CHAPTER 1

Non-invasive imaging of coronary artery disease

Including adaptations from:

Moss AJ, Newby DE.
CT coronary angiography evaluation of suspected anginal chest pain.
Heart. 2016;102(4):263-268.

Moss AJ, Williams MC, Newby DE, Nicol ED.
The updated NICE guidelines: Cardiac CT as 1st line test for coronary artery disease
Curr Cardiovasc Imaging Rep. 2017;10(5):15.

Moss AJ, Adamson PD, Newby DE, Dweck MR.
Positron emission tomography imaging of coronary atherosclerosis.
Future Cardiol. 2015;12(4):483-496.

1.1 Coronary computed tomography angiography

Despite decades of investment in the delivery of effective treatment, cardiovascular disease remains responsible for the vast majority of deaths worldwide. Even prior to the recent fluctuations in the global financial climate, many modern healthcare economies had sharpened their focus on delivering healthcare that is both clinically and cost effective. Ensuring cost-effective and efficacious treatment is central to maintaining sustainable healthcare programmes as populations increase in age and access healthcare in greater numbers. In the United Kingdom (UK), the National Institute for Health and Care Excellence (NICE) routinely reviews clinical evidence and publishes advice and recommendations based on the combination of clinical efficacy and cost effectiveness of both therapies and technologies. Established in 1997 it is now enshrined in UK law to ensure patients cared for in the English National Health Service (NHS) gain benefits from cost effective measures, and that NHS resources are optimised. It is in this context of a finite healthcare resource that the provision of non-invasive imaging of coronary artery disease will be reviewed.

Guidelines on the investigation and management of coronary artery disease have evolved significantly over the past two decades. In the early 1990's Braunwald's *Quick Reference Guide for Clinicians* recommended patients were offered treatment based on their pre-test probability of angina and a clear history of anginal chest pain was a pre-requisite for stratifying which patients required downstream investigation (Braunwald, Jones et al. 1994). Non-invasive testing (predominantly exercise-ECG) was reserved for identifying high-risk patient groups that may benefit from additional medical therapy and coronary revascularisation. Since Braunwald's early publication, the expansion of multi-modality cardiac imaging has generated a number of different testing strategies with improved sensitivity for diagnosing

coronary artery disease that have been incorporated into national and international guidelines (Knuuti, Wijns et al. 2019).

1.1.1 Non-invasive stress testing in coronary artery disease

There are a number of well-established stress testing modalities that are used across the world. When used to diagnose coronary artery disease, stress testing does have limitations, and all modalities have substantial false positive and negative rates (***Table 1.1***). It is also important to acknowledge that the identification of non-obstructive coronary artery disease is important and associated with substantial future cardiovascular risk (Nakazato, Arsanjani et al. 2014, Cho, Chang et al. 2012) that may be reduced by preventative therapy (Chow, Small et al. 2015).

There is heterogeneity in the response to both physical and pharmacological stress that can limit the identification of areas of reduced myocardial perfusion. Myocardial perfusion abnormalities may appear in the absence of symptoms demonstrating silent ischaemia and may also be evident in the absence of epicardial coronary artery disease (such as microvascular angina). The advantage of stress testing is that it provides an objective assessment of whether myocardial ischemia is responsible for the symptoms of angina, irrespective of aetiology. It also provides an objective measure of response to therapy, such as improved time to ischaemia with anti-anginal drugs. In addition, defining the areas of myocardial hypoperfusion can be used to guide coronary revascularisation strategies especially where there are intermediate severity stenoses or multiple potential territories of ischaemia.

Ultimately, stress testing is associated with both a false negative and false positive rate of one in six for the diagnosis of angina pectoris due to obstructive coronary

artery disease although the false negative rate is higher for exercise electrocardiography (***Table 1.1***) (Montalescot, Sechtem et al. 2013). As such, stress testing has limitations in those with a high (>85%) or low (<15%) pre-test probability of obstructive coronary artery disease. The pre-test probability of obstructive coronary artery disease can be determined from risk tables contained in both the European and American Guidelines, and can be used to assist in the selection of non-invasive investigations. However, these estimates are based on historical data, such as Diamond and Forrester's post-mortem study from over 40 years ago (Diamond and Forrester 1979), which markedly overestimate the probability of obstructive coronary artery disease and consequently this tends to lead to the over investigation of patients (Cheng, Berman et al. 2011).

	Diagnostic Performance		Markers of Risk	Limitations
	Sensitivity	**Specificity**		
Exercise Stress				Immobility, Deconditioning
Electrocardiogram	45-50%	85-90%	≥1 mm ST depression during first 2 stages of Bruce Protocol ≥2 mm ST depression at any time Fall or no rise in blood pressure Unable to complete stage 2 of Bruce Protocol	Bundle Branch Block, Digoxin, Left Ventricular Hypertrophy, Wolf-Parkinson-White Syndrome
Echocardiography	80-85%	80-88%	≥3 Dysfunctional segments	Suboptimal Imaging due to Limited Acoustic Window, Operator Dependent
Single Photon Emission Computed Tomography	73-92%	63-87%	Area of ischemia >10% Multiple territories of ischemia	Breast Attenuation, Ionising Radiation
Pharmacologic Stress				Variability in Responsiveness
Echocardiography	72-92%	82-95%	≥3 Dysfunctional segments	Suboptimal Imaging due to Limited Acoustic Window, Operator Dependent
Magnetic Resonance Imaging	67-94%	61-91%	≥2 Segments of ischemia ≥3 Dysfunctional segments	Contraindications such as Implanted Devices, Claustrophobia
Single Photon Emission Computed Tomography	90-91%	75-84%	Area of ischemia >10% Multiple territories of ischemia	Breast Attenuation, Ionising Radiation
Positron Emission Tomography	81-97%	74-91%	Area of ischemia >10% Multiple territories of ischemia	Expense, Availability, Ionising Radiation

Table 1.1 Comparison and performance of stress testing modalities.
(Moss and Newby 2015)

1.1.2 The ideal non-invasive investigation for coronary artery disease

Whilst there has been much research comparing different stress imaging modalities to detect obstructive coronary artery disease (Greenwood, Maredia et al. 2012), there is a no definitive evidence to recommend the superiority of one diagnostic test over another. To achieve a reduction in cardiac death and non-fatal myocardial infarction, the diagnostic test needs to influence downstream clinical decision-making through the avoidance of unnecessary invasive coronary angiography and the appropriate initiation of treatments that will ultimately reduce coronary events. The test should have a high level of diagnostic accuracy, the ability to better risk stratify individuals and be integrated into a cost-effective clinical pathway. Service provision should be tailored towards the needs of the population to optimise cost-efficacy and a testing strategy that is applicable to the low-intermediate pre-test probability group of patients would cover the majority of patients presenting to chest pain clinics (Skinner, Smeeth et al. 2010). However, consideration should also be given to the application of guideline driven care which may lead to avoiding investigation in presumed low-risk groups, but do so at the expense of misdiagnosing significant coronary artery disease in up to 10% of patients (Patterson, Nair et al. 2015). Thus a test with a high negative predictive value has great merit in patients with suspected angina due to coronary artery disease.

1.1.3 Diagnostic accuracy of coronary computed tomography angiography

The evolution of computed tomography (CT) platforms over the past 17 years has led to a substantial improvement in diagnostic performance. Modern scanners can now offer single-heartbeat angiograms with sub-millimetre sub-second spatial and temporal resolution (***Table 1.2***). The diagnostic accuracy of coronary CT angiography has been predominantly demonstrated with 64-slice scanners and has highlighted the high negative predictive value of coronary CT angiography to exclude the presence of obstructive and non-obstructive coronary artery disease when compared with invasive coronary angiography (Budoff, Dowe et al. 2008, Meijboom, Meijs et al. 2008, Miller, Rochitte et al. 2008). One potential limitation of anatomical assessment with coronary CT angiography is that it does not reliably predict the presence of myocardial ischaemia (Meijboom, Van Mieghem et al. 2008). However, CT perfusion imaging or CT fraction flow reserve are two approaches that can address this deficiency (Douglas, Pontone et al. 2015, Williams and Newby 2012, Williams, Reid et al. 2011).

	Computed Tomography	Magnetic Resonance Imaging
Scan Acquisition Scan Duration Spatial Resolution Temporal Resolution	 0.5-10 seconds Sub millimeter 280-420 milliseconds	 10-20 minutes Millimeter Less than 60 milliseconds
Radiation exposure	1 – 10 milliSieverts (depending on protocol)	No radiation exposure
Advantages	Shorter total scan time, - favoured by patients - improved scanner efficiency Better spatial resolution for visualising coronary anatomy Single breath hold of only 5-10 seconds	Radiation free imaging - serial scans - young patients - early disease Soft tissue characterisation Myocardial scar imaging
Limitations	Requirement for adequate rate control Contrast media reactions (Iodine) Contrast induced nephropathy Calcium blooming Radiation exposure	Claustrophobia Contrast media reactions (Gadolinium) Risk of nephrogenic systemic fibrosis if glomerular filtration rate <30 mL/min/1.73 m^2 Metallic implants (including pacemakers) Long scan times and limited spatial resolution

Table 1.2 Technical Comparison between CT and MRI in the evaluation of coronary artery disease.
(Dweck, Williams et al. 2016)

Is this anatomical-guided strategy supported by the evidence? Historically, invasive coronary angiography has been the definitive test to confirm of the presence of coronary artery disease against which all other non-invasive tests have been validated. However, invasive coronary angiography is the most expensive diagnostic investigation and, importantly, exposes individuals to the highest risk of procedural complications (NICE 2016). In the 2016 update, NICE determined the clinical effectiveness of the non-invasive modalities against a "gold-standard" of 50% stenosis on invasive coronary angiography, the same methodology that was used in the previous guidelines issued in 2010. Confirming the presence of a coronary artery luminal stenosis of 50% or greater is only part of the diagnostic assessment. Confirmation of inducible myocardial ischemia has been the principal goal prior to the initiation of appropriate of secondary prevention treatment and coronary revascularisation. In the NICE guidelines functional imaging is still recommended for those who have significant coronary artery disease or equivocal findings on CT coronary angiography. It should also be noted however that whilst non-invasive testing can assess multiple levels of the ischemia cascade, it is ultimately the confirmation of the anatomical burden of coronary artery disease which determines an individual's future risk of cardiac events (Maddox, Stanislawski et al. 2014).

1.1.4 Improving clinical outcomes with CT coronary angiography

The publication of two large multicentre randomised control trials (Douglas, Hoffman et al. 2015, SCOT-HEART investigators 2015) has provided insight into whether coronary CT angiography can be incorporated into chest pain care pathways to improve diagnostic accuracy and risk stratification of coronary artery disease. The PROspective Multicenter Imaging Study for Evaluation of chest pain (PROMISE)

trial conducted a head-to-head comparison of coronary CT angiography with stress imaging in the assessment of low-risk patients with intermediate probability of coronary artery disease whereas the Scottish COmputed Tomography of the HEART (SCOT-HEART) trial assessed the addition of coronary CT angiography to standard care across all patients (low, medium and high risk) presenting for assessment of suspected stable angina pectoris due to coronary artery disease (***Table 1.3***).

The PROMISE trial

The PROMISE trial recruited 10,003 patients aged 61±8 years from 193 centres across the United States of America and Canada to determine whether the use of coronary CT angiography (CCTA) or stress testing would reduce the long-term composite endpoint of major adverse cardiovascular and procedural events (Douglas, Hoffman et al. 2015). The study population was specifically selected to have an intermediate risk having excluded patients with a previous diagnosis of coronary artery disease and few patients (11%) having typical angina. The study population was therefore focused on a lower risk patient group and excluded patients with planned invasive coronary angiography. The functional testing performed differed significantly across the trial centres with 68% undergoing myocardial scintigraphy, 22% stress echocardiography and 10% exercise electrocardiography. This illustrates the diversity and lack of consensus surrounding the investigations for patients presenting with chest pain and the poor adherence to current North American guidelines (Fihn, Blankenship et al. 2014). In PROMISE, the number of invasive coronary angiograms increased (12.2% [CCTA] versus 8.1% [functional testing]) although the proportion of patients with normal coronary angiograms was reduced (3.4% [CCTA] versus 4.3% [functional testing]). Coronary CT angiography led to more coronary revascularisation procedures (6.2% [CCTA]

vs. 3.2% [functional testing]). Unfortunately there is little information regarding alterations in the clinician's diagnosis and management plan, or changes in the patients' drug therapies. Overall the two groups had similar rates of the composite primary end-point of death, myocardial infarction, hospitalisation for unstable angina or major procedural complication.

Study	**SCOT-HEART**		**PROMISE**	
Population	4,146 patients Chest pain 100% Typical Angina 35% Previous CAD 9%		10,003 patients Chest pain 73% Typical Angina 12% No previous CAD	
Randomisation	1:1		1:1	
Intervention	CCTA in addition to Standard Care		CCTA versus Functional Test	
Control	Standard Care Nuclear Stress imaging (9%) Stress Echocardiography (1%) Exercise ECG (85%)		Functional Test Nuclear Stress imaging (67.3%) Stress Echocardiography (22.5%) Exercise ECG (10.2%)	
Primary Outcome	Certainty of diagnosis of angina due to coronary heart disease at 6 weeks		All cause mortality, non-fatal MI, hospitalisation for unstable angina, major procedural complications	
Predicted Event Rate	13.1% (cardiac death & non-fatal MI) over 5 years		9% (all-cause death, non-fatal MI, hospitalisation for unstable angina, major procedural complication)	
	CCTA (n=2073)	Standard Care (n=2073)	CCTA (n=4996)	Functional Test (n=5007)
Positive test result	25%	-	10.7%	11.7%
Event rates (<2 years follow-up)*				
All-cause death/non-fatal MI	1.9%	2.7%	2.1%	2.2%
Cardiac Death/non-fatal MI¶	1.3%	2.0%	-	-
Non-fatal MI (n)	1.1% (22)	1.7% (35)	0.6% (30)	0.8% (40)
Revascularisation (n)	11.2% (233)	9.7% (201)	6.2% (311)	3.2% (158)
Event rate (4.8 year follow-up)				
Cardiac Death/non-fatal MI§	2.3% (48)	3.9% (81)	-	-
Non-fatal MI	2.1% (44)	3.5% (73)	-	-
Revascularisation	13.5% (279)	12.9% (267)	-	-

Table 1.3 SCOT-HEART and PROMISE trials.

* SCOT-HEART median follow-up 1.7 years, PROMISE median follow-up 2 years.
¶ Hazard ratio 0.62, 95% confidence interval 0.38 – 1.01, p=0.0527
§ Hazard ratio 0.59, 95% confidence interval 0.41 – 0.84, p=0.004

CAD coronary artery disease, CCTA coronary computed tomography angiography, MI myocardial infarction
(adapted from Moss, Williams et al. 2017)

The SCOT-HEART Trial

The SCOT-HEART trial recruited 4,146 patients aged 18-75 years referred from primary care to a cardiology clinic with suspected angina pectoris due to coronary artery disease (SCOT-HEART investigators 2015). Only a small number of exclusion criteria (inability to undergo CT scanning, renal failure (eGFR <30mL/min), acute coronary syndrome within 3 months) ensured that the trial population was inclusive and recruited 47% of all eligible patients presenting to the clinic, making the application of the findings broadly applicable and highly generalisable. Participants were more likely to have typical angina (35%) and a small proportion (9%) had a history of prior coronary artery disease. Importantly the vast majority of patients (85%) underwent exercise electrocardiography during clinic assessment and prior to 1:1 randomisation to standard care alone (including cardiovascular risk assessment) or standard care with coronary CT angiography. The majority of patients had either normal (38%) or non-obstructive (37%) coronary artery disease reflecting the modest prevalence of coronary artery disease seen in patients attending UK rapid access chest pain clinics (Sekhri, Feder et al. 2007, Skinner, Smeeth et al. 2010). Of those who underwent standard care alone, a minority (11%) underwent further stress testing usually in the form of myocardial scintigraphy.

Despite the use of stress testing in the clinic and wider spectrum of patient presentation, coronary CT angiography doubled the clinician's certainty of the diagnosis of coronary artery disease (relative risk 2.56 [95% CI, 2.33-2.79]) and angina pectoris due to coronary artery disease (relative risk 1.79 [95% CI, 1.62-1.96]; the primary end-point). Coronary CT angiography also led to substantial cancellation of unnecessary investigations and changed pharmacological therapy in approximately 25% of participants. These alterations were associated with

improvements in the selection of patients for invasive coronary angiography with rates of normal coronary angiography more than halved. Rates of detection of obstructive coronary artery disease were also increased and led to a trend to an increase in coronary revascularisation (Hazard Ratio 1·20 [95% CI 0·99-1·45], P=0·061) despite similar overall rates of invasive coronary angiography.

For patients being assessed for angina pectoris due to coronary artery disease, the most appropriate clinical outcome is coronary artery disease death or non-fatal myocardial infarction. At 5 years, there was a reduction in this combined endpoint (coronary heart disease death or non-fatal myocardial infarction) in the coronary CT angiography arm (2.3% vs. 3.9%, Hazard Ratio 0.59, 95% CI 0.41–0.84), principally driven by a reduction in non-fatal myocardial infarction (2.1% versus 3.5%, Hazard Ratio 0.60, 95% CI 0.41-0.87) (SCOT-HEART investigators 2018) (***Table 1.3***). To date, this is the only randomised controlled trial of non-invasive cardiac imaging that has demonstrated improved outcomes in this setting.

1.2 Coronary positron emission tomography imaging

Advances in cardiovascular molecular imaging offer the potential to unravel the complex *in vivo* cellular pathophysiology of a variety of cardiovascular disorders. Through a greater understanding of the pathogenesis of cardiovascular disease, molecular imaging may highlight novel risk factors and key targets for future treatments. Whereas traditional structural imaging modalities yield a generic approach to patient care, molecular imaging modalities give complementary information at the cellular level, informing about disease activity with the potential to facilitate personalised disease monitoring and direct targeted therapy.

Atherosclerosis is a chronic inflammatory disease characterised by the formation of lipid-rich plaques. As early as the mid-19th Century, Rudolf Virchow advocated the role inflammation plays in the formation of Grützbalg (grit-follicles) within the coronary vasculature, namely that 'inflammation of the inner arterial coat be the starting point of atheromatous degeneration' (Virchow 1860). Our understanding of the pro-inflammatory mechanisms associated with atherosclerotic events subsequently expanded through pathological studies of autopsy specimens and pre-clinical models (Narula, Nakano et al. 2013, Davies and Thomas 1984, Lendon, Davies et al. 1991, Burke, Farb et al. 1997). These demonstrated inflammation to be a central process at almost every stage of atherosclerosis but particularly important in the precipitation of acute plaque rupture, with macrophages secreting matrix metalloproteinases that serve to weaken the fibrous cap. Inflammation is therefore a key feature of plaques at risk of rupture in addition to other related characteristics such as a large necrotic core, a thin fibrous cap, angiogenesis and microcalcification. Each represents a potential imaging target, with molecular

imaging well placed to measure non-invasively the *in vivo* activity of these key processes.

The emergence of hybrid coronary positron-emission tomography in conjunction with computed tomography or magnetic resonance offers the opportunity to investigate pathophysiological processes on a molecular scale. Potentially any pathological feature can be targeted depending on the availability of an appropriate radiopharmaceutical. Current approaches have made use of established radiotracers developed for oncological imaging. However, the potential exists to create bespoke tracers targeted specifically at high-risk atherosclerotic plaque features, thereby providing even more accurate imaging. I will here review current and emerging PET tracers that hold promise in resolving the activity of these key processes underlying the progression of atherosclerosis in humans. I will also examine some of the technological challenges that will need to be met in order to translate these approaches in to the coronary arteries.

1.2.1 18F-Fluorodeoxyglucose and macrophage metabolism

2-[^{18}F]-Fluoro-2-deoxy-D-glucose (18F-FDG) is a glucose analogue that enters cells expressing glucose transporters (known as solute carrier family 2, facilitated glucose transport member [GLUT] 1 and 3) by facilitated diffusion. It accumulates in the cytosol following phosphorylation by hexokinase to 18F-FDG-6-phosphate. The stoichiometry of 18F-FDG-6-phosphate prohibits further breakdown via the glycolytic pathway leading to a rise in concentration of 18F-FDG-6-phosphate that is proportional to the metabolic demand of the cell (Gallagher, Fowler et al. 1978). Macrophages are the key cellular constituent of active, inflamed atheroma and have increased metabolic demands compared to surrounding cells in the vasculature. *Ex*

vivo studies have demonstrated a close histological correlation between 18F-FDG uptake and macrophage density (Tawakol, Migrino et al. 2006). Macrophage density correlates with plaque progression and the size of the necrotic core (Moreno, Falk et al. 1994, Swirksi, Pittet et al. 2006). Pre-clinical mouse models suggest that 18F-FDG may signal inflammation during the early phase of atherogenesis at the point of foam cell formation, whilst clinical studies have suggested uptake is less evident once macroscopic calcium has formed within the plaque (Ogawa, Nakamura et al. 2012, Tarkin, Joshi et al. 2014). Satomi *et al* reported that the polarisation of macrophages towards a pro-inflammatory M1 subtype results in increased tritiated fluorodeoxyglucose (3H-FDG) uptake through the upregulation of glucose transporters compared with a reparative M2 subtype (Satomi, Ogawa et al. 2013). A two-fold increase in 3H-FDG was associated with an increase in GLUT-1 and 3 and hexokinase gene expression in M1 macrophages. Additionally, there was downregulation of glucose-6-phosphorylase, the reverse reaction of hexokinase. The same was not observed in M2 macrophages, which instead appear to decrease their dependence on glycolysis, perhaps in order to gain a survival advantage in the hostile inflammatory environment (Tavakoli, Zamora et al. 2013). More recently, 18F-FDG accumulation in a Yucatan minipig model has raised questions of whether 18F-FDG uptake is an accurate measure of vascular macrophage activity (Libby, Bhatt et al, 2019). There was considerable accumulation of 18F-FDG in all arteries without atherosclerotic plaque with activity localised to metabolically active medial smooth muscle cells (Al-Mashhadi, Tolbod et al 2019). Discriminating increased 18F-FDG uptake activity in regions of macrophage-driven inflammation remains an ongoing challenge as the non-macrophage uptake accounts for the majority of signal intensity (Al-Mashhadi, Tolbod et al 2019).

The pivotal work of Rudd *et al* demonstrated that 18F-FDG uptake can be visualised in the atheromatous walls of the carotid artery (Rudd, Warburton et al. 2002). In eight patients with symptomatic carotid lesions, there were higher estimated 18F-FDG accumulation rates compared with asymptomatic lesions and no significant uptake in angiographically normal arteries. The carotids are especially well suited to vascular PET imaging because of their relatively large caliber, stationary nature and because vascular tissue is readily available for histological validation following endarterectomy. Optimisation of scanning protocols to determine the appropriate injected dose, circulation time and pre-scan fasting glucose have been conducted allowing quantification of carotid 18F-FDG with excellent scan-rescan reproducibility (Bucerius, Mani et al. 2014, Rudd, Myers et al. 2007, Rudd, Myers et al. 2007, Izquierdo-Garcia, Davies et al. 2009). This means that relatively few patients are required for clinical trials testing the anti-inflammatory effects of novel medication. This has facilitated the use of 18F-FDG–PET as a surrogate end point in phase 2 clinical trials of novel pharmaceuticals, with the results closely tracking with the outcomes of subsequent studies focusing on clinical end-points (Fayad, Mani et al. 2011, Fayad, Mani et al. 2011, Schwartz, Olsson et al. 2012). Phase 2 18F-FDG-PET clinical trials have demonstrated good agreement between modification of plaque activity and subsequent larger phase 3 clinical outcome studies (***Table 1.4***).

Translating 18F-FDG PET in to the coronary arteries is more challenging owing to the limited spatial resolution of clinical PET platforms and the impact of coronary motion. Assessment of the proximal coronary arteries and aortic root appears feasible with increased uptake observed in patients with recent acute coronary syndrome (Rogers, Nasir et al. 2010). However more detailed analysis of the mid and distal coronary vasculature is limited by spillover of signal from the myocardium,

such that even with optimal myocardial suppression protocols, half of all coronary territories cannot be interpreted (Joshi, Vesey et al. 2014, Dweck, Chow et al 2012). Clinical studies examining alternative methods for reducing physiological 18F-FDG uptake in the myocardium are under investigation in the hope that they will improve visualisation of coronary activity. Combined with the multitude of factors that may account for increased 18F-FDG uptake, these limitations have shifted attention to find more specific radiotracers that target inflammatory pathways, however none of these have made it through to clinical application to date.

	18F-FDG study (+)	**18F-FDG study (-)**
Clinical outcome (+)	**Atorvastatin** (Tawakol, Fayad et al, 2013, Singh, Emami et al, 2016) **Pioglitazone** (Nitta, Tahara et al, 2013)	
Clinical outcome (-)		**Dalceptrapib** (Fayad, Mani et al, 2011) **5-lipooxygenase inhibitor** (Gaztanaga, Farkouh et al, 2015) **Losmapimod** (Elkhawa, Rudd et al, 2012) **Oxidised low density lipoprotein antibody** (Lehrer-Graiwer, Singh et al, 2015)

Table 1.4 Use of 18F-fluoro-2-deoxyglucose positron emission tomography imaging to guide inflammatory response to treatment.

Phase 2 clinical trials demonstrating cardiovascular 18F-fluoro-2-deoxyglucose activity response to therapy compared with subsequent phase 3 clinical outcome trials.
Study references in brackets. 18F-FDG, 18F-fluoro-2-deoxyglucose.

1.2.1.1 18F-Fluorodeoxyglucose and biomarkers of inflammation

The association between 18F-FDG uptake and other biomarkers of inflammation offers insight into the complex processes governing atherosclerotic progression. Following the publication of the JUPITER trial, interest in evaluating the inflammatory state of atherosclerotic plaques continues to grow (Ridker, Danielson et al. 2008). The use of high sensitivity C-reactive protein (hsCRP) provides a snapshot of inflammatory activation within the body, however it cannot localise this activity to the vasculature let alone specific vascular territories or plaques. By contrast, co-localisation of 18F-FDG to the arterial wall gives a clearer signal of focal atherosclerotic inflammation. Unraveling the complex relationship between systemic inflammation and 18F-FDG uptake is challenging, especially as plaque rupture events following myocardial infarction may exacerbate atherosclerotic inflammation at remote sites (Rudd, Myers et al 2009, Joshi, Toor et al. 2015). Importantly, 18F-FDG plaque imaging appears more sensitive in detecting the anti-inflammatory effects of novel atherosclerosis therapies making it a useful end-point for phase 2 clinical trials (Fayad, Mani et al. 2011, Mani, Woodward et al. 2014). From a clinical standpoint, identifying 18F-FDG uptake within carotid arteries improves cardiovascular risk stratification independent of hsCRP suggesting that 18F-FDG offers incremental information to the assessment of atherosclerotic inflammation (Noh, Moon et al. 2013).

Pre-clinical 18F-FDG imaging has provided a deeper understanding of plaque pathophysiology and temporal fluctuations in plaque activity. Murine models using $ApoE^{-/-}$ mice fed on a high-fat Western diet exhibit higher 18F-FDG uptake within the descending aorta at 16 weeks. Lipid rich plaques that display focal regions of ^{18}F-FDG uptake recruit macrophages through the expression of vascular cell adhesion

molecule (VCAM-1). Associations between plaque inflammation and subsequent calcification have also been observed using 18F-FDG. 18F-FDG highlights regions of the vasculature associated with osteopontin, a marker of early vascular calcification, which has prognostic significance in human coronary atherosclerosis (Hay, Pedersen et al. 2012). High osteopontin levels are associated with increased major adverse cardiovascular events following myocardial infarction, stable coronary artery disease and in patients undergoing coronary intervention (Bjerre, Pedersen et al. 2013, Georgiadou, Iliodromitis et al. 2010, Kato, Momiyama et al. 2009). Over 5 years of follow-up, focal 18F-FDG uptake identified locations of subsequent calcium deposition and calcium progression in the thoracic aorta. Whilst plaques with novel calcification were associated with increased arterial inflammation, regions of dense calcification were associated with a decreased level of inflammatory activity (Abdelbaky, Corsini et al. 2013, Joshi, Ranjani et al. 2016). Understanding the exact link between inflammation and calcification in atherosclerosis is a key topic of investigation, which may be aided by 18F-sodium fluoride PET imaging and is discussed in greater detail below.

1.2.1.2 Link Between Inflammation and Calcification

Vascular calcification is a key process in atherosclerosis although its exact role remains incompletely understood. Large macroscopic calcific deposits can be visualised on computed tomography and are usually associated with advanced stable atherosclerotic plaque. Nevertheless, CT-determined calcium predicts future adverse events presumably on the basis that patients with high calcium scores will also have more non-calcific plaques at risk of rupture and causing an event. By contrast, the early stages of calcification appear to be associated with plaque instability and increased risk of rupture and events. Ruptured and culprit plaques

often demonstrate regions of microcalcification on histopathology. In keeping with this hypothesis, low-density calcium deposition on CT is associated with an increased risk of events compared to high-density calcium (Criqui, Denenberg et al. 2014). Similarly, the early stages of 'spotty' macrocalcification on CT appear to mark out a higher risk stage of the disease than the larger macroscopic deposits found in stable plaques (Motoyama, Kondo et al. 2007). CT imaging however, is unable to resolve true microcalcification, prompting investigation of alternative approaches with the capacity to detect this early form of calcium.

The association between plaque inflammation and subsequent calcification has been studied using molecular imaging in pre-clinical models of atherosclerosis. High-resolution molecular imaging with a bisphosphonate-derived near-infrared imaging agent (OsteoSense) identifies distinct regions of calcification activity in the vasculature that can be compared with macrophage staining (Aikawa, Nahrendorf et al. 2007). Indeed, OsteoSense binds preferentially to nascent, nanocrystalline deposits of hydroxyapatite that coalesce to form spheres of microcalcification of <50 μm. Microscopic analysis of these particles reveals a range in size from 5 μm down to individual matrix vesicles that are only 100 nm (Bertazzo, Gentleman et al 2013). Cell-derived matrix vesicles containing nanocrystals of hydroxyapatite are exocytosed from the cell membranes of macrophages and vascular smooth muscle cells. These are then released into the extracellular space where they form a nidus for microcalcification which then aggregate to form larger macroscopic deposits (New, Goesttsch et al. 2013, Hutcheson, Goettsch et al. 2016). This process is most evident in the necrotic core where nucleation and calcification growth occur in regions of collagen degradation (Hutcheson, Goettsch et al. 2016). Interestingly, hydroxyapatite may also be a contributor to the inflammatory process, rather than

merely an end product. Ectopic needle-shaped hydroxyapatite crystals stimulate IL-1β /IL-18-dependent inflammatory pathways (Jin, Frayssinet et al. 2011). Additionally, if pairs of microcalcified spheres migrate into the fibrous cap, increases in local mechanical stresses due to interfacial debonding can lead to plaque rupture (Maldonado, Kelly-Arnold et al. 2012).

1.2.2 18F-Sodium fluoride and microcalcification

[^{18}F]-Sodium fluoride (18F-fluoride) has been used as an oncological radiotracer for the past forty years. 18F-Fluoride binds to hydroxyapatite by substitution with a hydroxyl group on the surface of the hydroxyapatite matrix to form fluoroapatite ($Ca_{10}(PO_4)_6F_2$) (Hawkins, Choi et al. 1992). As hydroxyapatite is the dominant in vivo form of crystalline calcium, 18F-fluoride has been used to define areas of increased bone activity with greater accuracy in detecting bone metastases than other conventional imaging techniques (Schirrmeister, Gulmann et al. 1999).

Hydroxyapatite is also the major component of vascular calcification leading to interest in using 18F-fluoride as a marker of vascular calcification activity. Early studies demonstrated areas of increased PET uptake in the aorta, the valves of patients with aortic stenosis and the coronary arteries (Dweck, Chow et al. 2012, Dweck, Khaw et al. 2013, Dweck, Jones et al. 2012, Dweck, Jenkins et al. 2014, Jenkins, Vesey et al. 2015). The latter is of particular interest with 18F-fluoride localising to individual plaques with excellent signal-to-noise and very low uptake in the surrounding myocardium.

18F-Fluoride appears to provide different information to CT calcium scoring. Detailed electron microscopic analysis of carotid endarterectomy specimens has

shown that fluoride, like OsteoSense, binds preferentially to regions of microcalcification compared to the macroscopic deposits observed using computed tomography (Irkle, Vesey et al. 2015). This perhaps reflects the greater exposed surface area of hydroxyapatite in these nanocrystalline areas (Irkle, Vesey et al. 2015). Indeed, 41% of patients with coronary artery calcium scores >1,000 do not have any evidence of increased 18F-fluoride uptake (Dweck, Chow et al. 2012). As previously discussed, microcalcification is a key component of high-risk atherosclerotic plaques and consistent with this, plaques with increased 18F-fluoride uptake have been shown to have multiple high-risk characteristics on histology and intravascular ultrasound including inflammation, positive remodelling, microcalcification and a large necrotic core (***Figure 1.1***). Moreover, in patients with recent myocardial infarction increased 18F-fluoride uptake has been observed in >90% of the culprit plaques responsible for that event (Joshi, Vesey et al. 2014). The clinical challenge is to now determine whether identification of microcalcification in the coronary arteries using 18F-fluoride PET can improve risk stratification in individuals at high-risk of future coronary thrombotic events (Joshi, Vesey et al. 2014).

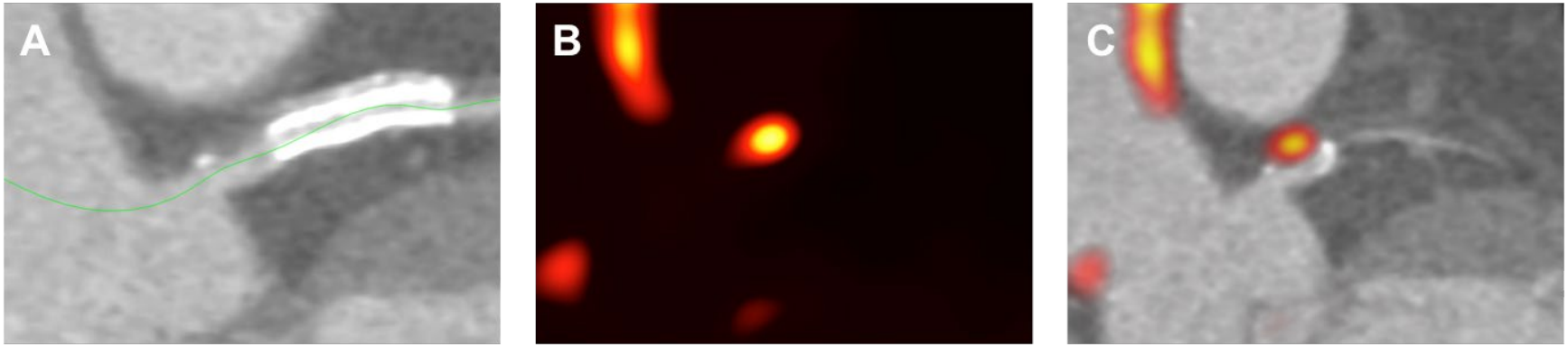

Figure 1. 18F-Sodium fluoride and plaque rupture

Patient presenting with acute myocardial infarction. Computed tomography demonstrating high-risk features (spotty calcification and low attenuation plaque) in that region (A). The culprit plaque also demonstrated increased 18F-fluoride PET activity on hybrid PET/CT image (B and C).

1.3 Novel tracers

1.3.1 Developments in coronary artery positron emission tomography

The development and expansion of positron emission tomography will depend on the development of novel tracers targeting a range of different pathological processes (***Figure 1.2***). A number of tracers are in development with many centered on providing more specific imaging of inflammation, whilst others have been targeted to related processes associated with active atheroma, disease progression and plaque rupture (***Table 1.5***). In addition, improvements in spatial resolution and techniques for correcting cardiac motion will be required if these new tracers are to prove of use in the small and highly mobile coronary arteries.

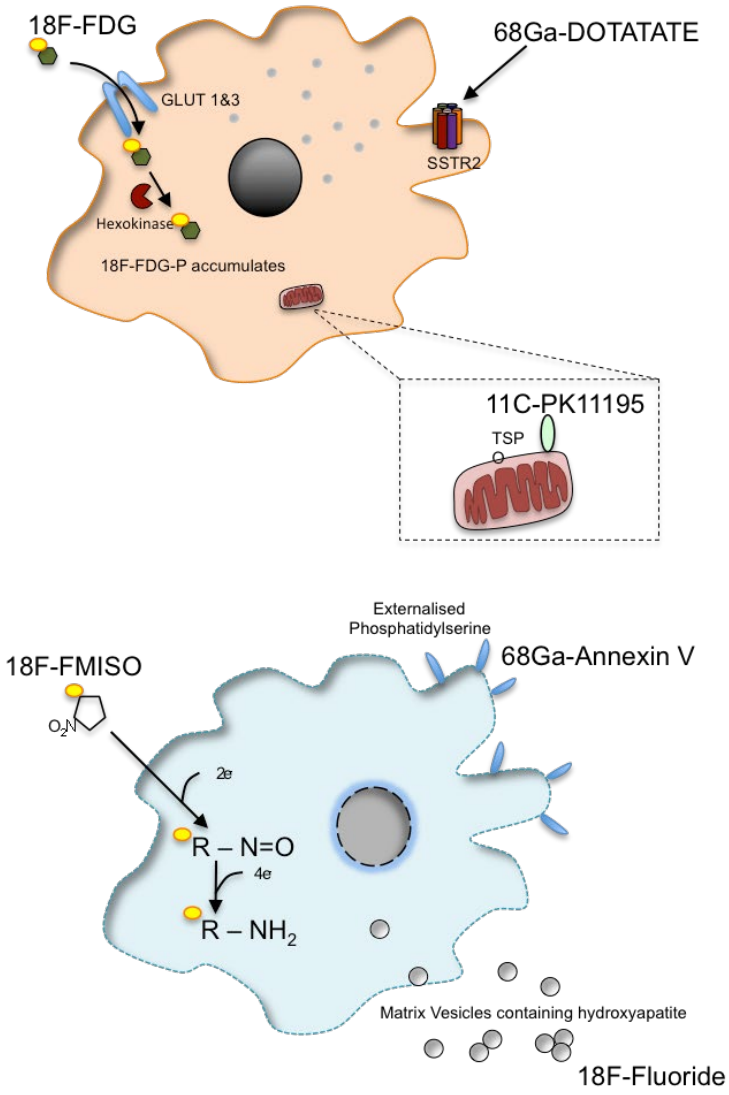

Figure 1.2 Radiotracer accumulation in atherosclerotic plaques as markers of inflammation, hypoxia, apoptosis and microcalcification activity.

Inflammatory pathways can be visualised *in vivo* using specific radiolabelled PET ligands. 18F-FDG accumulates in activated macrophages, but can also be influenced by local hypoxia. Other radiotracers such as 68Ga-DOTATATE and 11C-PK11195 may be more specific markers of macrophage activity than 18F-FDG. An imbalance in metabolic substrates reduces the oxygen tension in the plaque promoting necrosis and apoptosis of macrophages and smooth muscle cells. Generation of reactive oxygen species, externalization of phosphatidylserine and the extrusion of microcrystalline hydroxyapatite can be detected by 18F-FMISO, 68Ga-Annexin V and 18F-fluoride respectively.

DOTATATE, 1,4,7,10-tetraazacyclododecane-1,4,7,10-tetraacetic acid (DOTA)-octreotate; FDG, fluorodeoxyglucose; FDG-P, fluorodexoyglucose-6-phosphate; FMISO, fluoromisonadazole; GLUT, facilitated glucose transporter member; NaF, sodium fluoride; SSTR2, somatostatin receptor type 2; TSPO, translocator protein.
(Moss, Adamson et al. 2015)

Target	Ligand	Radiotracer	Application to date
Macrophage activation	GLUT (1&3) and conversion by hexokinase to 18F-FDG-6-phosphate	^{18}F-FDG	Prospective *in vivo* studies in extra-cardiac atherosclerosis Myocardial suppression required to evaluate coronary arteries
	Somatostatin receptor subtype 2	^{68}Ga-DOTATATE	Prospective *in vivo* studies in coronary artery disease
	Translocator protein 18-kDa	^{11}C-PK11195	Prospective *in vivo* study in carotid stenosis
	Translocator protein 18-kDa	^{11}C-PBR28	Clinical studies in healthy controls and multiple sclerosis
	Mannose receptor	^{18}F-FDM	Preclinical cell culture model
	Choline kinase phosphorylated to Phosphatidylcholine	^{18}F-choline	Preclinical murine model
Apoptosis	Phosphatidylserine	^{68}Ga-Annexin A5	Preclinical murine model
Hypoxia	Reduction to amine derivative in low O_2 environment	^{18}F-FMISO	Preclinical murine model
	Reduction to amine derivative in low O_2 environment	^{18}F-HX4	Proof of concept in carotid atherosclerosis
Microcalcification	Hydroxyapatite	^{18}F-Fluoride	Prospective *in vivo* studies in coronary and extra-cardiac atherosclerosis
Angiogenesis	$\alpha_V\beta_3$ & $\alpha_V\beta_5$ integrin	^{18}F-Fluciclatide	Proof of concept in aortic atherosclerosis
	$\alpha_V\beta_3$ integrin	^{18}F-RGD-K5	*Ex vivo* human carotid studies

Table 1.5 PET radiotracers for coronary atherosclerosis.
(Moss, Adamson et al. 2015)

1.3.2 68Ga-DOTATATE and macrophage somatostatin receptors

Somatostatin receptors are G-protein-coupled receptors that are expressed in a wide variety of tissues. 68Ga-DOTATATE binds to somatostatin receptor subtype 2 (SSRT2) which are expressed by the lipopolysaccharide-activated macrophages associated with plaque vulnerability (Armani, Catalani et al. 2007). Whereas 18F-FDG is hampered by diffuse myocardial uptake that often obscures coronary activity, 68Ga-DOTATATE permits clearer detection of macrophage accumulation in coronary plaques (***Figure 1.3***). In a retrospective analysis of 70 patients with neuroendocrine tumours, 44% had co-localisation of 68Ga-DOTATATE to atheromatous plaques in the proximal coronary arteries (Rominger, Saam, et al. 2010). Whilst in another retrospective study of 44 cancer patients 68Ga-DOTATATE again accumulated in individual coronary lesions suggesting that it may ultimately prove a better marker of inflammation activity in these vessels that 18F-FDG (Mojiahedi, Alavi et al. 2015). The Vascular Inflammation imaging using SomatostatiN receptor positron emission tomography study (NCT02021188) demonstrated improved specificity for carotid and coronary atherosclerotic macrophage imaging using 68Ga-DOTATATE compared with 18F-FDG (Tarkin, Joshi et al, 2017). RNA sequencing of the different macrophage phenotypes revealed SSRT2 expression to be highly specific for pro-inflammatory M1 macrophages, whilst there were very low levels of SSRT2 mRNA expression in unstimulated M0 or activated M2 subtypes (Tarkin, Joshi et al, 2017). Longitudinal studies exploring coronary plaque progression identified by 68Ga-DOTATATE are ongoing (NCT04043377).

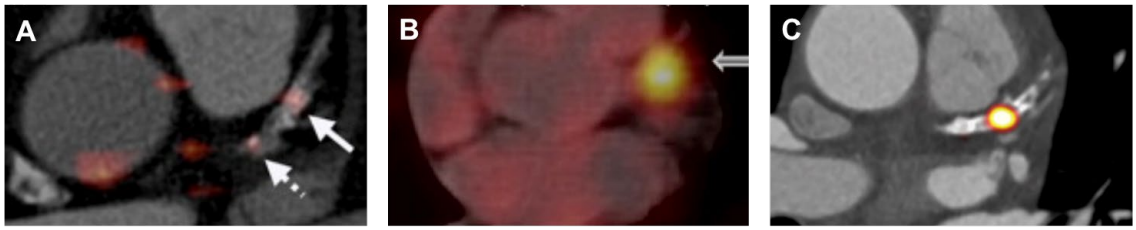

Figure 1.3 Coronary radiotracer uptake in calcified proximal left anterior descending arteries.

Comparison of different radiotracers in the proximal left anterior descending artery of three different patients. The relatively low diffuse 18F-FDG signal (A) contrasts with enhanced focal uptake of 68Ga-DOTATATE (B) and 18F-fluoride (C). Individual radiotracers can discriminate between the upregulation of different molecular pathways in macroscopically similar plaques.
(Moss, Adamson et al. 2015).

1.3.3 11C-PK11195 and translocator protein/peripheral benzodiazepine receptors

[^{11}C]-PK11195 is an isoquinoline-derived ligand of the translocator protein (TSPO), previously known as the peripheral benzodiazepine receptor that is found on the outer mitochondrial membrane. TSPO is involved in cholesterol transport across the mitochondrial intermembrane space and regulation of the mitochondrial respiratory chain. This critical role means that TSPO is widely expressed in cardiac tissues, however the highest density of receptors are found in activated macrophages undergoing bursts of oxidative stress (Carayon, Portier, et al. 1996, Canat, Carayon et al. 1993). In a proof of concept study, Pugliese *et al* visualised 11C-PK11195 uptake in 6 patients with large vessel vasculitis in the aortic arch and carotid arteries (Pugliese, Gaemperli et al. 2010). Symptomatic patients with active disease had higher signals in the vascular wall compared with asymptomatic patients with quiescent vasculitis. The same group performed 11C-PK11195 imaging in patients with carotid atherosclerosis demonstrating increased tracer uptake in the ipsilateral culprit carotid plaque of patients post stroke/TIA (Gaemperli, Shalhoub et al. 2012). In 8 patients undergoing carotid endarterectomy, *ex vivo* autoradiography using 3H-PK11195 confirmed radiotracer co-localisation with CD68^{+} macrophages. Novel fluoride-labelled 18 kDa translocator protein radiotracers are in development (MacAskill, Walton et al, 2019).

1.3.4 18F- Fluoro-D-mannose and M2 macrophages

Mannose, an isomer of glucose, also serves as a substrate for glycolysis in metabolically active macrophages. Similar to glucose, it is incorporated into cells through glucose transporters, but also binds to mannose receptors expressed on M2 macrophages (Finn, Nakano et al. 2012). As such, radiolabeled 2-deoxy-2-[^{18}F]-

fluoro-D-mannose (18F-FDM) has been explored as a viable alternative to 18F-FDG for imaging inflammation in atherosclerosis (Tahara, Mukerjee et al. 2014). This pre-clinical study highlighted an improved pharmacokinetic profile using 18F-FDM compared with 18F-FDG, which resulted in higher levels of 18F-FDM uptake in macrophages, predominantly due to less inhibition of hexokinase activity than is observed with 18F-FDG. Clinical translation of these results is now awaited.

Detection of M2 macrophages may serve as an indirect measure of plaque haemorrhage, since macrophage clearance of intracellular iron and haemoglobin generates an M2 subtype characterised by high mannose receptor expression (Finn, Nakano et al. 2014). Intraplaque haemorrhage results in rapid expansion of the necrotic core following the sudden release of cholesterol-rich erythrocyte membranes. It is therefore an important contributor to episodic plaque growth and may account for the sudden transformation of stable coronary artery disease to active disease state at increased risk of rupture (Kolodgie, Gold et al. 2003).

1.3.5 18F-Fluoromisonidazole and hypoxia

Hypoxia is a key feature of both the expanding necrotic core and atherosclerotic plaque growth. In early plaques oxygen freely diffuses across the initima and the adventitial vasa vasorum. However with plaque expansion, this oxygen diffusion falls (Zemplenyi, Crawford et al. 1989). Combined with the increasing metabolic demand from activated macrophages, an oxygen debt builds up that renders these advanced atherosclerotic plaques severely hypoxic. 18F-FDG may provide an indirect measure of oxygen sufficiency as expression of reactive oxygen species and hypoxia inducible factors stimulate 18F-FDG uptake (Folco, Sheikine et al. 2011, Lee, Quach et al. 2014). However radiolabelled nitroimidazoles offer greater

specificity as they accumulate in tissues that lack oxygen, acting as an electron carrier in the mitochondrial respiratory chain. Uptake of nitroimidazoles is inversely proportional to the oxygen tension, such that 3H-fluoromisonidazole uptake increases by twenty-fold at low partial pressures of oxygen (Krohn, Link et al. 2008). 18F-Fluoromisonidazole (18F-FMISO) has been used extensively in tumour imaging and is now under investigation in atherosclerosis (Mateo, Izquierdo-Garcia et al. 2014). In a pre-clinical study, 18F-FMISO uptake co-localised with pimonidazole defined regions of hypoxia that were nestled in deep in macrophage-dense cores. In contrast, superficial macrophages in a subintimal location were not hypoxic and less inflamed. Clinical studies with a similar nitroimidazole analogue ([^{18}F]-2-(4-((2-nitro-1H-imidazol-1-yl)methyl)-1H-1,2,3-triazol-1-yl)propan-1-ol) have been reported demonstrating increased uptake in patients with carotid stenoses (van der Valk, Sluimer et al. 2015).

1.3.6 18F-Fluciclatide and αVβ3 integrin receptors

Angiogenesis occurs in response to atherosclerotic plaque hypoxia, with fragile microvessels sprouting from the advential vasa vasorum to provide the necrotic core with a new blood supply. These thin-walled vessels have poor structural integrity and are prone to leakage, rupture, and ultimately haemorrhage in to the plaque (Sluimer, Kolodgie, et al. 2009). The vascular endothelial cells responsible for establishing this microvasculature express $\alpha_V\beta_3$ integrin, part of the integrin superfamily of heterodimeric receptors responsible for cell adhesion and signaling. The $\alpha_V\beta_3$ receptor is upregulated in immature endothelial cells as a response to angiogenic guidance molecules. The arginine-glycine-aspartate (RGD) motif has allowed investigators to target the $\alpha_V\beta_3$ binding site to inhibit atherosclerotic progression (Maile, Busby et al. 2010). 18F-Fluciclatide successfully visualises

tumour angiogenesis and can detect treatment responses to chemotherapy (Battle, Goggi et al. 2011, Mena, Owenius et al. 2014). Pre-clinical experiments with a similar analogue, 18F-RGD-K5, demonstrated a moderate correlation between PET uptake and endothelial cell staining of *ex vivo* carotid plaques (Golestani, Mirfeizi et al. 2015). Our group has recently performed the first prospective clinical study (NCT01813045) using 18F-Fluciclatide to assess aortic atherosclerotic uptake (Jenkins, Vesey et al. 2017, Jenkins, Vesey et al. 2019). The expression of $\alpha_V\beta_3$ integrin quantified using 18F-Fluciclatide is associated with aortic plaque burden and higher signal intensity was found in patients with recent myocardial infarction suggesting it may hold potential to quantify plaque angiogenesis and inflammation in high-risk individuals (Jenkins, Vesey et al. 2017, Jenkins, Vesey et al. 2019).

1.3.7 68Ga-Annexin A5 and macrophage apoptosis

The lipid-rich necrotic core is a key feature of the vulnerable plaque and is derived from the death of macrophages and smooth muscle cells within the plaque due to a combination of apoptosis and necrosis. Externalisation of phosphatidylserine onto the extracellular surface of the plasma membrane is an almost universal feature of apoptosis. This makes it a useful target for detection using Annexin based radiotracers (Kolodgie, Petro et al. 2003).

Clinical SPECT imaging of atherosclerotic apoptosis using 99mTc-Annexin A5 was first performed by Kietselaer *et al* in four patients prior to carotid endarterectomy. In two patients who had suffered a recent transient ischaemic attack (TIA), the ipsilateral carotid artery showed Annexin A5 uptake (Kietselaer, Reutelingsperger et al. 2004). Interestingly, the other two patients with remote transient ischaemic attacks (3-4 months) had no observable Annexin A5 uptake. Histology

demonstrated a correlation between Annexin A5 binding and both macrophage staining and intraplaque haemorrhage. Development of the PET tracer 68Ga-Annexin A5 has demonstrated promise in murine models of myocardial infarction. However, translation into clinical studies has been delayed because of suboptimal pharmacokinetics with accumulation in the liver and kidneys (Lehner, Todica et al. 2014). Interestingly Annexin A5 also co-localises with matrix vesicles containing hydroxyapatite in atherosclerosis, indicating that cell death may be an important trigger to microcalcification (New, Goettsch et al. 2013).

1.4 Improving PET image quality

1.4.1 Technical aspects of coronary PET imaging

Clinical application of PET imaging to coronary atherosclerosis will require technical improvement with respect to spatial resolution and motion correction. Clinical positron emission tomography has a fundamental limit of spatial resolution in the range of 4–5 mm for 18F-radiotracers. This means assessment of the coronary arteries with a luminal diameter of 2–5 mm is at the very limit of the capabilities of current clinical PET systems. This is a particular problem because of the complex motion of the coronary vessels, which can displace the right coronary artery by as much as 20 mm (Schecter, Resar et al. 2006). Visualising and quantifying radiotracer uptake on this scale is additionally confounded by partial volume effects. Namely, the signal increases when surrounded by areas of high activity (e.g. myocardium with 18F-FDG) and attenuates when surrounded by areas of low activity (e.g. the lung with most tracers) (Soret, Bacharach et al. 2007). This combination of image blurring (limited spatial resolution) and partial voluming (distribution of signal across voxels) can result in discrepancy between fused PET and CT data sets, requiring careful co-alignment to delineate coronary artery segments with increased radiotracer uptake. ECG gating of the PET data can help substantially, but necessitates discarding much of the data resulting in reduced counts and noise. Cardiac motion correction algorithms that make use of all of the data are emerging and appear to improve the accuracy of co-registration (Le Meunier, Slomka et al. 2011, Slomka, Diaz-Zamudio et al. 2015). A recent feasibility study has found that these algorithms can improve signal detection in the coronary arteries by a third, with particular reductions in the blurring of the PET image and background noise (Rubeaux, Joshi et al. 2016).

1.4.2 Positron Emission Tomography Magnetic Resonance

Hybrid positron emission tomography is now being explored in conjunction with magnetic resonance (MR) platforms. Given that radiotracer uptake resides in the vessel wall rather than the coronary lumen, PET-MR can potentially provide additional information on soft tissue characterisation, of particular use in assessing carotid plaque characteristics (Vesey, Dweck et al. 2016). Ripa *et al* performed the first feasibility study of carotid atherosclerotic imaging using 18F-FDG PET-MR in six patients without flow-limiting luminal stenosis (Ripa, Knudsen et al. 2013). There was a strong correlation between PET-MR and PET-CT measurements in the absence of significant disease. Whilst the attenuation corrected computed tomography and magnetic resonance maps differ across the two platforms, quantification of radiotracer uptake appears to be comparable (Bini, Robson et al. 2015). Enthusiasm for extending the use of PET-MR to assessment of the coronary vasculature in high-risk groups is tempered by the temporal and spatial resolution required for coronary imaging and compounded by artefact from coronary stenting. However reliable imaging of the proximal vessels using magnetic resonance angiography is now possible and one major potential advantage is the ability to continuously monitor cardiac motion using magnetic resonance, which can then be used to correct the PET data. In addition, radiation exposure can potentially be reduced by more than half. Studies are currently underway to further explore the utility of cardiac PET-MR imaging (NCT01418313).

1.5 Future perspective

Whilst an increasing number of radiotracers are in development to specifically evaluate coronary atherosclerosis, what steps are required to take PET imaging in to the primetime of non-invasive coronary imaging? For aspirations to become a clinical reality, the next decade of coronary artery PET research should focus on addressing three key objectives. Firstly, can PET imaging identify individuals at risk of future cardiovascular events? Following the model established by other non-invasive imaging modalities, clinical outcome studies should evaluate whether PET imaging can stratify individuals at the greatest risk of myocardial infarction or cardiovascular death in primary and secondary disease settings. Secondly, can PET imaging assess an individual's response to therapy? Identifying whether individuals are responders or non-responders to treatment is a perceived strength of molecular imaging and this may allow clinicians to 'bridge the gap' towards the delivery of personalised medicine, particularly when integrated with genetic profiling. Finally and possibly the highest bar for any imaging test to attain, can PET imaging assist in the selection of appropriate therapy to improve cardiovascular outcomes and save lives? This is likely to require randomised controlled trials testing whether the addition of molecular imaging can improve current paradigms. Ultimately if PET imaging is to have a clinical role this is likely to be in refining risk stratification in those already felt to be at risk.

Hybrid positron emission tomography provides insight into the pathophysiology of atherosclerosis that until recently has been available only through autopsy examinations. The rapidly expanding number of radiotracers for the assessment of atherosclerosis now allows us to measure directly disease activity and to evaluate the molecular mechanisms governing plaque progression and rupture. Translating

this information into the clinic may ultimately provide a more stratified approach to risk prediction, ensuring that effective treatment is directed appropriately to those with active atherosclerosis, who are most likely to gain benefit. However considerable work remains to test this important hypothesis.

1.6 Thesis aims and Hypotheses

Whilst the unifying theme of this thesis is to explore novel non-invasive imaging approaches to identify vulnerable plaques in patients with coronary atherosclerosis, the aims can be divided into four component parts. The first aim, using coronary plaque analysis from the SCOT-HEART study, is to assess the utility of CT coronary angiography in stratifying patients at increased risk of cardiovascular events based adverse plaque characteristics. The second aim is to evaluate whether novel coronary positron emission tomography using 18F-fluoride can be used as a reproducible metric of disease activity to support the use of this technique in randomised clinical trials. The third aim is to determine whether coronary 18F-fluoride uptake is a measure of atherosclerotic plaque activity using histological correlation with coronary artery specimens. The final aim is to test whether the use of coronary 18F-fluoride positron emission tomography can be used to guide intensification of antiplatelet therapy in a randomised clinical trial.

The following hypotheses will be tested:

i. The identification of adverse plaque characteristics using coronary CT angiography adds incremental information to luminal stenosis severity to stratify patients at increased risk of cardiovascular events (Chapter 3).

ii. Coronary 18F-fluoride positron emission tomography is a reproducible imaging technique in patients with stable and unstable coronary artery disease (Chapter 4).

iii. 18F-Fluoride uptake identifies hydroxyapatite deposition in coronary plaques in regions of active plaque mineralization (Chapter 5).

iv. Dual antiplatelet therapy using P2Y12 inhibition with ticagrelor reduces myocardial injury, as measured using high-sensitivity troponin I, in patients with coronary 18F-fluoride uptake (Chapter 6).

CHAPTER 2

METHODOLOGY

2.1 Summary

The Scottish Computed Tomography of the HEART trial was an open-label, multicentre, randomised controlled trial investigating the addition of coronary computed tomography angiography to the rapid access chest pain standard of care pathway in 12 centres across Scotland. Post-hoc analyses of coronary computed tomography angiography scan acquisitions detailed plaque composition and associations with clinical outcomes are presented in chapter 3. The methodology for coronary plaque analysis using 18F-fluoride positron emission tomography was optimised with scan-rescan reproducibility testing in chapter 4 using nested cohorts from two clinical trials of an investigational medicinal product, the Dual antiplatelet therapy to Inhibit coronary Atherosclerosis and MyOcardial injury in patients with Necrotic high-risk coronary plaque Disease (DIAMOND) trial and Prediction of Recurrent Events with 18F-Fluoride to Identify Ruptured and High-risk Coronary Artery Plaques in Patients with Myocardial Infarction (PRE^{18}FFIR). Histological examination of post-mortem coronary artery specimens was undertaken using 18F-fluoride micro-positron emission tomography scanning and presented in chapter 5. Finally, the DIAMOND trial primary analysis, a controlled trial of an investigational medicinal product (Ticagrelor AZD6410, 90mg tablet, AstraZeneca, Södertälje, Sweden) is presented in chapter 6. Specific study design, methodology and statistical analysis relevant to each study are detailed in the respective chapters.

2.2 Patient Cohorts

2.2.1 Scottish Computed Tomography of the HEART Trial sub-study population

The study population of the Scottish Computed Tomography of the HEART (COT-HEART) trial has been previously described (SCOT-HEART investigators, 2015). Briefly, the trial was a pragmatic, open-label, parallel-group, multicentre randomised control trial of 4,146 patients attending the rapid access chest pain clinic for the assessment of suspected cardiac chest pain. Participants were recruited from 12 cardiology clinics across Scotland between November 2010 and September 2014. Inclusion criteria were necessarily broad and included participants aged 18-75 years who were between 18 and 75 years old and had been referred by their primary care physician to a dedicated cardiology chest pain clinic with stable chest pain due to suspected coronary artery disease. Of note, participants with acute chest pain were referred directly to the emergency department and were not included in this study population. Exclusion criteria included the inability to undergo coronary computed tomography angiography, renal impairment (serum creatinine >250 μmol/L or estimated glomerular filtration rate <30 mL/min/1.73 m^2), previous recruitment to the trial, major allergy to iodinated contrast, inability to give informed consent, known pregnancy, and recent acute coronary syndrome within 3 months (SCOT-HEART investigators, 2015). Participants were randomised 1:1 to standard care (n=2,073) or standard care plus computed tomography calcium score and coronary computed tomography angiography (n=2,703), of whom 1,778 underwent coronary computed tomography angiography at one of the study sites. The Chief Investigator for this study was Professor David Newby.

The sub-study of adverse plaque characteristics of participants randomised to computed tomography angiography from the SCOT-HEART trial presented in Chapter 3 is a secondary post-hoc analysis. To perform a detailed analysis of plaque characteristic, all images were re-analysed by trained readers in coronary computed tomography angiography at Edinburgh Imaging facility, Royal Infirmary of Edinburgh, Edinburgh, United Kingdom.

2.2.2 Dual antiplatelet therapy to Inhibit coronary Atherosclerosis and MyOcardial injury in patients with Necrotic high-risk coronary plaque Disease trial population

The Dual antiplatelet therapy to Inhibit coronary Atherosclerosis and MyOcardial injury in patients with Necrotic high-risk coronary plaque Disease (DIAMOND) trial was an investigator-initiated, controlled trial of an investigational medicinal product (Ticagrelor AZD6410, 90mg tablet, AstraZeneca, Södertälje, Sweden) conducted at a single centre in Edinburgh, United Kingdom (Clinical Trials.gov Study Identification Number: NCT02110303). Participants were recruited between March 2015 and March 2017 and included individuals with stable coronary artery disease aged ≥40 years and already receiving aspirin therapy with angiographically proven multivessel coronary artery disease defined as at least two major epicardial vessels with any combination of either (a) >50% luminal stenosis, or (b) previous revascularization (percutaneous coronary intervention or coronary artery bypass graft surgery). Participants were excluded if they had any of the following criteria: an acute coronary syndrome within the last 12 months, any ongoing indication for dual anti-platelet therapy, or concurrent thienopyridine (clopidogrel or prasugrel) or oral anticoagulant therapy, or percutaneous coronary intervention or coronary artery

bypass graft surgery within the last 3 months. Full eligibility criteria are provided in the ***Table 2.1***.

Participants were recruited from a local registry at the Royal Infirmary of Edinburgh and underwent hybrid coronary positron emission tomography computed tomography angiography at the Edinburgh Imaging facility, Royal Infirmary of Edinburgh, Edinburgh, United Kingdom. The Chief Investigator for this study was Professor David Newby.

Inclusion Criteria
For inclusion in the study subjects should fulfil the following criteria: 1. Patients aged ≥40 years with angiographically proven multivessel coronary artery disease defined as at least two major epicardial vessels with any combination of either (a) >50% luminal stenosis, or (b) previous revascularization (percutaneous coronary intervention or coronary artery bypass graft surgery) 2. Provision of informed consent prior to any study specific procedures 3. Receiving aspirin
Exclusion Criteria
Subjects should not enter the study if any of the following exclusion criteria are fulfilled: 1. An acute coronary syndrome within the last 12 months 2. An indication for dual anti-platelet therapy, such as drug eluting stent 3. Receiving thienopyridine therapy such as clopidogrel or prasugrel 4. Percutaneous coronary intervention or coronary artery bypass graft surgery within the last 3 months 5. Inability or unwilling to give informed consent 6. Women who are pregnant, breastfeeding or of child-bearing potential (women who have experienced menarche, are pre-menopausal and have not been sterilised) will not be enrolled into the trial 7. Known hypersensitivity to ticagrelor or one of its excipients 8. Active pathological bleeding or bleeding diathesis 9. Significant thrombocytopenia: platelets <100 x 10^9 /L 10. History of intracranial hemorrhage 11. Moderate to severe liver impairments (Child's Grade B or C) 12. Maintenance therapy with strong CYP3A4 inhibitors, such as ketoconazole, nefazodone, ritonavir, indinavir, atazanavir, or clarithromycin 13. Major intercurrent illness of life expectancy <1 year 14. Renal dysfunction (eGFR ≤30 mL/min/1.73m^2) 15. Contraindication to iodinated contrast agents 16. Planned coronary revascularization or major non-cardiac surgery in the next 12 months 17. Maintenance therapy with simvastatin or lovastatin at doses greater than 40mg daily 18. Receiving oral anticoagulants including warfarin, rivaroxaban, dabigatran or apixaban

Table 2.1. Inclusion and exclusion criteria for DIAMOND trial

2.2.2.1 18F-Fluoride Positron Emission Tomography Computed Tomography Angiography reproducibility population in patients with stable coronary artery disease

A pre-specified sub-study of the DIAMOND population included 20 participants whom underwent repeat coronary positron emission tomography computed tomography angiography to assess scan-rescan reproducibility within 2 weeks using the same image acquisition protocol. The sub-study comprised of 10 participants with increased coronary 18F-fluoride uptake and 10 participants without increased coronary 18F-fluoride uptake. Inclusion and exclusion criteria were the same of those detailed in the DIAMOND trial (***Table 2.1***).

2.2.3 18F-Fluoride Positron Emission Tomography Computed Tomography Angiography reproducibility population in patients with recent acute coronary syndrome

This study is a single centre observational cohort study nested within the Prediction of Recurrent Events with 18F-Fluoride to Identify Ruptured and High-risk Coronary Artery Plaques in Patients with Myocardial Infarction (PRE^{18}FFIR). PRE^{18}FFIR is an international multicentre observational controlled trial of an investigational medicinal product ([18F] sodium fluoride 250 Megabecquerel) recruiting participants in the United Kingdom, Australia and United States of America (Clinical Trials.gov Study Identification Number: NCT02110303). To assess the scan-rescan reproducibility of 18F-fluoride positron emission tomography computed tomography angiography, 10 participants with recent myocardial infarction were recruited from a single centre in Edinburgh, United Kingdom to undergo serial coronary positron emission tomography computed tomography angiography within 2 weeks using the same

image acquisition protocol. Full eligibility criteria are provided in the ***Table 2.2***. The Chief Investigator for this study was Professor David Newby.

Inclusion Criteria
For inclusion in the study subjects should fulfil the following criteria: 1. Patients aged ≥50 years with recent (<21 days) type 1 myocardial infarction and angiographically proven multi-vessel coronary artery disease defined as at least two major epicardial vessels with any combination of either (a) >50% luminal stenosis, or (b) previous revascularization (percutaneous coronary intervention or coronary artery bypass graft surgery). 2. Provision of informed consent prior to any study specific procedures 3. Already consented to the main PRE^{18}FFIR study
Exclusion Criteria
Subjects should not enter the study if any of the following exclusion criteria are fulfilled: 1. Inability or unwilling to give informed consent 2. Women who are pregnant, breastfeeding or of child-bearing potential (women who have experienced menarche, are pre-menopausal and have not been sterilised) will not be enrolled into the trial 3. Major intercurrent illness with life expectancy <2 years 4. Renal dysfunction (eGFR ≤30 mL/min/1.73m^2) 5. Contraindication to iodinated contrast agents, positron emission tomography or computed tomography 6. Permanent or persistent atrial fibrillation 7. Previous screening as part of this sub-study

Table 2.2. Inclusion and exclusion criteria for PRE^{18}FFIR-Reproducibility study.

2.3 Coronary computed tomography angiography

2.3.1 Scan acquisition

Computed tomography calcium score and computed tomography coronary angiography were performed using 64, 128 or 320-multidetector scanner. Protocols were optimised in accordance with manufacturers recommendations and have been described previously (Newby, Williams et al. 2012).

2.3.2 Coronary plaque analysis

Coronary artery calcium score was assessed on non-contrast computed tomography using the Agatston scoring method as previously described (Agatston, Janowitz et al. 1990). Coronary artery calcium scores were classified into four categories (0, 1-99, 100-399 and ≥400 Agatston units).

On coronary computed tomography angiography images, per-segment assessment of atherosclerotic plaque was performed using a 15-segment model by 6 trained observers, with complex cases classified by consensus (Austen, Edwards et al. 1975). Normal coronary arteries were defined by the absence of obstructive or non-obstructive atherosclerotic plaque. Non-obstructive coronary artery disease was defined by the presence of atherosclerotic plaque occupying a cross-sectional area stenosis of up to 70%. Obstructive coronary artery disease was defined as a stenosis of more than 70% in one or more major epicardial vessels or more than 50% in the left main stem. Observer agreement for the identification of coronary artery disease on coronary computed tomography angiography and coronary artery calcium score in the SCOT-HEART study has previously been shown to be excellent (Williams, Golay et al. 2015).

For each segment, the presence or absence of four coronary artery plaque characteristics was assessed (***Figure 2.1***), namely positive remodeling, low attenuation plaque, spotty calcification and the “napkin ring” sign. Positive remodeling was defined as an outer vessel diameter which was 10% greater than the mean of the diameter of the segments immediately proximal and distal to the plaque (Motoyama, Sarai et al. 2009). Low attenuation plaque was defined as a focal central area of plaque with an attenuation density of <30 Hounsfield Units (Motoyama, Kondo et al. 2007). Spotty calcification was defined as focal calcification within the coronary artery wall which measured <3 mm in maximum diameter (Motoyama, Sarai et al. 2009). The ‘napkin ring’ sign was defined as previously described as a central area of low attenuation plaque which had a peripheral rim of high attenuation (Maurovich-Horvat, Schlett et al. 2012). Observer agreement for the assessment of coronary artery plaque characteristics has overall been shown to be fair (Mauroles, Hamilton-Craig et al. 2018).

An individual adverse plaque was defined as one with positive remodeling or low attenuation plaque, as described previously by Motoyama *et al* (Motoyama, Sarai et al. 2009). Participants with one or more adverse plaques were defined as having adverse plaque.

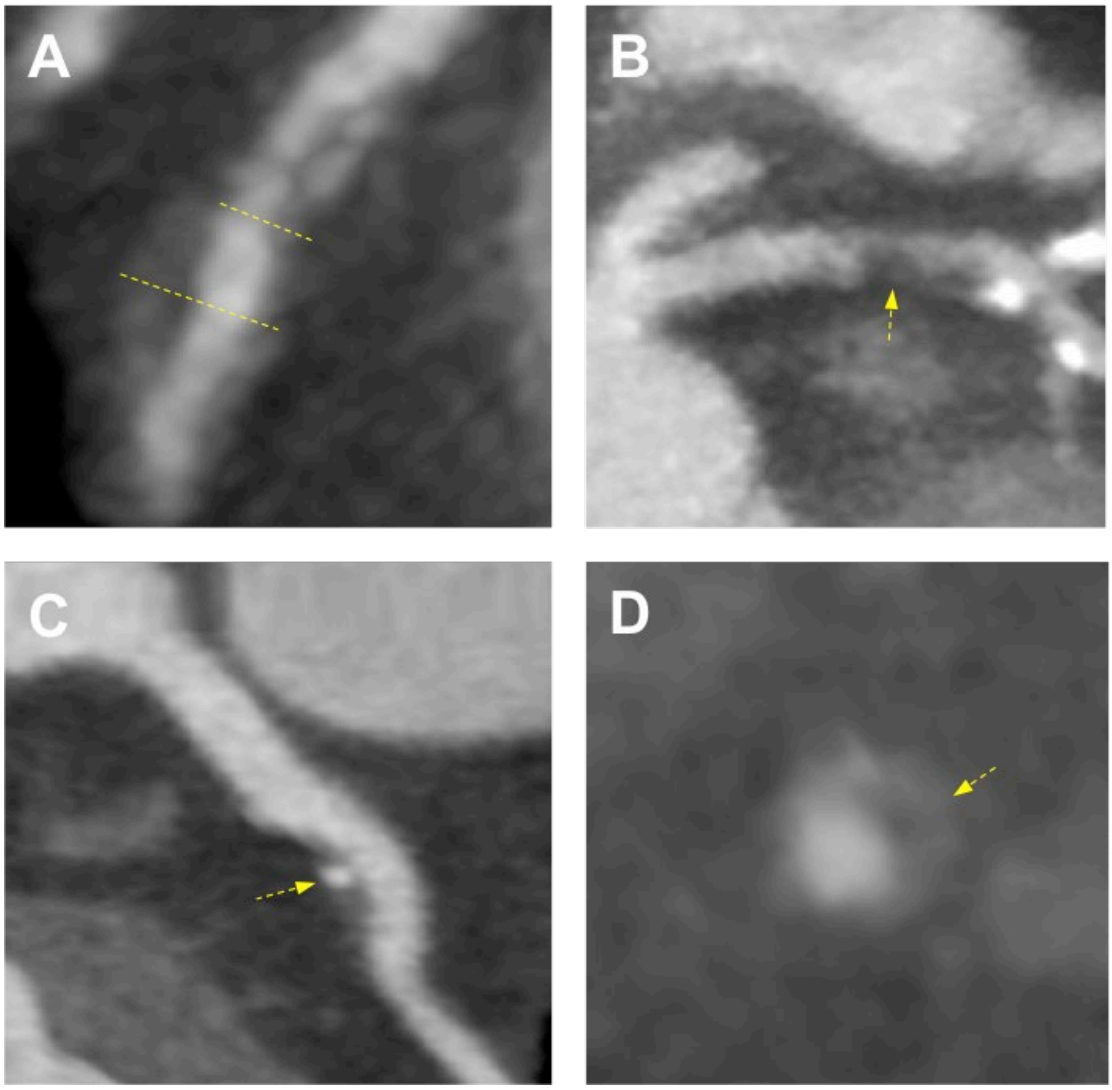

Figure 2.1 Coronary plaque characteristics identified on computed tomography coronary angiography.

Coronary atherosclerotic plaque features detected using computed tomography coronary angiography including (A) positive remodelling, (B) low attenuation plaque, (C) spotty calcification and (D) the 'napkin ring' sign. Positive remodelling (A) was defined as an outer vessel diameter (large yellow line) which was 10% greater than the mean diameter of the segments immediately proximal (small yellow line) and distal to the plaque. Low attenuation plaque (B) was defined as a focal central area of plaque with an attenuation density of <30 Hounsfield Units (yellow arrow). Spotty calcification (C) was defined as focal calcification within the coronary artery wall which measured <3 mm in maximum diameter (yellow arrow). The 'napkin ring' sign (D) was defined as a central area of low attenuation plaque with a peripheral rim of high attenuation (yellow arrow).

2.4 18F-Fluoride Positron Emission Tomography

2.4.1 Scan acquisition

All participants underwent coronary 18F-fluoride positron emission tomography computed tomography angiography. Participants were administered 50-100 mg oral metoprolol if their resting heart rate was >65 beats/min prior to the intravenous administration of 250 MBq 18F-fluoride. After 60 min, patients were imaged with a hybrid positron emission tomography computed tomography scanner (64-multidetector Biograph mCT, Siemens Medical Systems, Erlangen, Germany). Attenuation correction CT scans were performed in held expiration prior to the acquisition of electrocardiographic-gated (ECG-gated) list-mode PET data using a single 30-min bed position centred on the heart. Finally, an ECG-gated coronary computed tomography angiogram was performed in mid-diastole during held expiration. All participants received sublingual glyceryl trinitrate prior to coronary computed tomography angiogram.

2.4.2 Scan analysis

ECG-gated PET images were reconstructed in diastole (50-75% of the R-R interval, 2 iterations, 21 subsets Siemens Ultra-HD algorithm) and fused with contrast enhanced CCTA. Analysis of the CT images was performed using dedicated software (Vitrea Advanced, Toshiba Systems) with multi-planar reformatting for plaque analysis used as necessary. Coronary arteries with a diameter ≥ 2 mm were assessed according to the 18-segment Society of Cardiac Computed Tomography model (Leipsic, Abbara et al. 2014). The analysis of coronary 18F-fluoride activity has been described previously (Dweck, Chow et al. 2012, Joshi, Vesey et al. 2014). The pre-specified coronary 18F-fluoride analysis protocol for the DIAMOND study is detailed below. Visual assessment for increased coronary 18F-fluoride activity was

performed on both a per-patient level and per-segment basis. For a signal to be co-localised to the coronary artery, an atherosclerotic plaque had to be present on the CCTA and the increased pattern of radiotracer had to arise from the coronary artery and follow its course over >5 mm in three dimensions on orthogonal views. Semi-quantitative PET analysis was undertaken for all proximal coronary segments in addition to any atherosclerotic segment with focal 18F-fluoride activity as described above. Maximum standardized uptake values (SUV_{MAX}) were measured within regions of interest. Correction was made for uptake in a referent proximal coronary plaque with no evidence of increased 18F-fluoride activity. To calculate coronary target to background ratios (TBR), coronary SUV_{MAX} was divided by these background measures providing TBR_{MAX}. Coronary 18F-fluoride activity with TBR_{MAX} >1.25 was classified a high-risk plaque. Further exploratory methods of 18F-fluoride analysis are discussed in Chapter 4.

2.5 Micro-Positron Emission Tomography

2.5.1 Scan acquisition

Micro-positron emission tomography was performed at the Pre-clinical Edinburgh Imaging facility, Royal Infirmary of Edinburgh, Edinburgh, United Kingdom. Micro-positron emission tomography acquisitions used 1:5 coincidence mode and computed tomography with semi-circular full trajectory, maximum field of view, 480 projections, 50 kVp, 300 ms and 1:4 binning (Mediso nanoScan PET/CT, Mediso Medical Imaging Systems, Hungary) and total activity counts over 30 min were measured. PET data were reconstructed using Mediso's iterative Tera-Tomo 3D reconstruction algorithm using 4 iterations, 6 subsets, full detector model, normal regularization, spike filter on, voxel size 0·6 mm and 400-600 keV energy window. Micro-PET-CT images were analysed on an OsiriX workstation (OsiriX version 7.5.1, 64-bit, OsiriX Imaging Software, Geneva, Switzerland).

2.5.2 Saturation binding assays to quantify 18F-fluoride binding kinetics and selectivity to hydroxyapatite

Saturation radioligand binding experiments to determine the number of binding sites (Bmax) and the dissociation constant (K_d) of 18F-fluoride were undertaken using nanocrystalline hydroxyapatite phantoms prior to performing *ex vivo* imaging. Five-milligram vials of hydroxyapatite were incubated with 18F-fluoride (110, 230, 470 or 700 kBq/mL) for 20 min. The supernatant fraction was then removed and hydroxyapatite was twice washed in 10 mL 0.9% sodium chloride for 5 min to remove unbound 18F-fluoride. Hydroxyapatite phantoms were scanned using high-resolution micro-PET (1:5 coincidence mode) and computed tomography. Regions of interest were drawn around contours of phantoms on the CT and mapped to corresponding fused 18F-fluoride positron emission tomographic images. Total

binding activity curves and Scatchard plots were generated to calculate Bmax and K_d of 18F-fluoride for subsequent *ex vivo* experiments. To ensure saturation of binding sites, 2x K_d was used to evaluate the selectivity of 18F-fluoride for hydroxyapatite compared with phantoms of calcium phosphate, calcium oxalate and calcium pyrophosphate using the method described above.

2.5.3 Cadaveric coronary arteries and 18F-fluoride micro-positron emission tomography computed tomography

Atherosclerotic sections of left coronary arteries were obtained from victims of sudden death (both cardiac and non-cardiac) with ethical approval and informed relative authorisation from the next of kin (National Health Service South East Scotland Research Ethics Committee 14/SS/1090). Tissue was independently obtained at time of autopsy by the performing pathologist. Legislation regarding the regulation of tissue in victims of sudden death meant that only left main and proximal left anterior descending coronary artery specimens could be obtained for detailed research analysis. These were obtained with the surrounding myocardium and did not necessarily include the specific culprit plaque for patients who had suffered acute myocardial infarction. Tissue was immediately fresh frozen at -80 degrees Celsius. Thawed non-decalcified coronary artery specimens were incubated for 20 min in 18F-fluoride 100 kBq/mL solution (10.5 MBq 18F-fluoride in 99.5 mL 0.9% sodium chloride). Specimens were twice washed in 10 mL 0.9% sodium chloride for 5 min to remove unbound 18F-fluoride. Specimens were scanned using the micro-PET-CT protocol described above. Regions of interest were drawn in background regions, myocardium, non-calcified and calcified segments in coronary artery plaques using micro-CT images and the maximum 18F-

fluoride activity in each region was recorded on co-registered micro-PET images. Maximum activity recorded in a region equal to or above 100 kBq/mL was defined as high 18F-fluoride intensity (>5x myocardium activity), whereas values with a maximum activity of less than 100 kBq/mL was defined as low intensity. After whole specimen imaging, the coronary arteries were fixed in 10% (w/v) neutral buffered formalin.

2.6 Sample preparation and histological examination

Formalin-fixed coronary arteries were sectioned into 2-4 mm slices by a vascular biology/pathology lab. The resulting slices were embedded in paraffin which provided 1-8 tissue cross-sections analysed per sample depending on the size of tissue initially isolated. Paraffin sections (4 μm) were used for histology and immunohistochemistry as described below. In all cases, images were generated using an Aperio Slide Scanner using ImageScope software (Leica Biosystems, Germany). Histological examination was performed using haematoxylin and eosin staining for overall pathology, followed by Movat's pentachrome and trichome staining to differentiate fibrosis and elastic fibres. Von Kossa and Alizarin-red staining were used to assess for the presence of calcification.

2.6.1 Fluorescein-bisphosphonate immunofluorescence of cadaveric coronary arteries

To determine whether the binding of 18F-fluoride in regions of Von Kossa and Alizarin-red S was specific for hydroxyapatite deposition, categorisation of these regions using a fluorescein-bisphosphonate probe was undertaken. Fluorescein-bisphosphonate is a highly sensitive and specific probe for identifying regions of microcrystalline hydroxyapatite. Incubation and binding in tissue has previously been described in detail (Sim, Rashdan et al. 2018). Briefly, sections were de-waxed in xylene and incubated with Fluorescein-bisphosphonate (1 μM) for 2 h, washed in water (2x) followed by incubation with 2% Alizarin Red S (250 μL) for 5 min. Sections were washed in water (3x) and subsequently incubated with 4', 6-diamidino-2-phenylindole (500 nM) for 5 min. Sections were washed with water (1x)

and then mounted using ProLong Gold Antifade. Fluorescence signal was detected under a Leica DMRB fluorescence microscope.

2.6.2 Raman Spectroscopy

Coronary artery specimens were embedded in paraffin wax, sectioned and subsequently placed on calcium fluoride slides. Once dried, the slides were placed in xylene for 15 min followed by dehydration in ethanol. As soon as they were dehydrated, the sections were ready for imaging and did not require additional processing. Alizarin Red S staining was used to discriminate regions of calcification. Sections from tissue presenting no calcification, calcification with low fluoride intensity (<100 kBq/mL), and no calcification with high fluoride intensity (≥100 kBq/mL) were selected in order to address whether there were any differences in the apatite crystal or molecular substitution in the structure. Raman imaging was carried out using an InVia Renishaw Microscope with a 785-nm laser excitation source which was used to excite the sample through a 50, N.A. 0.75 objective. The total data acquisition was performed during 60 s for spectra with a 100% laser power using the WiRE software (Renishaw, Gloucestershire, United Kingdom). All of the spectra acquired were background subtracted using a background correction algorithm.

2.6.3 Immunohistochemical categorisation of osteogenic markers

Immunohistochemistry was completed using osteopontin (OPN) (Sigma-Aldrich Catalog No: 07264, 1:100 dilution), runt-related transcription factor 2 (Runx2) (Abcam Catalog No: Ab76956, 1:50 dilution), transforming growth factor beta 1 (TGFβ1) (Abcam Catalog No: Ab64715, 1:25 dilution), wingless/integrated 3a (Wnt3A) (Abcam Catalog No: Ab28472, 1:200 dilution) and Caspase 3 (Cell Signalling No: 9664, 1:100 dilution). Staining was performed via automated staining with a Leica Bond Rx system using Bond Epitope Retrieval Solution 1 (pH=6, Catalog No: AR9961) and Bond Polymer Refine Red Detection (Catalog No: DS9390). The omission of the primary antibody served as negative controls. Blinded qualitative categorization of staining intensity was performed by a pathologist using a 4-point classification: 0, no notable staining, 1, <20% of plaque or relevant cells are weakly positive, 2, <50% of plaque or some relevant cells are strongly positively, 3, 50-100% of plaque or all relevant cells are strongly positive. For comparison of immunohistochemical analysis with 18F-fluoride activity, plaques with a classification 3 were defined as ‘positive’ and classification <3 was defined as ‘negative’ for osteopontin, runt-related transcription factor 2, transforming growth factor beta 1 and wingless/integrated 3a. Plaques with classification 2 were defined as ‘positive’ and classification <2 were defined as ‘negative’ for Caspase 3.

2.7 DIAMOND Trial study procedures

2.7.1 DIAMOND trial allocation and randomisation

Patients were randomly assigned 1:1 to either ticagrelor 90 mg twice daily or matched placebo tablets (AstraZeneca, UK). Randomization was performed using a web-based system that ensured allocation concealment, with treatment allocation incorporating minimization based on age (<65, ≥65 years old), sex, baseline plasma high-sensitivity troponin I concentration (≤5.1, >5.1 ng/L) and the presence or absence of coronary 18F-fluoride uptake. A random element was included with a 1 in 10 chance of the determined treatment allocation being switched to the other treatment arm.

2.7.2 High-sensitivity cardiac troponin I

Plasma high-sensitivity cardiac troponin I concentrations were measured using the ARCHITECT$_{STAT}$ assay (Abbott Laboratories, Abbott Park, Illinois). The limit of detection is 1.0 ng/L with an inter-assay co-efficient of variation <10% at 4.7 ng/L (9) (Shah, Anand et al. 2015). The upper reference limit (99th centile) based on 4,590 samples from healthy men and women is 34 ng/L for men and 16 ng/L for women (10) (Shah, Griffiths et al. 2015). Samples were collected at baseline, 30 days and 3, 6, 9 and 12 months. A value of 0.5 ng/L was imputed for troponin values below the limit of detection.

2.7.3 Platelet function analysis

Platelet and monocyte activation in response to adenosine diphosphate (ADP) was determined by flow cytometry, as described previously (Harding, Din et al. 2007). These analyses were performed by a single technician blinded to study allocation

with the results of these investigations withheld from the study team until after trial database lock. Briefly, peripheral venous blood was obtained from all participants at the baseline and 1-month visits. Blood was drawn by clean venepuncture of a large antecubital vein using a 19-gauge needle, and care was taken to ensure a smooth blood draw without venous stasis. Blood was collected into tubes containing the direct thrombin inhibitor, D-Phenylalanine-L-prolyl-L-arginine chloromethyl ketone (PPACK, Cambridge Biosciences). Tubes were gently inverted to ensure mixing of whole blood with anticoagulant.

Immunolabelling and flow cytometry were performed in whole blood to avoid centrifugation and washing steps which can lead to artefactual platelet activation. All chemicals were obtained from BD Biosciences. (Oxford, UK). Aliquots of whole blood (50 µL) were incubated with anti-CD14-Allophycocyanin (APC), anti-CD42a-fluorescein isothiocyanate (FITC), anti-CD11b-PE-Cyanine(Cy)7, anti-CD62p-Phycoerythrin (PE) and isotype matched controls for 20 min at room temperature in Eppendorfs with and without ADP (at final concentration of 20 µmol/L). Thereafter, samples were fixed with 1% paraformaldehyde (p-selectin) or FACS-Lyse (platelet-monocyte aggregates). All samples were analysed within 24 hours using a FACSCalibur flow cytometer (Becton-Dickinson). Data analysis was performed using FlowJo v10 (Treestar, Oregon, USA). A medium flow setting was used to minimize leukocyte-platelet coincident events. Monocytes were identified based on their forward and side scatter characteristics and then by triggering on FL-4 to identify CD14-PE positive monocytes and exclude large granular lymphocytes. For each measurement a minimum of 2,500 monocytes were collected. Platelet-monocyte aggregates were defined as monocytes positive for CD42a. All results are

expressed as geometric mean of fluorescence. P-selectin expression was defined as CD42a-FITC positive platelets that were also positive for CD62p-PE.

2.7.4 Study Endpoints

The pre-specified primary endpoint was high-sensitivity cardiac troponin I concentrations at 30 days in patients with increased coronary 18F-fluoride activity. Secondary endpoints were plasma high-sensitivity cardiac troponin I concentration at 30 days in patients without coronary 18F-fluoride activity, and plasma high-sensitivity troponin I concentration over 1 year. Adverse events were recorded in all patients who received a single dose of study medication and included bleeding events categorized according to PLATO criteria as major life-threatening, other major, minor or minimal bleeding (Wallentin, Becker et al. 2009).

2.7.5 Sample Size

In patients with increased coronary 18F-fluoride uptake, we previously reported that mean troponin concentrations were more than double those in patients without increased coronary 18F-fluoride uptake (7.9 [SD 9.3] vs. 3.1 [SD 1.9] ng/L, p=0.047) (Joshi, Vesey et al. 2014). It was estimated that ticagrelor would reduce troponin concentration by half. Forty-eight patients per treatment arm were required to achieve 80% power at two-sided $p<0.05$. After allowing for 15% dropout, we estimated that fifty-five patients would be required per treatment arm. Previous studies had found that 45% of patients with advanced but stable coronary artery disease demonstrated increased coronary 18F-fluoride uptake, so a total sample size of 250 patients was estimated to be required to identify 110 patients with increased coronary 18F-fluoride activity. Termination of further recruitment could be authorized by the trial steering committee once a per-protocol population of 110

patients with increased coronary 18F-fluoride activity had been randomized and completed the primary endpoint at 30 days.

2.8 Ethical considerations

All participants for whom data has been included in the results chapters provided written informed consent prior to any involvement in the respective study. Each study was approved by the local institutional review board, the Scottish Research Ethics Committee and in appropriate cases the Medicines and Healthcare products Regulatory Agency and the United Kingdom Administration of Radiation Substances Advisory Committee.

2.9 Statistical analysis

Full details of the statistical methods are provided in the respective results chapters. Pre-specified statistical analysis undertaken as part of a controlled trial of investigational medicinal product is included in this thesis. As stipulated by regulations governing clinical trial of investigational medicinal products, primary outcome statistical analyses were designed and performed by a clinical trial statistician at the Edinburgh Clinical Trial Units, Edinburgh, United Kingdom. Post-hoc analyses were performed by clinical investigators independent of a clinical trial statistician.

CHAPTER 3

Adverse coronary artery plaque characteristics in patients with coronary artery disease *A SCOT-HEART sub-study*

Williams MC, **Moss AJ**, Dweck M, Adamson PD, Alam S, Hunter A, Shah ASV, Pawade T, Weir-McCall JR, Roditi G, van Beek EJR, Newby DE, Nicol ED.
Coronary artery plaque characteristics associated with adverse outcomes in the SCOT-HEART study.
J Am Coll Cardiol. 2019;73(3):291-301.

3.1 Summary

Objectives

Unlike most non-invasive imaging modalities, coronary computed tomography angiography (CCTA) can characterise subtypes of atherosclerotic plaque. The objective of this study was to investigate the prognostic implications of adverse coronary plaque characteristics in patients with suspected coronary artery disease.

Methods

In this post-hoc analysis of the SCOT-HEART trial, the presence of adverse plaque (positive remodelling or low attenuation plaque), obstructive disease and coronary artery calcification within 15 coronary segments was assessed on CCTA of 1,769 patients who were followed up for 5 years.

Results

Among study participants (mean age 58±10 years; 56% male), 608 (34%) patients had one or more adverse plaque features. Coronary heart disease death or non-fatal myocardial infarction was three-times more frequent in patients with adverse plaque (n=25/608 (4.1%) *versus* n=16/1161 (1.4%), p<0.001; hazard ratio 3.01 (95% confidence interval 1.61 to 5.63); p=0.001) and was twice as frequent in those with obstructive disease (n=22/452 (4.9%) *versus* n=16/671 (2.4%), p=0.024; hazard ratio 1.99 (95% confidence interval 1.05 to 3.79); p=0.036). Patients with both obstructive disease and adverse plaque had the highest event rate with a 10-fold increase in coronary heart disease death or non-fatal myocardial infarction compared to patients with normal coronary arteries (hazard ratio 11.50 (95% confidence interval 3.39 to 39.04); p<0.001). However, these associations were not

independent of coronary artery calcium score, a surrogate measure of coronary plaque burden.

Conclusion

Adverse coronary plaque characteristics and overall coronary plaque burden confer an increased risk of coronary heart disease death or non-fatal myocardial infarction.

3.2 Introduction

The investigation of patients with suspected coronary artery disease has previously focused on functional assessments that attempt to identify the presence of myocardial ischaemia as a downstream surrogate marker of proximal coronary artery stenoses. In contrast, non-invasive imaging with coronary computed tomography angiography (CCTA) has the ability to provide precise structural information of the coronary artery wall, and can assess for the presence and constituents of atherosclerotic plaque even in the absence of flow limiting disease.

Pathological studies in patients with myocardial infarction have identified an association between plaque rupture and adverse plaque characteristics that include positive remodelling, a large necrotic core, microcalcification and a thin fibrous cap (Virmani, Burke et al, 2003). Correlates of these features have been described for non-invasive imaging with CCTA and include the presence of positive remodelling, low attenuation plaque, spotty calcification and the 'napkin ring' sign (Motoyama, Ito et al. 2015). These plaque characteristics are associated with an increased risk of subsequent acute coronary syndromes (Motoyma, Ito et al. 2015, Motoyama, Sarai et al, 2009, Thomsen, Abdulla et al, 2016). Recent data have suggested that positive remodelling and low attenuation plaque in particular provide the most useful prognostic information (Motoyama, Ito et al. 2015, Conte, Annoni et al. 2017), although it remains unclear whether this is of incremental value to traditional cardiovascular risk factors or coronary plaque burden.

In the Scottish COmputed Tomography of the HEART (SCOT-HEART) prospective multi-centre randomised controlled trial of patients with stable chest pain, the addition of CCTA to routine care led to improved diagnostic certainty and patient

care that ultimately reduced the rate of coronary heart disease death or non-fatal myocardial infarction (SCOT-HEART investigators. 2015, SCOT-HEART investigators. 2018, Williams, Hunter et al, 2016). These benefits were largely attributable to subsequent changes in patient management and treatment which had been guided by the presence of obstructive or non-obstructive coronary artery disease as determined by CCTA. However, it may be that further risk stratification and targeted intensification of therapy in patients with adverse plaque characteristics could achieve additional benefits which go beyond the presence of obstructive or non-obstructive coronary artery disease.

In this secondary analysis of the SCOT-HEART trial, we aimed to determine the extent of adverse coronary artery plaque characteristics on CCTA and their association with subsequent clinical outcomes. If confirmed, the identification of these coronary artery plaque characteristics may help risk stratification and guide the intensity of therapy.

3.3 Methods

3.3.1 Study design

The SCOT-HEART trial was a multicentre randomised controlled trial of CCTA in out-patients with suspected angina pectoris due to coronary artery disease (Newby, Williams et al. 2012). The primary results have been reported previously (SCOT-HEART investigators. 2015, SCOT-HEART investigators. 2018, Williams, Hunter et al, 2016). This is a secondary post-hoc analysis of the SCOT-HEART study.

3.3.2 Participants

In brief, 4,146 patients who attended the cardiology outpatient clinic were randomised to standard care alone or standard care plus CCTA, and were followed up for symptoms, management and outcomes. Of the 2,073 participants who were randomised to the intervention arm, 1,778 underwent CCTA. CCTA and non-contrast imaging for calcium scoring was performed as described previously (SCOT-HEART investigators 2015). Cardiovascular risk was assessed using the ASSIGN score. This score has been validated for the Scottish population and, in addition to traditional cardiovascular risk factors, incorporates social deprivation and family history of cardiovascular disease (Woodward, Brindle et al. 2007).

3.3.3 Clinical Management and Outcomes

Outcome information including invasive coronary angiography and coronary revascularisation (percutaneous coronary intervention or coronary artery bypass graft surgery) was obtained from the electronic Data Research and Innovation Service (eDRIS) of the National Health Service (NHS) Scotland, and where

appropriate, confirmed by review of the patient health records. Categorisation of outcomes was performed blinded to the CCTA or other study data. The primary clinical endpoint for this study was the occurrence of coronary heart disease death or non-fatal myocardial infarction. Outcome data were updated in March 2018 (SCOT-HEART investigators. 2018).

3.3.4 Statistical analysis

Statistical analysis was performed using R version 3.5.0 (R Foundation for Statistical Computing, Vienna, Austria). Normally distributed quantitative variables are presented with mean and standard deviation. Non-normally distributed data are presented with median and interquartile range. Statistical significance was assessed using Pearson's Chi-square test, Fisher's exact test, Student's t-test, Mann-Whitney U test, Kruskal-Wallis test or ANOVA as appropriate. Outcome data investigating whether the presence of adverse plaque characteristics predicted coronary heart disease death or non-fatal myocardial infarction in patients with non-obstructive disease were analysed using Cox proportional hazards regression and presented graphically using cumulative incidence plots. A time-to-event analysis was performed using coronary heart disease death or non-fatal myocardial infarction as the endpoint, with the primary independent variable being the presence or absence of adverse plaque on CT. Deaths not classified as coronary heart disease deaths were censored for both the Cox regression analysis and the cumulative incidence plots. Hazard ratios (HR) and 95% confidence intervals (CI) are presented. Coronary artery calcium score and cardiovascular risk score were log transformed for analysis (log base 2 of 1 plus the parameter). Variables were included in multivariable analysis if they were statistically significant on univariable analysis. The assumption of proportional hazards was checked using SPSS. A statistically

significant difference was defined as a two-sided *P* value <0.05.

3.4 Results

Of the 1,778 individuals who underwent a CCTA, 1,769 participants had images that were available and of suitable quality for analysis (***Figure 3.1***). Patients had a mean age of 58±10 years and 56% were male with a range of cardiovascular risk factors and symptoms (***Table 3.1***). Of these patients, 37% (n=646) had normal coronary arteries, 38% (n=671) had non-obstructive coronary artery disease, and 26% (n=452) had obstructive coronary artery disease. Coronary heart disease death or non-fatal myocardial infarction occurred in 41 patients (2.3%) over a median of 4.7 years of follow up (interquartile range (IQR) 4.0 to 5.7 years).

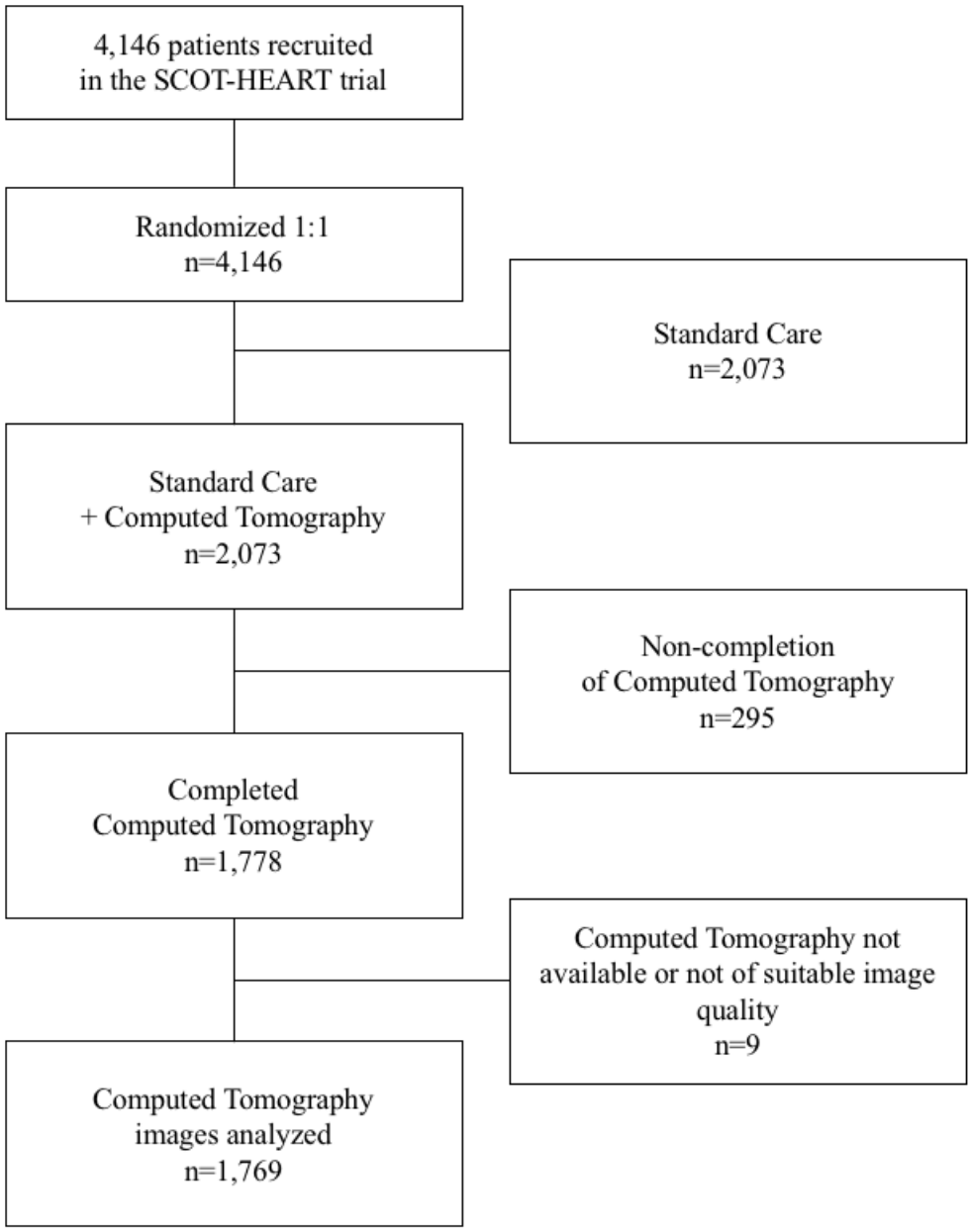

Figure 3.1 CONSORT diagram of SCOT-HEART sub-study.
(Williams, Moss et al. 2019)

		All participants n=1769	Participants without adverse plaque n=1161	Participants with adverse plaque n=608	P-value
Male		997 (56%)	545 (47%)	452 (74%)	**<0.001**
Age		57.6 ± 9.5	55.9 ± 9.8	60.8 ± 7.8	**<0.001**
Body mass index (kg/m^2)		29.6 ± 5.5	30.0 ± 5.8	28.8 ± 4.8	**<0.001**
Atrial fibrillation		34 (1.9%)	20 (1.7%)	14 (2.3%)	0.399
Smoking status	Current smoker	330 (19%)	208 (18%)	122 (20%)	**<0.001**
	Ex-smoker	593 (34%)	357 (31%)	236 (39%)	
	Non-smoker	845 (48%)	595 (51%)	250 (41%)	
Hypertension		608 (35%)	373 (32%)	235 (39%)	**0.005**
Diabetes		196 (11%)	128 (11%)	68 (11%)	0.919
Family history		765 (43%)	507 (44%)	258 (42%)	0.552
Previous CHD		178 (10%)	75 (6.5%)	103 (17%)	**<0.001**
Anginal symptoms	Typical angina	654 (37%)	347 (30%)	307 (51%)	**<0.001**
	Atypical angina	432 (24%)	293 (25%)	139 (23%)	
	Non-anginal	683 (39%)	521 (45%)	162 (27%)	
ASSIGN		17.9 ± 11.0	16.1 ± 10.9	21.4 ± 10.6	**<0.001**
Coronary artery calcium score (Agatston units)		21 [0 - 230]	0 [0 - 34]	281 [89 - 775]	**<0.001**

Table 3.1 Characteristics of SCOT-HEART sub-study participants according to presence or absence of adverse plaque.

N (%), mean ± standard deviation or median [interquartile range]; CHD (Coronary heart disease)

3.4.1 Plaque Characteristics

CCTA characteristics of atherosclerotic plaque were assessed in 26,535 segments in 1,769 patients. This demonstrated positive remodelling in 1,163 segments (4.4%), low attenuation plaque in 213 segments (0.8%), spotty calcification in 472 segments (1.8%), and the napkin ring sign in 78 segments (0.3%). All plaque characteristics were more common in the proximal coronary artery segments, in particular the proximal left anterior descending coronary artery (***Table 3.2, Table 3.3, Table 3.4, Table 3.5***). Adverse plaques were present in 608 (34%) patients. Patients with adverse plaques were older, had a higher body-mass index, and were more likely to be male. They were also more likely to have a previous history of coronary heart disease or hypertension, to be a smoker, or to have typical angina (***Table 3.1***). Patients with adverse plaques had a higher cardiovascular risk score and higher calcium score. Coronary heart disease death or non-fatal myocardial infarction was three-times more frequent in patients with adverse plaque compared to those without (n=25/608 (4.1%) versus n=16/1161 (1.4%), p<0.001; hazard ratio (HR) 3.01, 95% confidence interval (CI) 1.61 to 5.63; p=0.001; ***Figure 3.2***). Most events occurred in patients with adverse plaques in the proximal segments rather than the mid and distal segments (n=23/489 (4.7%) versus n=2/119 (1.7%); p=0.197). Adverse plaque features appeared to have a greater prognostic value in women and those under the age of 60 years, with a body-mass index of greater than 30 kg/m^2 or with a lower cardiovascular risk score, but these differences were not statistically significant (***Table 3.6***). The presence of one or more segments of spotty calcification or the napkin ring sign was not associated with a difference in coronary heart disease death or non-fatal myocardial infarction on per patient assessment (***Table 3.7***).

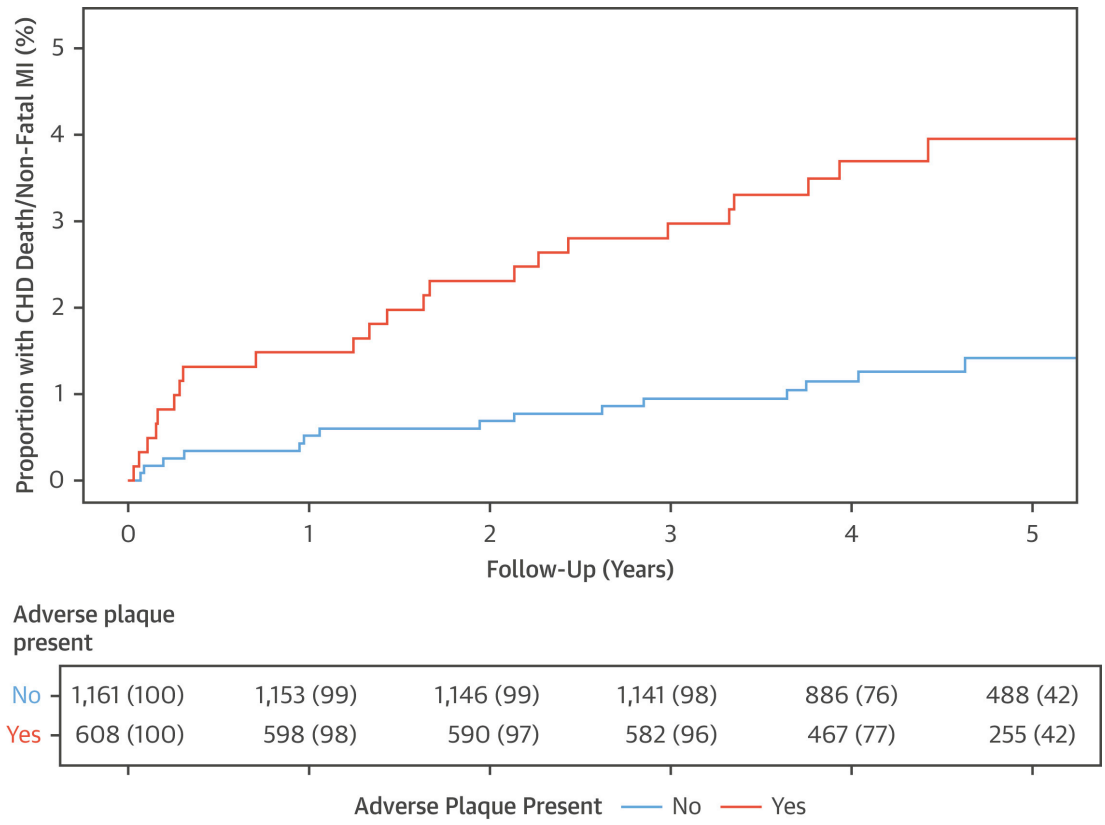

Figure 3.2 Coronary heart disease death or non-fatal myocardial infarction across the total cohort in patients with and without adverse plaque.

The effect of the presence of one or more adverse plaques (defined by the presence of low attenuation or positive remodelling) on subsequent coronary heart disease death or non-fatal myocardial infarction. Cumulative incidence plot for patients with and without adverse plaque features.
(Williams, Moss et al. 2019)

	Adverse plaque *		Positive remodelling		Low attenuation plaque		Spotty calcification		Napkin ring sign	
	N	%	N	%	N	%	N	%	N	%
Left Main Stem	60	3.4	59	3.3	12	0.7	13	0.7	5	0.3
Prox LAD	388	21.9	385	21.8	78	4.4	117	6.6	33	1.9
Mid LAD	234	13.2	224	12.7	50	2.8	84	4.7	13	0.7
Dist LAD	21	1.2	19	1.1	5	0.3	14	0.8	1	0.1
D1	19	1.1	19	1.1	1	0.1	20	1.1	1	0.1
D2	5	0.3	5	0.3	0	0	8	0.5	0	0
Prox Cx	109	6.2	106	6.0	18	1.0	39	2.2	6	0.3
OM1	27	1.5	26	1.5	4	0.2	13	0.7	1	0.1
AV Cx	11	0.6	11	0.6	1	0.1	4	0.2	1	0.1
OM 2	1	0.1	1	0.1	0	0	2	0.1	0	0
Mid Dist Cx	5	0.3	5	0.3	0	0	1	0.1	0	0
Prox RCA	116	6.6	112	6.3	20	1.1	56	3.2	6	0.3
Mid RCA	132	7.5	130	7.3	19	1.1	63	3.6	10	0.6
Distal RCA	51	2.9	51	2.9	4	0.2	25	1.4	1	0.1
RCA/CX PD	10	0.6	10	0.6	1	0.1	13	0.7	0	0

Table 3.2 Frequency of plaque characteristics in each of the 15 coronary artery segments.

** Positive remodelling or low attenuation plaque.*
Prox, proximal; RCA, right coronary artery; Cx, circumflex; PD, posterior descending; LM, left main; LAD, left anterior descending; D1, first diagonal; D2, second diagonal; OM1, obtuse marginal; AV, atrioventricular.

	Patients with non-obstructive disease N = 671		**Patients with obstructive disease N = 452**	
	N	%	N	%
Left Main Stem	19	2.8	41	9.1
Prox LAD	170	25.3	218	48.2
Mid LAD	81	12.1	153	33.8
Dist LAD	4	0.6	17	3.8
D1	4	0.6	15	3.3
D2	1	0.1	4	0.9
Prox Cx	28	4.2	81	17.9
OM1	6	0.9	21	4.6
AV Cx	2	0.3	9	2.0
OM 2	0	0	1	0.2
Mid Dist Cx	2	0.3	3	0.7
Prox RCA	34	5.1	82	18.1
Mid RCA	30	4.5	102	22.6
Distal RCA	9	1.3	42	9.3
RCA/CX PD	2	0.3	8	1.8

Table 3.3 Frequency of adverse plaque in patients with non-obstructive and obstructive coronary artery disease in each of the 15 coronary artery segments.

Prox, proximal; RCA, right coronary artery; Cx, circumflex; PD, posterior descending; LM, left main; LAD, left anterior descending; D1, first diagonal; D2, second diagonal; OM1, obtuse marginal; AV, atrioventricular.

	Positive remodelling AND low attenuation plaque	
	N	%
Left Main Stem	11	0.6
Prox LAD	75	4.2
Mid LAD	40	2.3
Dist LAD	3	0.2
D1	1	0.1
D2	0	0.0
Prox Cx	15	0.8
OM1	3	0.2
AV Cx	1	0.1
OM 2	0	0
Mid Dist Cx	0	0
Prox RCA	16	0.9
Mid RCA	17	1.0
Distal RCA	4	0.2
RCA/CX PD	1	0.1

Table 3.4 Presence of positive remodelling and low attenuation plaque in different coronary artery segments.

Prox, proximal; RCA, right coronary artery; Cx, circumflex; PD, posterior descending; LM, left main; LAD, left anterior descending; D1, first diagonal; D2, second diagonal; OM1, obtuse marginal; AV, atrioventricular.

		Patients **n (%)**	**Fatal or non-fatal myocardial infarction**	
			n (%)	**Hazard ratio** (95% confidence intervals)
Positive remodeling	**Present**	602 (34%)	25 (4.1%)	3.05 (1.63, 5.71) P<0.001
	Absent	1166 (66%)	16 (1.4%)	
Low attenuation plaque	**Present**	168 (10%)	6 (3.6%)	1.60 (0.67, 3.80) p=0.289
	Absent	1601 (91%)	35 (2.2%)	
Spotty calcification	**Present**	299 (17%)	6 (2.0%)	0.83 (0.35, 1.97) p=0.669
	Absent	1470 (83%)	35 (2.4%)	
Napkin ring	**Present**	76 (4.3%)	2 (2.6%)	1.16 (0.28. 4.79) p=0.841

Table 3.5 Per patient assessment of plaque characteristics and subsequent fatal or non-fatal myocardial infarction across the total population.

	Age < 60 years	**Age ≥ 60 years**
Adverse plaque features on CCTA	3.65 (1.54, 8.65) p=0.003	2.44 (0.97, 6.13) p=0.057
	Male	**Female**
Adverse plaque features on CCTA	2.44 (1.14, 5.22) p=0.021	3.27 (1.00, 10.71) p=0.051
	BMI < 30 kg/m^2	**BMI ≥ 30 kg/m^2**
Adverse plaque features on CCTA	1.76 (0.83, 3.74) p=0.143	9.06 (2.53, 32.50) p=0.001
	Low cardiovascular risk score*	**High cardiovascular risk score***
Adverse plaque features on CCTA	3.12 (1.35, 7.21) p=0.008	2.64 (1.00, 6.94) p=0.050

Table 3.6 Univariable analysis for fatal or non-fatal myocardial infarction in patients with adverse plaque features on CCTA stratified by age, sex and body mass index.

* High cardiovascular risk score defined as an ASSIGN score greater than or equal to 20.
CCTA – Coronary Computed Tomography angiography; BMI – Body-mass index

		Non obstructive disease			Obstructive disease		
		No adverse plaque n=403	**With adverse plaque n=268**	**P-value**	**No adverse plaque n=112**	**With adverse plaque n=340**	**P-value**
Male		208 (52%)	179 (67%)	**<0.001**	74 (66%)	273 (80%)	**0.002**
Age		59.0 ± 8.7	59.7 ± 8.2	0.282	61.4 ± 8.7	61.6 ± 7.4	0.823
Body mass index (kg/m^2)		30.0 ± 5.2	28.4 ± 4.9	**<0.001**	29.9 ± 5.3	29.2 ± 4.6	0.210
Atrial fibrillation		7 (1.7%)	5 (1.9%)	1.000	1 (0.9%)	9 (2.6%)	0.463
Smoking status	Current smoker	66 (16%)	62 (23%)	**0.019**	26 (23%)	60 (18%)	0.393
	Ex-smoker	145 (36%)	105 (39%)		38 (34%)	131 (39%)	
	Non-smoker	192 (48%)	101 (38%)		48 (43%)	149 (44%)	
Hypertension		157 (39%)	86 (32%)	0.070	53 (48%)	149 (45%)	0.565
Diabetes		56 (14%)	31 (12%)	0.379	20 (18%)	37 (11%)	0.054
Family history		177 (44%)	111 (41%)	0.229	43 (38%)	147 (43%)	0.553
Previous CHD		32 (7.9%)	32 (12%)	0.084	24 (21%)	71 (21%)	0.902
Anginal symptoms	Typical angina	122 (30%)	88 (33%)	0.439	70 (63%)	219 (65%)	0.643
	Atypical angina	103 (26%)	75 (28%)		19 (17%)	64 (19%)	
	Non-anginal	178 (44%)	105 (39%)		23 (21%)	57 (17%)	
ASSIGN		19.3 ± 11.4	19.4 ± 10.0	0.921	24.0± 11.7	23.0 ± 10.8	0.428
Coronary artery calcium score (Agatston units)		33 [3, 108]	129 [35, 307]	**<0.001**	206 [42, 590]	546 [196, 1188]	**<0.001**

Table 3.7 Characteristics of study participants with non-obstructive disease and obstructive disease with and without adverse plaque.

N (%), mean ± standard deviation or median [interquartile range]

3.4.2 Coronary Artery Stenosis

Patients with obstructive coronary artery disease were twice as likely to suffer coronary heart disease death or non-fatal myocardial infarction (n=22/452 (4.9%)) than patients with non-obstructive disease (n=16/671 (2.4%), Chi-squared p=0.024; HR 1.99, 95% CI 1.05 to 3.79; p=0.036). Patients with obstructive coronary artery disease were also more likely to undergo coronary revascularisation (n=215/452 (48%) versus n=35/671 (5%); p<0.001) and be prescribed preventative medications at 6 weeks (n=427/452 (95%) versus n=538/671 (80%); p<0.001) than patients with non-obstructive disease.

Adverse plaques were observed in 40% of patients with non-obstructive disease (n=268/671) and three quarters of patients with obstructive coronary artery disease (n=340/452). Patients with both obstructive disease and adverse plaque had the worst outcome during follow-up (***Figure 3.3***). Although the presence of adverse plaque is suggestive of a worse prognosis at 2 years in patients with non-obstructive disease, at 5 years the outcomes of patients with non-obstructive disease and obstructive disease without adverse plaque were similar (***Figure 3.3***). Indeed, compared to patients with normal coronary arteries, patients with obstructive disease and adverse plaque had a greater than 10-fold increase in the rate of coronary heart disease death or non-fatal myocardial infarction at 5 years (***Table 3.8***).

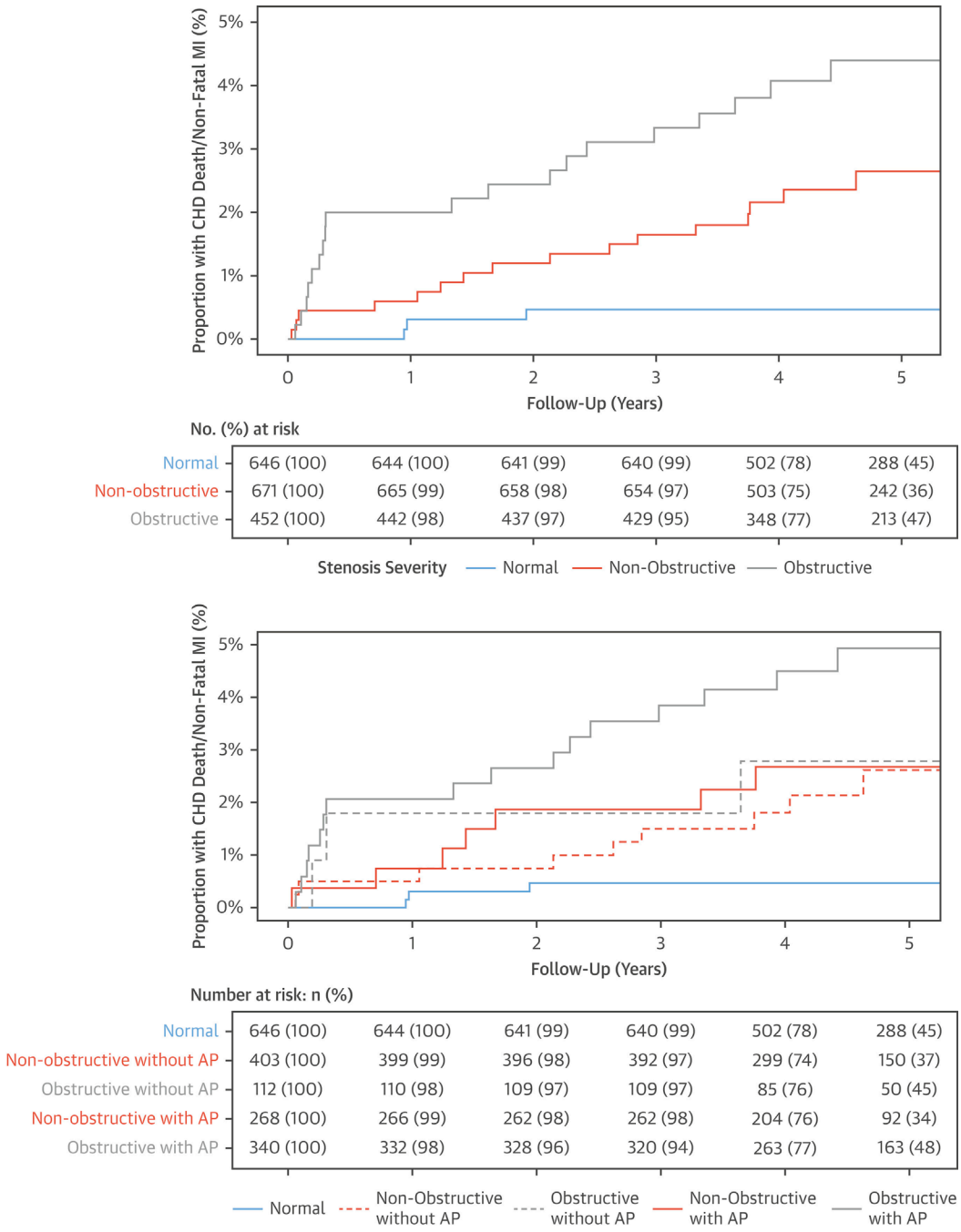

Figure 3.3 Coronary heart disease death and non-fatal myocardial infarction in patients with different stenosis severity and coronary artery plaque characteristics.

Cumulative incidence plot for coronary heart disease death and non-fatal myocardial infarction in patients (top panel) with normal coronary arteries, non-obstructive disease and obstructive disease and (bottom panel) normal coronary arteries, non obstructive disease with and without adverse plaque characteristics and obstructive disease with and without adverse plaque features. AP, adverse plaque.
(Williams, Moss et al. 2019)

	Univariable analysis	**Multivariate analysis #**
Non-obstructive disease without adverse plaque *	4.95 (1.34, 18.29) p=0.016	2.79 (0.64, 12.18) p=0.172
Non-obstructive disease with adverse plaque *	5.81 (1.50, 22.46) p=0.011	2.67 (0.53, 13.43) p=0.234
Obstructive disease without adverse plaque *	7.73 (1.73, 34.54) p=0.007	3.20 (0.52, 19.61) p=0.208
Obstructive disease with adverse plaque *	11.50 (3.39, 39.04) p<0.001	4.10 (0.76, 22.0) p=0.100
Coronary Artery Calcium Score **	1.23 (1.13, 1.35) p <0.001	1.12 (0.98, 1.28) p=0.107
Cardiovascular Risk score $	1.65 (1.13, 2.41) p=0.01	1.10 (0.71, 1.70) p=0.673

Table 3.8 Univariable and multivariable analysis for coronary heart disease death or non-fatal myocardial infarction compared to patients with normal coronary arteries.

Hazard ratios and 95% confidence intervals.
** Adverse plaque defined as the presence of positive remodelling or low attenuation plaque.*
*** Per doubling of coronary artery calcium score*
$ ASSIGN score, per doubling of cardiovascular risk score
 # Log rank statistic 27.29, p<0.001; Harrell's C statistic 0.728 (standard error 0.046)

3.4.3 Coronary Artery Calcium Score

Patients with a coronary artery calcium score ≥1000 AU had a thirteen-fold increase in coronary heart disease death or non-fatal myocardial infarction compared to patients without coronary artery calcification. There was a clear gradation of risk with calcification associated with increasing risk (***Figure 3.4***). Patients with obstructive coronary artery disease had an eight-fold higher coronary artery calcium score than patients with non-obstructive coronary artery disease (435 [IQR 138 to 1127] versus 54 [IQR 12 to 190] Agatston units (AU); $p<0.001$). In multivariable analysis, the presence of both adverse plaque and obstructive plaque were dependent on coronary artery calcium score as a predictor of coronary heart disease death or non-fatal myocardial infarction (***Table 3.9***).

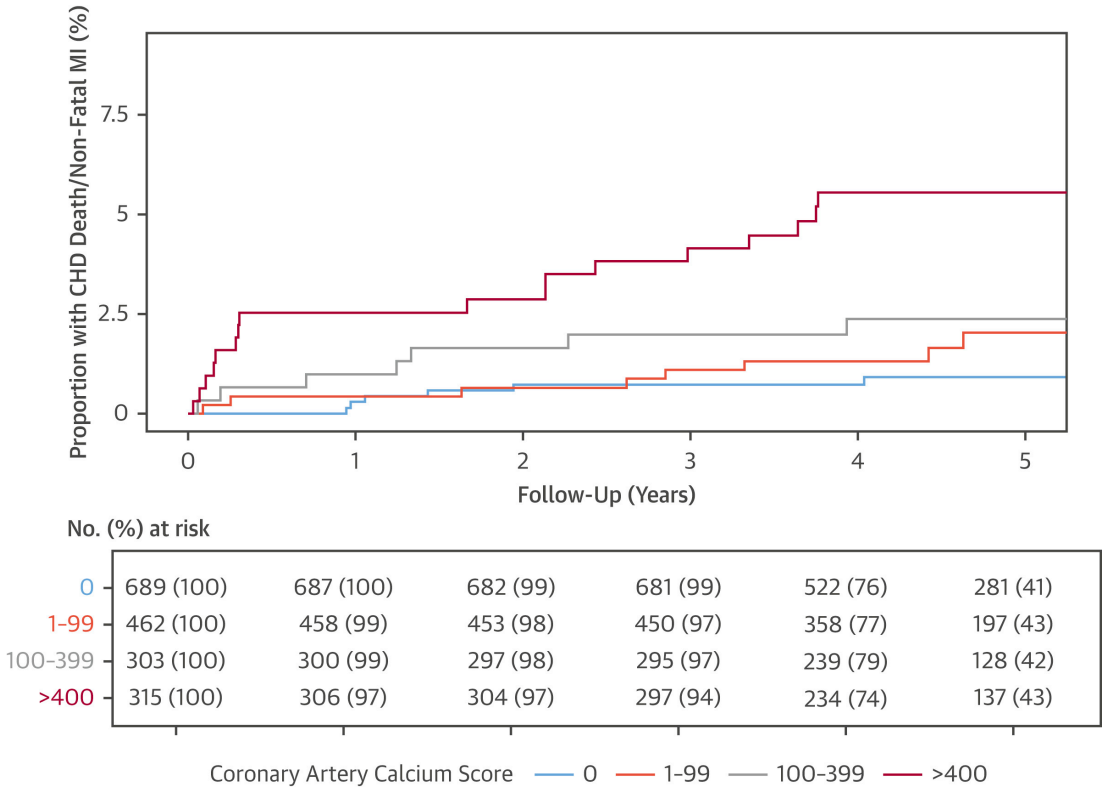

Figure 3.4 Coronary heart disease death and non-fatal myocardial infarction in patients with different severity of coronary artery calcification.

Cumulative incidence plots of the effect of different severity of coronary artery calcification on subsequent coronary heart disease death or non-fatal myocardial infarction.
(Williams, Moss et al. 2019)

	Univariable analysis	**Multivariable analysis #**
Adverse plaque *	3.01 (1.61, 5.63) p=0.001	1.18 (0.55, 2.52) p=0.671
Coronary Artery Calcium Score **	1.23 (1.13, 1.35) p <0.001	1.17 (1.04, 1.33) p=0.011
Obstructive coronary artery disease	3.35 (1.81, 6.19) p <0.001	1.36 (0.63, 2.93) p=0.439
Cardiovascular Risk score $	1.65 (1.13, 2.41) p=0.01	1.14 (0.74, 1.75) 0.563

Table 3.9 Univariable and multivariable analysis for coronary heart disease death or non-fatal myocardial infarction across the total population.

Hazard ratios and 95% confidence intervals.
** Compared to patients without adverse plaque in the total population. Adverse plaque defined as the presence of positive remodelling or low attenuation plaque.*
*** Per doubling of coronary artery calcium score*
$ ASSIGN score, per doubling of cardiovascular risk score
 # Log rank statistic 26.74 (p<0.001), Harrell's C statistic 0.723 (standard error 0.046)

3.5 Discussion

In a large multicentre prospective study of CCTA, we have demonstrated that adverse coronary plaque characteristics are associated with a tripling of the risk of coronary heart disease death or non-fatal myocardial infarction. The presence of obstructive disease was also a major predictor of risk, with the combination of adverse plaque with obstructive disease appearing to confer the greatest risk. However, overall the only independent predictor of risk was the coronary artery calcium score, a measure of overall plaque burden. These results suggest that whilst plaque composition and its haemodynamic consequences are associated with future myocardial infarction, the predominant factor governing patient outcomes is the burden of coronary atherosclerosis.

Adverse coronary plaque is associated with subsequent cardiovascular events in patients with stable coronary artery disease (Motoyama, Ito et al. 2015, Thomsen, Abdulla et al. 2016, Conte, Annoni et al. 2017, Motoyama, Kondo et al, 2007). In keeping with previous work (Motoyama, Ito et al. 2015, Motoyama, Sarai et al. 2009, Motoyama, Kondo et al. 2007, Scheltt, Maurovich-Horvat et al. 2013, Narula, Nakano et al. 2013), we found that the plaque characteristics which were the most helpful in predicting future coronary events were positive remodelling and low attenuation plaque. These CT characteristics are markers of pathological vulnerability (Obaid, Calvert et al. 2017), and are potential culprit lesions for subsequent acute coronary events. Motoyama *et al* identified that the presence of adverse plaque was predictive of acute coronary syndrome at 4 years in a study of 3,158 patients with 88 events (2.8%) (Motoyama, Ito et al. 2015). In the Prospective Multicentre Imaging Study for Evaluation of Chest Pain (PROMISE) trial, adverse plaques were present in 15% of patients and were associated with an increased risk

of the combined endpoint of death, myocardial infarction or unstable angina (Ferencik, Mayrhofer et al. 2018). However, overall adverse plaques have a low positive predictive value for the identification of subsequent coronary events. This is in keeping with the known theory of continuous plaque remodelling where adverse plaques may stabilise with or without sub-clinical rupture, rather than cause a clinically apparent acute coronary syndrome.

Acute myocardial infarction occurs when there is rupture or erosion of a coronary atherosclerotic plaque and there is associated thrombus formation causing vessel occlusion (Davies. 2000). The presence of pre-existing flow limitation due to obstructive atheroma is not a pre-requisite for this process. Indeed, it should be remembered that the majority (~80%) of myocardial infarctions are attributable to non-obstructive coronary plaques on antecedent angiography (Maddox, Stanislawski et al. 2014). Moreover, the risk of future myocardial infarction is similar whether the coronary plaque causes 50-85% or >85% luminal stenosis (Van Lierde, De Geest et al. 1990). A nested-case control study of patients without known coronary artery disease within the Coronary CT Angiography Evaluation for Clinical Outcomes: An International Multicentre (CONFIRM) registry identified that >65% of patients who developed acute coronary syndromes had non-obstructive disease on their baseline CCTA (Chang, Lin et al. 2018). This reflects the important nature of the biology of the atherosclerotic plaque rather than the functional consequence of luminal stenosis (Mann, Davies. 1999). For the prediction of subsequent coronary events, the presence of atherosclerotic plaque is more important than the presence of coronary stenoses. Indeed, in our study, patients with a combination of both obstructive coronary artery disease and adverse plaque had the worst outcomes. Moreover, patients with non-obstructive disease and adverse plaque had similar

outcomes to patients with obstructive disease without adverse plaque. Thus, our study provides evidence that coronary artery disease should no longer be defined based on luminal severity, but by the volume and type of disease.

When examined across the cohort as a whole, adverse plaques did not provide independent prognostic information when CT calcium scoring was included. CT calcium scoring is a surrogate marker of plaque burden and its prognostic utility has been established in large studies of symptomatic and asymptomatic patients (Shah, Bellam et al. 2014, McClelland, Chung et al. 2006). It is likely that patients with higher plaque burden are more likely to have adverse plaques and are more likely to have severe coronary artery stenoses. Few studies have assessed the clinical implications of this overlap. A small study of 339 patients with suspected coronary artery disease found that both adverse plaques and CT calcium score were independent predictors of cardiac events at 2 years (Takamura, Fujimoto et al. 2017). Clearly the greater the burden of disease, the greater the risk of events. However, for the individual patient, the assessment of coronary artery calcium alone is not sufficient to guide management as the presence and volume of coronary artery calcification is not directly related to the degree of coronary artery stenosis and cannot inform on the pathophysiological status of the atherosclerotic plaque (Newby 2017). Indeed, in the PROMISE study, CCTA provided better prognostic discrimination compared to coronary artery calcium score (Budoff, Mayrhofer et al. 2017).

It is perhaps not surprising that the identification of plaque characteristics at a single time point by CCTA may not be sufficient to predict future events in long term follow-up. Atherosclerotic plaque undergoes continuous remodelling driven by a variety of

genetic and environmental factors, and we know that medications, such as statins, alter the constituents of atherosclerotic plaque (Lee, Chang et al. 2018). Autopsy studies show that atherosclerosis is present in young people (Joseph, Ackerman et al. 1993) and normograms for CT calcium score (McClelland, Chung et al. 2006) and plaque burden (Naoum, Berman et al. 2017) are in clinical use. Concerns have been raised about over medicalising patients with the routine use of preventative therapies for patients with non-obstructive disease (Redberg, Katz et al. 2017). However, the event rate in patients with non-obstructive disease in our study highlights that atherosclerosis is not “normal”. Similarly in the PROMISE study CCTA identified patients with non-obstructive disease who were at risk of subsequent events (Hoffmann, Ferencik et al. 2017). Indeed, future studies should assess whether the identification of coronary artery disease per se can guide treatment changes and improve outcomes for the wider population.

3.5.1 Limitations

There are a number of study limitations that we should acknowledge. First, the relatively low number of events over 5 years of follow-up limits our power to assess multiple subgroups. This in part reflects our selection of the hard clinical end-point of coronary heart disease death or non-fatal myocardial infarction as well as the low to intermediate risk of the population recruited in the SCOT-HEART trial. Second, the SCOT-HEART study was not designed or powered for this secondary analysis, and our findings are exploratory. Third, we used a simple and pragmatic approach to the identification of adverse plaques that would not greatly add to the time spent analysing CT scans. Automated software that can identify plaque characteristics may further improve observer variability in the classification of adverse plaques and help standardisation. Finally, the trial did encourage the use of secondary

preventative therapies in patients found to have either obstructive or non-obstructive disease. This will have inevitably reduced the number of events as well as reduced our ability to identify associations between plaque characteristics and clinical events because they will have been modified by the initiation of antiplatelet and statin therapies.

3.6 Conclusion

In conclusion, we have demonstrated that adverse plaque characteristics provide prognostic information out to 5 years, but that this is not independent of plaque burden assessed by coronary artery calcium score. Patients with obstructive disease and adverse plaques have the highest event rates throughout follow-up. This may aid the identification of a subgroup of patients who would benefit from more intensive medical therapy.

CHAPTER 4

Molecular coronary plaque imaging using 18F-fluoride

Moss AJ, Doris MK, Andrews JPB, Bing R, Daghem M, van Beek EJR, Forsyth L, Shah ASV, Williams MC, Sellers S, Leipsic J, Dweck MR, Parker RA, Newby DE, Adamson PD.
Molecular coronary plaque imaging using 18F-fluoride
Circ Cardiovasc Imaging. 2019;12:e000929.

4.1 Summary

Objectives

Coronary 18F-fluoride positron emission tomography (PET) identifies ruptured and high-risk atherosclerotic plaque. The optimal method to identify, to quantify and to categorize increased coronary 18F-fluoride uptake and determine its reproducibility has yet to be established. This study aimed to optimise the identification, quantification, categorisation and scan-rescan reproducibility of increased 18F-fluoride activity in coronary atherosclerotic plaque.

Methods

In a prospective observational study, patients with multi-vessel coronary artery disease underwent serial 18F-fluoride PET. Coronary 18F-fluoride activity was visually assessed, quantified and categorised with reference to maximal tissue to background ratios (TBR_{MAX}). Levels of agreement for both visual and quantitative methods were determined between scans and observers.

Results

Thirty patients (90% male, 20 patients with stable coronary artery disease, and 10 with recent type 1 myocardial infarction) underwent paired serial PET-CCTA imaging within an interval of 12±5 days. A mean of 3.7±1.8 18F-fluoride positive plaques per patient were identified following recent acute coronary syndrome, compared with 2.4±2.3 positive plaques per patient in stable coronary artery disease. The bias in agreement in TBR_{MAX} measurements in visually positive plaques was low between observers (mean difference -0.01, 95% limits of agreement -0.32 to 0.30) or between scans (mean difference 0.06, 95% limits of agreement -0.49 to 0.61). Good agreement in the categorisation of focal 18F-

fluoride uptake was achieved using visual assessment alone (κ = 0.66) and further improved at higher TBRmax values.

Conclusions

Coronary 18F-fluoride activity is a precise and reproducible metric in the coronary vasculature. The analytical performance of 18F-fluoride is sufficient to assess the prognostic utility of this radiotracer as a non-invasive imaging biomarker of plaque vulnerability.

Clinical Trial Registration Information

Clinical Trials.gov Study ID: NCT02110303, NCT02278211

4.2 Introduction

Atherosclerotic plaque rupture is the commonest cause of acute coronary syndromes (Libby, 2013). Cardiovascular imaging modalities have focused on identifying the presence and severity of luminal stenoses to stratify the risk of plaque rupture events. However, luminal stenosis is a relatively late feature of coronary atherosclerosis and the majority of rupture events occur at sites of non-obstructive plaque on antecedent angiography (Van Lierde, De Geest et al. 1990, Chang, Lin et at. 2018, Ahmadi, Leipsic et al. 2015). As such, interest has grown in identifying adverse atherosclerotic plaque characteristics and regions of increased disease activity within the arterial wall that may better predict subsequent plaque rupture and clinical events. One promising approach has been to use combined positron emission tomography (PET) and computed tomography (CT) angiography that co-registers the detailed anatomy of the arterial wall with the *in vivo* biological activity of disease (Dweck, Chow et al. 2012).

To date, PET-CT has predominantly been used to evaluate the presence of inflammatory processes in large calibre arteries using the radiotracer 18F-fluorodeoxyglucose (18F-FDG) (Rudd, Warburton et al. 2002). However, the application of this tracer to the coronary circulation is limited because background myocardial 18F-FDG uptake obscures and prevents assessment of coronary plaque activity (Joshi, Vesey et al. 2014). Recent studies have found that 18F-sodium fluoride (18F-fluoride) holds major promise in identifying culprit plaques in the coronary circulation following myocardial infarction (Dweck, Chow et al. 2012, Joshi, Vesey et al. 2014). Validation work in the carotid arteries indicates that 18F-fluoride also identifies culprit plaques following neurovascular events and preferentially binds to microcalcification, a key component of high-risk atherosclerotic plaque

(Irkle, Vesey et al. 2015, Vesey, Jenkins et al. 2017). Studies are now ongoing to assess the prospective prognostic capability of coronary 18F-fluoride PET and whether the signal can help guide the use of novel therapies (NCT02110303 and NCT02278211). However, coronary 18F-fluoride imaging is challenging due to the small calibre of the vessels and their near continuous motion throughout the cardiac cycle (Demer, Tintut et al. 2017, Alavi, Werner et al. 2016). Moreover, there is a lack of consensus regarding image analysis techniques with a number of differing approaches having been used. Hence, there is a need to optimise and to standardise coronary PET imaging methodology to facilitate the widespread application of coronary molecular imaging.

To address these issues, we undertook a prospective observational clinical study in patients with stable and unstable coronary artery disease that aimed to establish a reproducible methodology for identifying, quantifying and characterising 18F-fluoride activity in the coronary arteries.

4.3 Methods

4.3.1 Study Population

Participants were recruited within pre-specified reproducibility substudies of the DIAMOND (Dual antiplatelet therapy to Inhibit coronary Atherosclerosis and MyOcardial injury in patients with Necrotic high-risk coronary plaque Disease) and PRE^{18}FFIR (Prediction of Recurrent Events with 18F-Fluoride to Identify Ruptured and High-risk Coronary Artery Plaques in Patients with Myocardial Infarction) trials. Inclusion required the presence of multi-vessel coronary artery disease on invasive angiography, either following recent myocardial infarction (PRE^{18}FFIR), or in the context of stable coronary artery disease (DIAMOND). Exclusion criteria included inability to receive iodinated contrast, renal impairment (estimated glomerular filtration rate ≤30 mL/min/1.73 m^2) or women of child-bearing potential. The study was approved by the local institutional review board, the Scottish Research Ethics Committee (REC reference: 14/SS/0089 and 15/SS/0203), and the United Kingdom (UK) Administration of Radiation Substances Advisory Committee. It was performed in accordance with the Declaration of Helsinki. All patients provided written informed consent prior to any study procedures.

4.3.2 18F-Fluoride Positron Emission Tomography And Coronary Computed Tomography Angiography

All patients underwent 18F-fluoride PET-CT and coronary CT angiography scanning on two occasions two weeks apart using the same protocol. Patients were administered 50-100 mg oral metoprolol if their resting heart rate was >65 beats/min prior to the intravenous administration of 250 MBq 18F-fluoride. After 60 min, patients were imaged with a hybrid PET-CT scanner (64-multidetector Biograph

mCT, Siemens Medical Systems, Erlangen, Germany). Attenuation correction CT scans were performed in held expiration prior to the acquisition of electrocardiographic-gated (ECG-gated) list-mode PET data using a single 30-min bed position centred on the heart. Finally, an ECG-gated coronary CT angiogram (CCTA) was performed in mid-diastole during held expiration. All patients received sublingual glyceryl trinitrate prior to CCTA.

4.3.3 Image Analysis

ECG-gated PET images were reconstructed in diastole (50-75% of the R-R interval, 2 iterations, 21 subsets Siemens Ultra-HD algorithm) and fused with contrast enhanced CCTA. Analysis of the CT images was performed using dedicated software (Vitrea Advanced, Toshiba Systems) with multi-planar reformatting for plaque analysis used as necessary. Coronary arteries with a diameter ≥ 2 mm were assessed according to the 18-segment Society of Cardiac Computed Tomography model (Leipsic, Abbara et al. 2014). Qualitative and semi-quantitative analysis of the PET images from all sixty scans was performed independently by trained observers using an OsiriX workstation (OsiriX version 3.5.1 64-bit; OsiriX Imaging Software, Geneva, Switzerland).

4.3.4 Identification of Coronary 18F-Fluoride Uptake

Co-registration of PET and CCTA images was undertaken to aid image interpretation in a two stage process. First, 18F-fluoride blood pool activity on the PET scan was aligned with contrast enhanced CCTA images of the cardiac chambers in three dimensions using axial, sagittal and coronal views of the heart. This approach is made possible by the increased blood pool activity of 18F-fluoride in comparison to the myocardium, allowing the contours of the cardiac chambers to

be determined on the PET images. Second, axial, coronal and sagittal views were again interrogated in three dimensions to ensure optimal alignment of any tracer uptake in the aortic valve, aortic root, and the inner curve of the ascending aorta with the contrast CCTA (***Figure 4.1***).

Visual assessment for increased coronary 18F-fluoride activity was performed on both a per-patient level and per-segment basis. For a signal to be co-localised to the coronary artery, a coronary atherosclerotic plaque had to be present on the CCTA and the increased pattern of radiotracer had to arise from the coronary artery and follow its course over >5 mm in three dimensions on orthogonal views. Care was taken to exclude 18F-fluoride activity arising from adjacent structures such as the aortic valve, mitral valve annulus, left atrial appendage and the pulmonary artery.

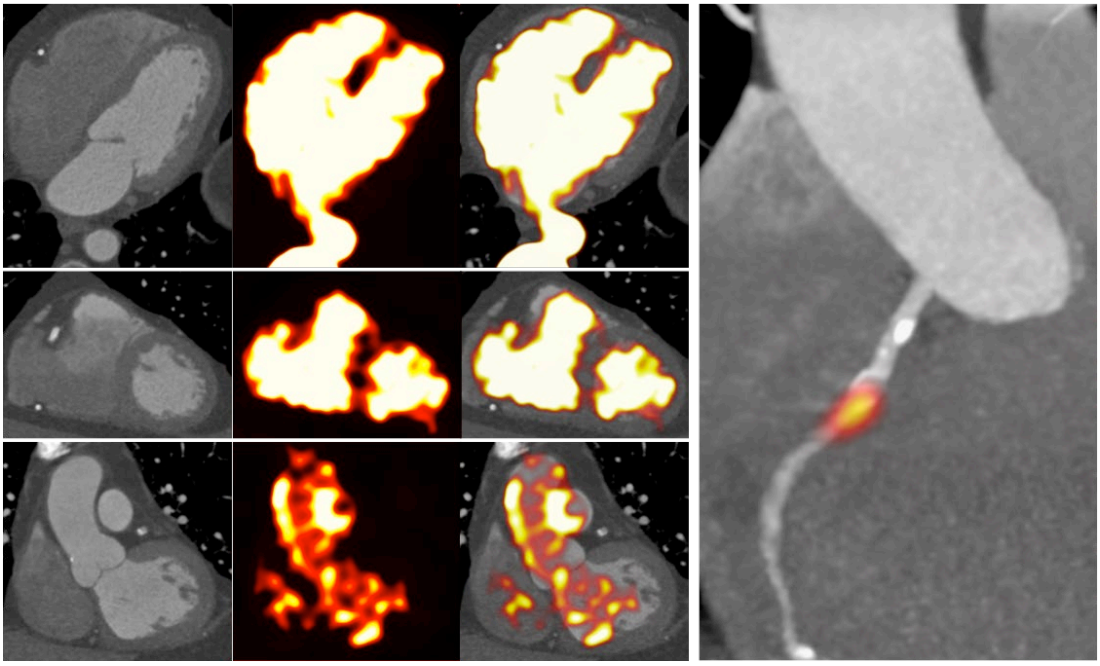

Figure 4.1 Co-registration of 18F-fluoride positron emission tomography with contrast-enhanced computed tomography.

Patient and cardiac motion between the acquisition of positron emission tomography (PET) and coronary computed tomography angiography (CCTA) datasets can be enhanced by co-alignment of diastolic phase electrocardiogram-gated PET reconstructions (50-75% of cardiac cycle) with the diastolic phase of CCTA. 18F-Fluoride activity in cardiac chambers facilitates accurate 3-dimension co-alignment in axial and coronal views. At low levels of activity, 18F-fluoride is predominantly restricted to the intravascular compartment with minimal activity observed in the myocardium. 18F-Fluoride activity that co-localises to the inner and outer curvature of the ascending aorta and aortic valve can be used as markers for co-registration. 18F-Fluoride activity in coronary arteries is referenced to blood pool activity allowing coronary 18F-fluoride activity to be differentiated from the surrounding structures in multiplanar views.

4.3.5 Quantification of Coronary 18F-Fluoride Uptake

Semi-quantitative PET analysis was undertaken for all proximal coronary segments in addition to any atherosclerotic segment with focal 18F-fluoride activity as described above. First, maximum standardised uptake values (SUV_{MAX}) were measured within regions of interest drawn around these areas. Due to the difficulties of drawing reproducible regions of interest around the perimeter of coronary segments, mean SUV values were not recorded.

SUV_{MAX} values were corrected for background activity using several different methods. First, correction was made for uptake in a referent proximal coronary plaque with no evidence of increased 18F-fluoride activity (Dweck, Chow et al. 2012, Joshi, Vesey et al. 2014). Second, correction was made for blood pool activity using elliptical regions of interest drawn within the brachiocephalic vein, superior vena cava, and all four cardiac chambers with mean standardized uptake values (SUV_{MEAN}) recorded for each region. To calculate coronary target to background ratios (TBR), coronary SUV_{MAX} was divided by these background measures providing $TBR_{REFERENT}$ and TBR_{MAX} values respectively.

4.3.6 Categorisation of Coronary 18F-Fluoride Uptake

18F-Fluoride activity in plaques meeting visual criteria for positivity was quantified and use to categorise plaques into the following groups: uptake below (TBR <0.9), similar to (TBR 0.9-1.1), and above (TBR >1.1) blood pool activity. This categorisation was then applied to both patients with recent acute coronary syndromes and stable coronary artery disease to assess the frequency of 18F-fluoride active lesions with the different thresholds. Discrepancies in reporting were

resolved by consensus adjudication (two out of three blinded observers) of the presence of focal coronary 18F-fluoride activity.

4.3.7 Reproducibility of Coronary 18F-Fluoride Uptake

Repeat anonymised scans for all 30 patients were presented to three experienced observers in random order. Each observer performed scan analysis independent of the other readers. First, they determined the presence of coronary plaques with increased visual activity using the criteria for visual identification described above. Second, they quantified activity in the coronary plaques which was referenced to background activity in the referent plaque, right atrium, left atrium, right ventricle, left ventricle, superior vena cava and brachiocephalic vein. Coefficients of variation for each of these background measurements were then calculated. Subsequently, coefficients of variation were calculated for each metric of coronary 18F-fluoride activity (e.g. SUV_{MAX}, TBR_{MAX}, $TBR_{REFERRENT}$ etc.). Finally, we assessed the agreement of these metrics across serial scans using visual categorisation in isolation, and in combination with a low semi-quantitative threshold (TBR >0.9) or a high semi-quantitative threshold (TBR >1.1).

4.3.8 Statistical analysis

Continuous variables are reported as mean ± standard deviation (SD) or median and interquartile range (IQR). Categorical variables are reported as absolute number and percentages. Paired *t*-tests were used to determine statistical significance for comparisons of means with normal distribution. Consensus observer agreement (two out of three observers) of coronary segment tracer localisation was used to adjudicate positive focal tracer uptake and the presence of a single positive segment was sufficient for a patient level diagnosis of 18F-fluoride positivity. Limits

of agreement analysis was conducted to assess scan-rescan and inter-observer repeatability for all coronary segments and visually positive coronary plaques using TBR_{MAX} adjusted for the left atrial blood pool. Following the mixed effects limits of agreement methodology of Parker et al. (Parker, Weir et al. 2016), a mixed effects model was fitted to the TBR_{MAX} between-scan paired differences with segment included as a random effect nested within patient, adjusting for study (DIAMOND or PRE^{18}FFIR) and observer as fixed effects. The mixed model for the TBR_{MAX} between-observer paired differences was similar but with scan number and observer comparison as fixed effects instead of observer. In both cases, the mean bias was separately estimated based on a model only including the nested random effects of segment within patient (Parker, Weir et al. 2016). Variance components concordance correlation coefficients (CCC) were computed as an additional measure of scan-rescan and inter-rater agreement using mixed effects methodology suitable for repeated measures data (Carrasco, Phillips et al. 2013). Specifically, we fitted a mixed effects model to the raw outcome data including nested random effects of segment within patient and adjusting for observer, study (DIAMOND or PRE^{18}FFIR), scan (first or second), and the global mean as fixed effects. For assessment of scan-rescan agreement we included the scan re-scan variance in the denominator of the repeated measures CCC formula, whereas for inter-observer agreement we included the between-observer variance in the denominator instead. Note that the CCC is strongly dependent on the between-segment and between-patient variability. Pan et al. (Pan, Rose et al. 2013) suggest that the CCC variance components method calculated using mixed effects modelling could also be applied to binary outcome data, and concludes that the method works well when the proportions are “not too extreme”. Therefore, the same CCC method was used to measure agreement of the binary visual uptake outcome to produce a kappa-type

statistic κ. The κ values were interpreted as follows: poor ≤0.20, fair 0.21 to 0.4, moderate 0.41 to 0.60, good 0.61 to 0.80, and very good ≥0.81. A non-parametric bootstrap method was used to compute 95% bias-corrected percentile confidence intervals for the CCC estimates. Statistical analysis was performed using R version 3.5.3 (R Foundation for Statistical Computing, Vienna, Austria). Statistical significance was taken as $P<0.05$.

4.4 Results

Thirty patients (90% male, 20 patients with stable coronary artery disease, and 10 with recent type 1 myocardial infarction) underwent serial PET-CCTA imaging within 12±5 days. Cardiovascular risk factors were common and twenty-eight (93.3%) patients had undergone prior coronary revascularisation (22 percutaneous coronary intervention and 9 coronary artery bypass grafting) (***Table 4.1***).

	All Patients	Patients With Recent Myocardial Infarction	Patients With Stable Coronary Heart Disease
N	30	10	20
Age, years	67.3±7.6	62.83±6.30	69.53±7.32
Male	27 (90)	10 (100)	17 (85)
Body Mass Index, kg/m^2	28.3±4.2	29.8±4.40	27.51±3.97
Medical history			
Previous Myocardial Infarction	23 (77)	10 (100)	13 (65)
Coronary Revascularisation	28 (93.3)	9 (90)	16 (80)
Percutaneous Coronary Intervention	22 (63)	9 (90)	13 (50)
Coronary Artery Bypass Grafting	9 (20)	0	9 (30)
Hypertension	17 (57)	3 (30)	14 (70.0)
High Cholesterol	26 (87)	6 (60)	20 (100)
Diabetes Mellitus	5 (17)	3 (30)	2 (10)
Prior Stroke/Transient Ischemic Attack	1 (3)	0	1 (5)
Atrial Fibrillation	1 (3)	0	1 (5)
Peripheral Vascular Disease	1 (3)	0	1 (5)
Medications			
Aspirin	30 (100)	10 (100)	20 (100)
P2Y12 Antagonist	10 (33)	10 (100)	0
Statin	30 (100)	10 (100)	20 (100)
Beta-Blocker	13 (43)	4 (40)	9 (45)
Angiotensin Converting Enzyme Inhibitor/Angiotensin II Receptor Blocker	25 (83)	8 (80)	17 (85)
Creatinine, mg/dL	0.9±0.2	1.0±0.2	0.9±0.1
Estimated Glomerular Filtration Rate, mL/min/1.73m^2	98.5±16.9	94.6±17.6	100.4±16.7
Interscan Interval, days	12.3±5.1	13.9±6.1	11.5±4.5

Table 4.1 Baseline characteristics of 18F-fluoride reproducibility population.

Values are n (%) or mean ± standard deviation.

4.4.1 Blood Pool 18F-Fluoride Activity

18F-Fluoride blood pool activity was consistently higher in all four cardiac chambers than in the myocardium (blood pool SUV_{MEAN} 1.14 *versus* interventricular septum SUV_{MEAN} 0.80) (***Figure 4.2, Figure 4.3, Figure 4.4***). This facilitated accurate manual co-registration of the PET and CCTA data sets as described above (***Figure 4.1***). Background measurements in the referent plaque, brachiocephalic vein and the superior vena cava were consistently lower than cardiac blood pool with high coefficients of variation. The regions with the least variability in serial measurements of background activity (SUV_{MEAN}) were the cardiac atria with coefficients of variation in the left and right atria of 5.9±2.8% and 6.5±2.5% respectively (***Figure 4.2, Table 4.2***).

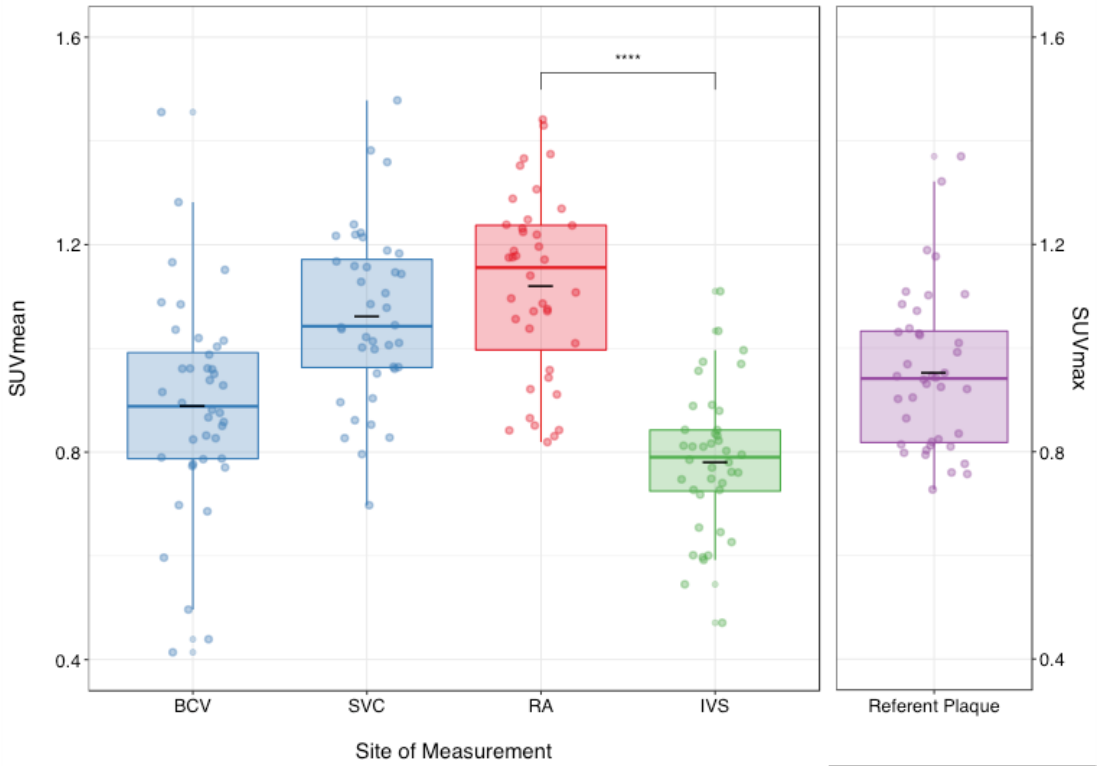

Figure 4.2 Standardised Uptake Values of Blood Pool and Cardiac 18F-Fluoride activity.

Box-plot of the median and the interquartile range of mean standardise uptake values for brachiocephalic, superior vena cava, right atrium, interventricular septum (black line, mean). Note the low myocardial and background coronary arterial 18F-fluoride uptake compared to blood pool in the right atrium.
BCV, brachiocephalic vein, IVS, interventricular septum, LA, left atrium, LV, left ventricle, RA, right atrium, RV, right ventricle, SVC, superior vena cava.
NS, non-significant; *, p≤0.05, †, p≤0.01, ‡, p≤0.001, §, p≤0.0001.

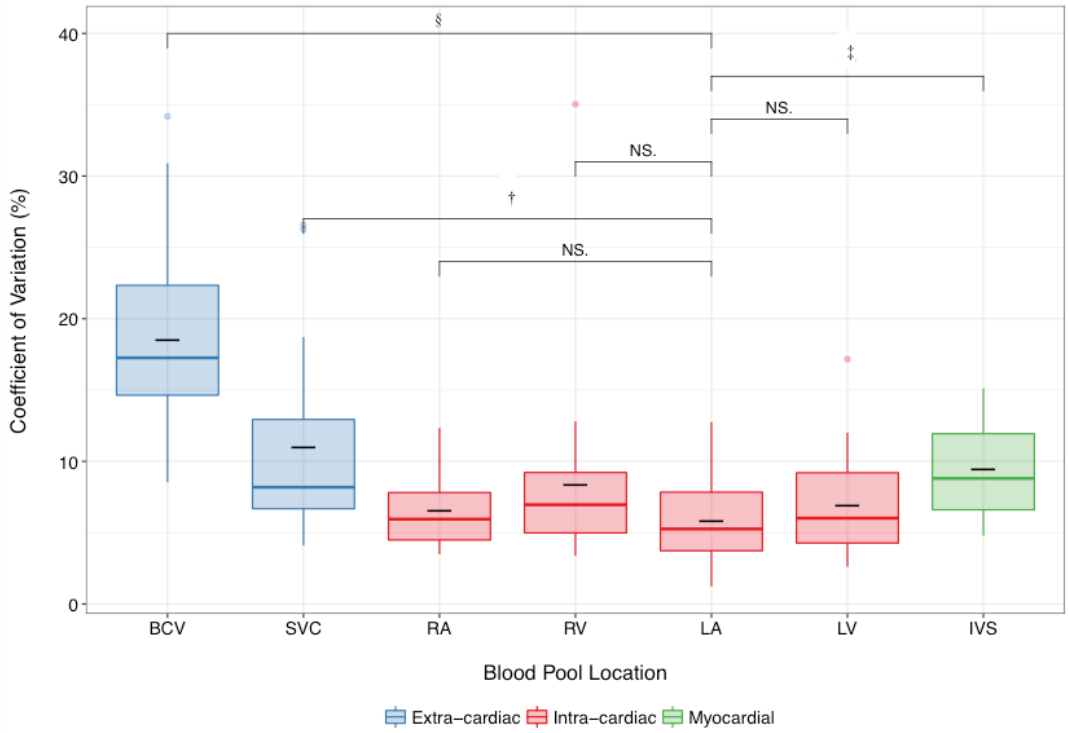

Figure 4.3 Coefficients of variation of Blood Pool and Cardiac 18F-Fluoride Activity.

The mean standardised uptake value (SUV_{MEAN}) (g/mL) in each region was compared by three observers across two scans. (**A**) Box-plot of the median and the interquartile range of coefficients of variation for each region (black line, mean). There was no difference in the coefficients of variation of 18F-fluoride SUV_{MEAN} within intra-cardiac chambers (red), but there were increased coefficients of variation using systemic venous blood pool measurement ($p<0.001$) and interventricular septal myocardium ($p<0.001$) compared with measurement of SUV_{MEAN} 18F-fluoride activity in the left atrium.

BCV, brachiocephalic vein, IVS, interventricular septum, LA, left atrium, LV, left ventricle, RA, right atrium, RV, right ventricle, SVC, superior vena cava.
NS, non-significant; *, $p\leq0.05$, †, $p\leq0.01$, ‡, $p\leq0.001$, §, $p\leq0.0001$.

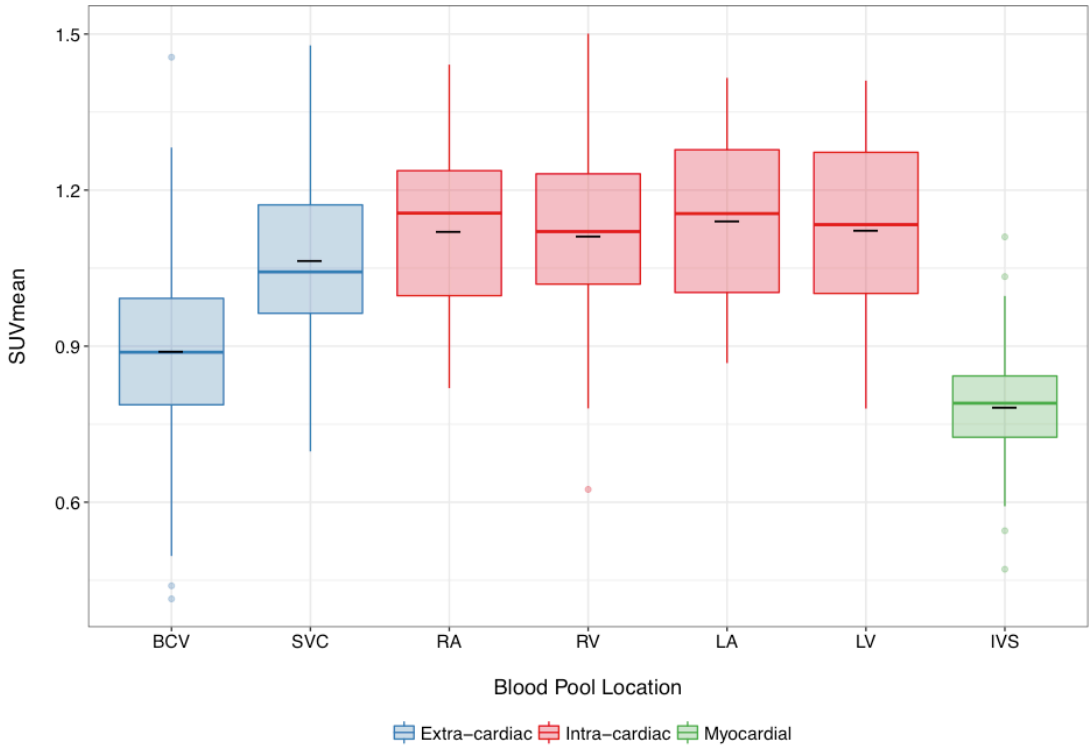

Figure 4.4 Background cardiac 18F-fluoride activity.

The mean standardised uptake value SUV_{MEAN} (g/mL) in each location in all patients with coronary artery disease. The horizontal bar inside each box is the median, the lower and upper hinges correspond to the first and third quartiles (the 25th and 75th percentiles). The upper and lower whiskers extend from the hinge to the largest or smallest value no further than 1.5 times the interquartile range from the hinge. The short black horizontal line corresponds to the mean value.
BCV, brachiocephalic vein, IVS, interventricular septum, LA, left atrium, LV, left ventricle, RA, right atrium, RV, right ventricle, SVC, superior vena cava.

	BLOOD POOL SUV_{MEAN}			
LOCATION		DIFFERENCE		
	OVERALL MEAN	MEAN	SD	95% LIMITS OF AGREEMENT
(A)				
BRACHIOCEPHALIC VEIN	0.903	-0.08	0.16	-0.394 to 0.233
INTERVENTRICULAR SEPTUM	0.771	0.028	0.052	-0.074 to 0.131
LEFT ATRIUM	1.159	-0.018	0.043	-0.103 to 0.067
LEFT VENTRICLE	1.142	-0.016	0.064	-0.142 to 0.110
RIGHT ATRIUM	1.13	-0.009	0.053	-0.112 to 0.095
RIGHT VENTRICLE	1.124	-0.019	0.051	-0.118 to 0.080
SUPERIOR VENA CAVA	1.084	-0.013	0.174	-0.355 to 0.328
(B)				
BRACHIOCEPHALIC VEIN	0.863	-0.056	0.188	-0.423 to 0.312
INTERVENTRICULAR SEPTUM	0.785	-0.038	0.098	-0.229 to 0.154
LEFT ATRIUM	1.15	-0.024	0.114	-0.248 to 0.200
LEFT VENTRICLE	1.134	-0.048	0.119	-0.282 to 0.185
RIGHT ATRIUM	1.126	-0.029	0.131	-0.286 to 0.227
RIGHT VENTRICLE	1.114	-0.022	0.134	-0.284 to 0.240
SUPERIOR VENA CAVA	1.078	-0.049	0.17	-0.382 to 0.285

Table 4.2 Bland-Altman analysis of background 18F-fluoride cardiac activity.

Between observer (A) and between scan (B) reproducibility.

4.4.2 Identification of Coronary 18F-Fluoride Uptake

Low myocardial 18F-fluoride uptake enabled visual separation between areas of focal 18F-fluoride binding in the coronary arteries and background blood pool activity in the cardiac chambers. After accurate co-registration, these factors facilitated the identification of radiotracer originating from the coronary arteries even at levels of intensity similar to background blood pool activity that would otherwise not be discernible (***Figure 4.5***). Using this method, focal coronary 18F-fluoride activity of variable intensity could be visually identified in all culprit plaques (n=10) in patients with recent type 1 myocardial infarction.

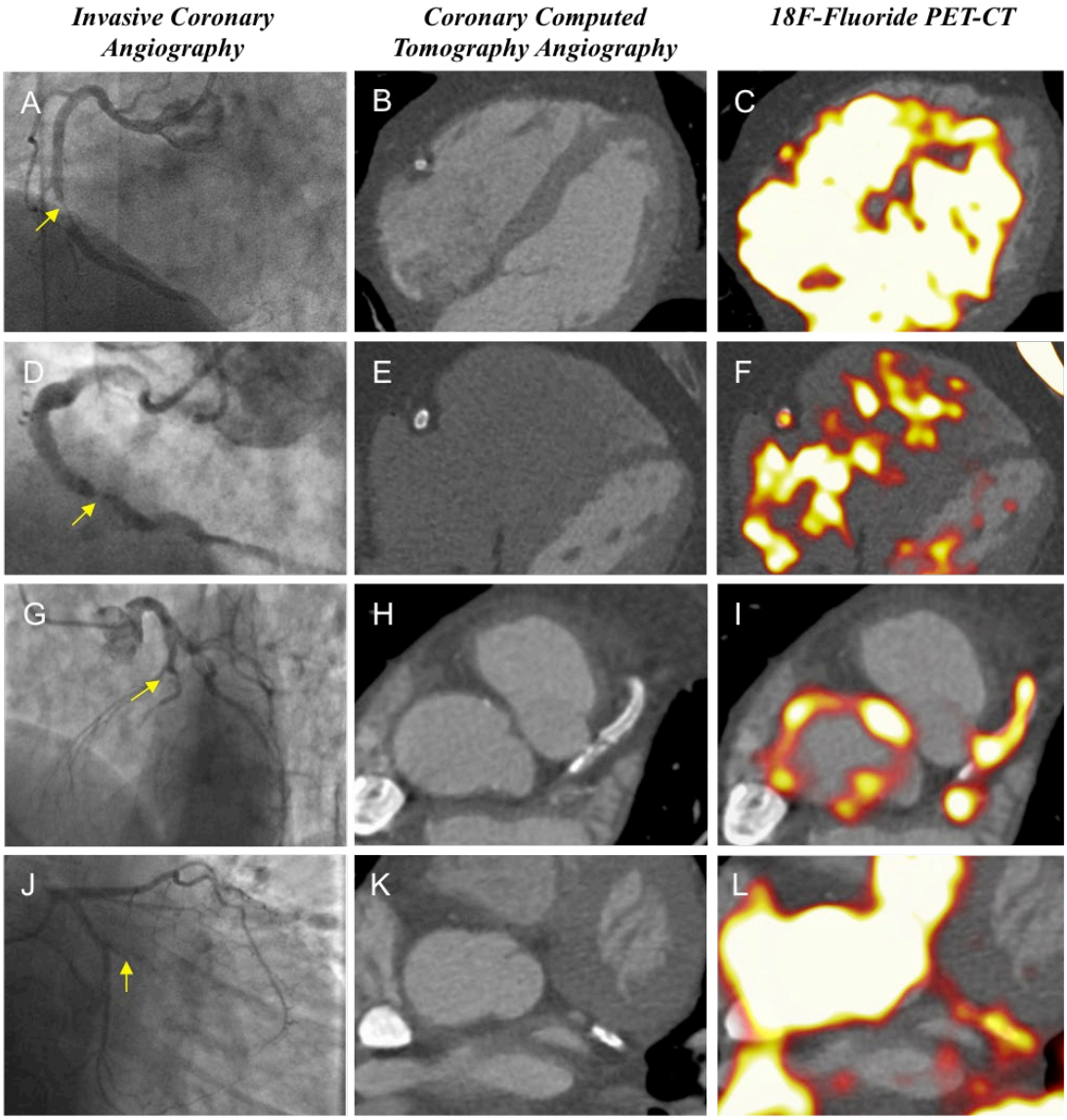

Figure 4.5 Culprit plaque 18F-fluoride activity on positron emission tomography-coronary computed tomography angiography.

Following acute myocardial infarction, culprit plaque 18F-fluoride activity can be measured in the right coronary artery (A-F), left anterior descending artery (G-I) and atrioventricular circumflex artery (J-L).

4.4.3 Quantification of Coronary 18F-Fluoride Uptake

Quantification of coronary 18F-fluoride activity within the plaque of interest, standardised according to a proximal non-diseased coronary artery segment ($TBR_{REFERENT}$) demonstrated a high degree of variability on repeated measurements. The coefficients of variation reduced in a stepwise manner when using the brachiocephalic vein and superior vena cava as the sites of measurement for blood pool activity and were lowest for target to background ratios determined after standardisation for intracardiac blood pool activity using either the left or right atria ($p<0.05$ for all comparisons, ***Figure 4.6***). Therefore, subsequent analyses used TBR_{MAX} values standardized according to the atrial blood pool, with 18F-fluoride originating in the coronary arteries categorised into levels below (TBR_{MAX} <0.9), similar to (TBR_{MAX} 0.9-1.1) and above (TBR_{MAX} >1.1) atrial blood pool activity (***Figure 4.7***).

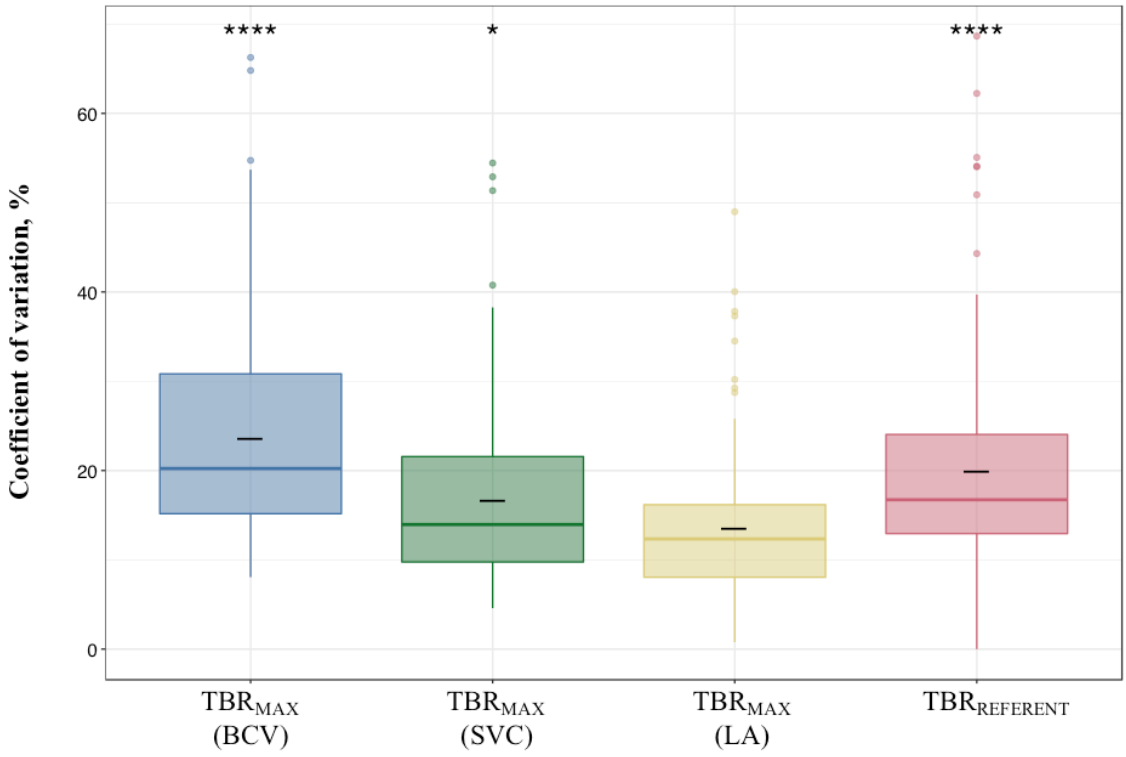

Figure 4.6 Coefficients of variation of different measures of coronary 18F-fluoride activity.

Variation of coronary 18F-fluoride measurements using different anatomical sites for measurement of background tracer activity.
Paired t-tests used compared with TBR_{MAX} (LA): *, p≤0.05, ****, p ≤0.0001.
TBR, target-to-background ratio; BCV, brachiocephalic vein; SVC, superior vena cava; LA, left atrium.

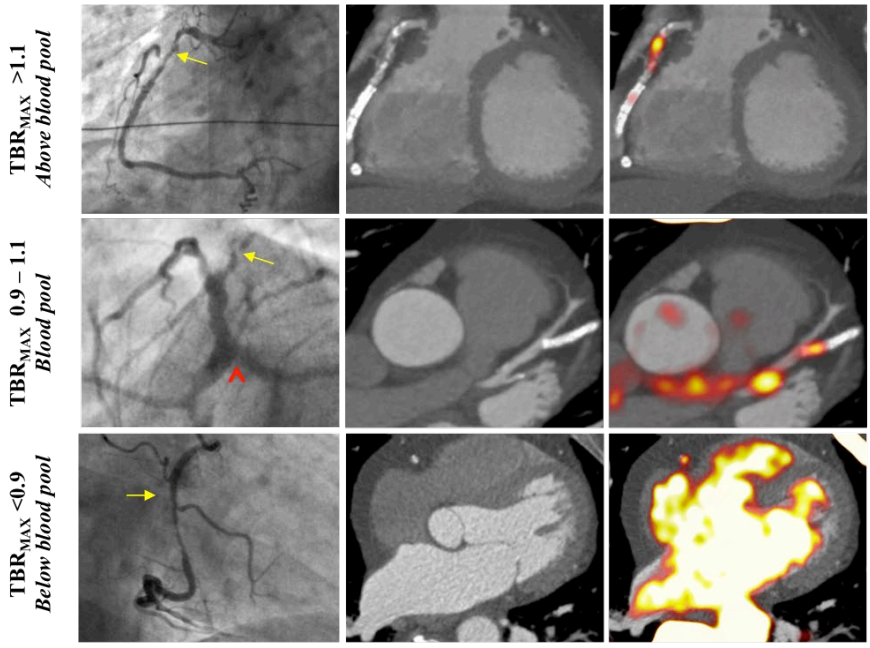

	Ruptured plaque n=10	**Stable plaque n=530**
18F-fluoride Visual Uptake n, (%)	10 (100)	73 (13.8%)
Absent 18F-fluoride visual uptake n, (%)	0	457 (86.2)
Coronary 18F-fluoride intensity in positive plaques		
TBR$_{MAX}$ >1.1 n, (%)	2 (20.0)	57 (78.1)
TBR$_{MAX}$ 0.9-1.1 n, (%)	5 (50.0)	11 (15.1)
TBR$_{MAX}$ <0.9 n, (%)	3 (30.0)	5 (6.8)

Figure 4.7 Quantification of coronary 18F-fluoride activity.

Visual identification of coronary 18F-fluoride activity was present in all ruptured plaques and 13.8% of stable coronary segments. The signal intensity of 18F-fluoride activity in coronary plaque was assessed both visually and semi-quantitatively by referencing to atrial blood pool activity (maximum target-to-background ratio [TBR$_{MAX}$]). Activity in coronary plaques was categorised into activity above blood pool (TBR$_{MAX}$ >1.1), at or around blood pool (TBR$_{MAX}$ 0.9-1.1), or below blood pool (TBR$_{MAX}$ <0.9). Higher intensity signals were observed in stable segments compared with ruptured plaques.

4.4.4 Categorisation of Coronary 18F-Fluoride Uptake

Using atrial blood pool as a point of reference allowed comparison of coronary 18F-fluoride TBR_{MAX} between patients with recent acute coronary syndromes and stable coronary artery disease. At the patient level, there were 3.7±1.8 positive plaques in patients with recent acute coronary syndrome compared with 2.4±2.3 positive plaques in patients with stable disease. Amongst patients with recent myocardial infarction, 100% (n=10/10) of culprit plaque segments met the criteria for visual uptake compared with 13.7% (n=73/530) of all segments not associated with plaque rupture. Visual assessment of coronary segment positivity achieved good inter-observer reliability (κ = 0.66, 95% confidence interval 0.63 to 0.70). Minor discrepancies between reporters occurred in regions adjacent to high background activity including the right atrial blood pool, pulmonary artery and mitral valve annulus that limited assessment in regions of the right, left anterior descending artery and atrioventricular circumflex arteries respectively. Agreement increased amongst coronary segments with higher TBR_{MAX} values and the application of a semi-quantitative method of determining 18F-fluoride positivity, requiring both visual evidence of tracer localization to a coronary region of interest and TBR_{MAX} above the pre-specified intensity thresholds achieved good scan-rescan agreement at both pre-defined cut points (TBR_{MAX} >0.9, κ = 0.72, 95% confidence interval 0.67 to 0.77; TBR_{MAX} >1.1 κ = 0.77, 95% confidence interval 0.71 to 0.83; ***Figure 4.7, Figure 4.8***). When applied to patients with recent myocardial infarction, the use of TBR_{MAX} thresholds resulted in fewer culprit plaques being classified as positive for focal 18F-fluoride uptake (n=7/10 (70%) at TBR_{MAX} ≥0.9; n=2/10 (20%) at TBR_{MAX} >1.1).

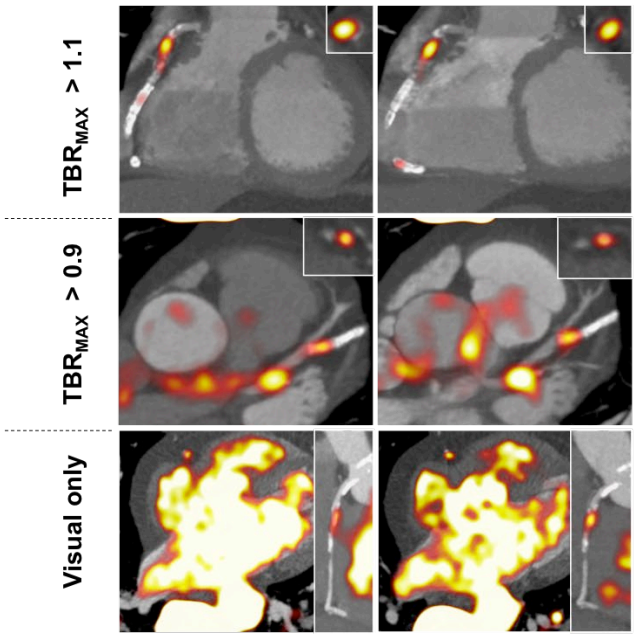

ACS	Scan 1 +	Scan 1 -
Scan 2 +	17	1
Scan 2 -	2	36

Stable CAD	Scan 1 +	Scan 1 -
Scan 2 +	37	4
Scan 2 -	3	71

ACS	Scan 1 +	Scan 1 -
Scan 2 +	27	2
Scan 2 -	5	22

Stable CAD	Scan 1 +	Scan 1 -
Scan 2 +	41	4
Scan 2 -	1	69

ACS	Scan 1 +	Scan 1 -
Scan 2 +	34	0
Scan 2 -	5	17

Stable CAD	Scan 1 +	Scan 1 -
Scan 2 +	42	6
Scan 2 -	2	65

Figure 4.8 Scan-rescan repeatability of coronary 18F-fluoride uptake.

Examples of repeated 18F-fluoride positron emission tomography and computed tomography scans across different thresholds of uptake. There were high levels of agreement between scans using a TBR_{MAX} >0.9 (93.0%, TBR_{MAX} >0.9, 94.2%, TBR_{MAX} >1.1).

4.4.5 Reproducibility of Coronary 18F-Fluoride Uptake

There were no differences in scan variables between the serial scans (***Table 4.3***). Patients with stable coronary artery disease had an increased dose-length product than patients with recent myocardial infarction due to the wider field of view on coronary CT angiography required for assessing the origin of the left internal mammary artery in cases of previous coronary artery bypass grafting. In all measured coronary segments (n=519), there was a mean bias of -0.03 between observers (95% limits of agreement -0.39 to 0.33) and a mean bias of 0.04 between scans (95% limits of agreement -0.41 to 0.49) (***Table 4.4, Figure 4.9***). In visually positive plaques, mixed effects biases were low between observers (mean bias -0.01, 95% limits of agreement -0.32 to 0.30) and between scans (mean bias 0.06, 95% limits of agreement -0.49 to 0.61). (***Table 4.4***) There was very good concordance between observers (concordance correlation coefficient 0.88, 95% confidence interval 0.85 to 0.90) and between scans (concordance correlation coefficient 0.86, 95% confidence interval 0.83 to 0.89). At the level of the patient, there was 100% agreement between the repeat scans on whether a patient demonstrated any increased coronary 18F-fluoride activity in at least one plaque. At the per-segment level, there was excellent agreement (92.4%) between scans using the visual assessment alone, although further improvements in agreement were achieved by applying the TBR_{MAX} thresholds (93.0% agreement rate TBR_{MAX} ≥0.9; 94.2% agreement rate TBR_{MAX} >1.1) (***Figure 4.8***).

(A)	SCAN 1	SCAN 2
NUMBER	10	10
HEART RATE, /MIN	63.7±9.1	59.6±9.9
DOSE LENGTH PRODUCT, MGY	278±103	336±112
18F-FLUORIDE DOSE, MBQ	242±9	239±9
TRACER ADMINISTRATION TO SCAN, MIN	61±4	62±3

(B)	SCAN 1	SCAN 2
NUMBER	20	20
HEART RATE, /MIN	56.8±8.0	57.3±10.3
DOSE LENGTH PRODUCT, MGY	448±259	394±226
18F-FLUORIDE DOSE, MBQ	249±9	248±9
TRACER ADMINISTRATION TO SCAN, MIN	66±7	66±10

Table 4.3 Scanning variables in patients with myocardial infarction and stable coronary artery disease.

Patient with myocardial infarction (A) and stable coronary artery disease (B).
Values are mean ± standard deviation.

	All segments	Visually Positive Plaques
Between scan CCC	CCC 0.88, 95% CI 0.87 to 0.90	CCC 0.86, 95% CI 0.83 to 0.89
Between observer CCC	CCC 0.89, 95% CI 0.87 to 0.90	CCC 0.88, 95% CI 0.85 to 0.90
Between scan Kappa VU	CCC 0.69, 95% CI 0.65 to 0.72	
Between observer kappa VU	CCC 0.66, 95% CI 0.63 to 0.70	
Between scan Limits of Agreement	Mean bias 0.04, 95% Limits of Agreement are from -0.41 to 0.50. Between segment SD 0.12, Between patient SD 0.12, Residual SD 0.15	Mean bias 0.06, 95% Limits of Agreement are from -0.49 to 0.61. Between segment SD 0.16, Between patient SD 0.18, Residual SD 0.15
Between observer Limits of Agreement	Mean bias -0.027, 95% Limits of Agreement are from -0.386 to 0.332, Between segment SD 0.065, Between patient SD 0.030, Residual SD 0.169	Mean bias -0.0068, 95% Limits of Agreement are from -0.316 to 0.303. Between segment SD 0.040, Between patient SD 0.023, Residual SD 0.151

Table 4.4 Mixed effects limits of agreement analysis.

Between scans and observers for all segments and visually positive plaques. CCC, concordance correlation coefficient, CI confidence interval, SD standard deviation.

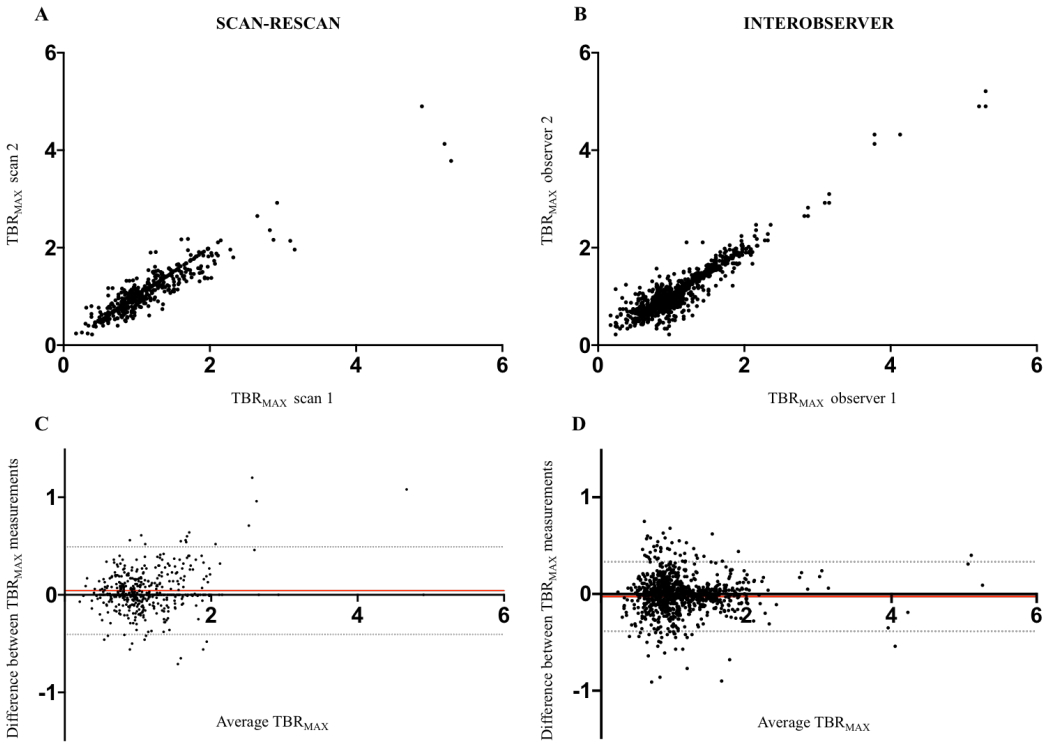

Figure 4.9 Bland-Altman plots of coronary 18F-fluoride activity.

Correlation and Bland-Altman plots for scan-rescan reproducibility for coronary plaques at different levels of coronary 18F-fluoride activity (TBR_{MAX}) (A, C respectively). Correlation and Bland-Altman plots for interobserver reproducibility between two observers at different levels of 18F-fluoride activity (TBR_{MAX}) (B, D respectively). The shaded circles represent individual observations whilst the red and grey hatched lines represent the mean difference and 95% mixed effects limits of agreement respectively.

4.5 Discussion

This study describes an optimised methodology for assessing coronary 18F-fluoride activity *in vivo*. Using this approach there is good agreement in the identification of plaques with increased coronary 18F-fluoride uptake between observers and on different scans. The tissue (SUV_{MAX}) to background (left atrial SUV_{MEAN}) ratio (TBR_{MAX}) has a low bias between observers and between scans. At TBR_{MAX} thresholds >0.9, there is low sampling variability and high interobserver agreement in the adjudication of coronary 18F-fluoride activity. 18F-Fluoride demonstrates optimal characteristics for coronary plaque molecular imaging, namely, low myocardial and background coronary artery activity, which allows regions of increased coronary 18F-fluoride uptake to be more readily detected at low levels of intensity. This technique has direct application to ongoing clinical trials using the identification of atherosclerotic plaque mineralisation to predict coronary events and improve the stratification of emerging therapeutic interventions (NCT02278211 and NCT02110303).

This study has a number of notable strengths. First, it is the largest prospective study to investigate the scan-rescan reproducibility of coronary imaging with repeated 18F-fluoride PET-CT scans. Second, the study population comprising thirty patients with established, multi-vessel coronary disease represents a high-risk cohort for whom imaging biomarkers have genuine potential to improve prognostic stratification and guide therapeutic interventions. Third, it directly compared several proposed methods for quantifying focal tracer activity within coronary atherosclerotic lesions and determined the interobserver and scan-rescan agreement for these metrics. Lastly, it derived a standardized semi-quantitative approach to image analysis that allows consistency in the reporting of diagnostic findings.

For an imaging biomarker to have clinical utility, it should demonstrate precise and reproducible analytical performance (Vasan, 2006). Specifically, *precision* refers to the closeness of agreement between independent observations under stipulated conditions (free from random error) and *reproducibility* reflects to the differences observed over separate scan acquisitions. The methodology of coronary 18F-fluoride assessment presented here has been optimised to define a precise measure of background activity (cardiac atria) that yields a precise measure of coronary activity (TBR_{MAX}) across serial scan acquisitions. Demonstrating the reliability of this metric is an important step towards implementing coronary PET imaging in clinical practice and prospective research trials. Future studies should apply similar acquisition and image analysis protocols to that described here, and continue to explore the clinical significance of such measurements.

To discriminate 18F-fluoride uptake from levels of background signal, focal coronary artery activity has previously been referenced to proximal non-diseased coronary artery segments ($TBR_{REFERENT}$) (Dweck, Chow et al. 2012, Joshi, Vesey et al. 2014). Although this practice differs from non-coronary 18F-fluoride PET imaging, it has been considered more appropriate to reference to a similar sized structure rather than a large blood pool region to avoid artificially low TBR values related to partial volume effects. However, this metric was found to have a high degree of variability on serial testing, due to inconsistency in measurements in the referent plaque. This likely reflects the inherent difficulty in reproducibly measuring a coronary segment without visual 18F-fluoride activity compared with the much easier agreement between observers when drawing a region of interest around a focal site of tracer uptake. Of note, this study identified 18F-fluoride activity within distal and

sidebranch vessels that may be more susceptible to partial volume averaging effects. In these regions, activity may 'spill out' into surrounding structures, thereby decreasing counts in plaques which would otherwise have increased activity. Similarly, coronary segments in close proximity to calcified tissue in the aortic and mitral annulus may be subjected to 'spill-in' of 18F-fluoride activity in regions that would otherwise have low activity. These small changes in localisation of maximal activity explain the variation observed when measuring structures below the field-width half maximum of 18F-fluoride (6mm). Future work using an increased delay between injection and acquisition (Kwiecinksi, Berman et al. 2019), optimising the reconstruction algorithm and motion-correcting the list mode data (Doris, Otaki et al. 2018) may improve quantitative reproducibility. Thus, quantification of activity should only be undertaken in plaques that meet the visual criteria stipulated in the methodology.

This optimised methodology for estimating background blood pool activity also differs from previous 18F-FDG cardiovascular PET studies. In 18F-FDG studies, background blood pool activity was measured within the large venous capacitance vessels, such as the superior vena cava (Rudd, Myers et al. 2007, Tarkin, Joshi et al. 2017). This is preferred over measurements from within the cardiac chambers because 18F-FDG is taken up by viable myocardium and blood pool activity can be contaminated by signal over spill from the myocardium. In contrast, there is very low myocardial uptake of 18F-fluoride and thus estimating atrial blood pool activity is not susceptible to this confounding issue. The superior vena cava can be a relatively small compressed structure sensitive to sampling error and partial volume effects whereas the atria present larger spherical volumes of activity that can be more readily and reliably sampled, providing a measurement with higher precision and

reproducibility. Thus for tracers with a low background myocardial uptake, background blood pool activity would appear to be best measured in the cardiac atria. Consequently, although standardisation of coronary activity with reference to the atrial blood pool (TBR_{MAX}) resulted in numerically lower values than when standardised according to either a referent coronary segment or an extracardiac blood pool, the coefficients of variation were much reduced. Indeed, because the referent plaque uptake is lower (0.7-0.8 of that in the atrial blood pool), the previous TBR_{MAX} threshold of 1.25 equates to a TBR_{MAX} threshold 0.9-1.0 when using the atrial blood pool activity. This finding has important implications for future studies that seek to measure change in tracer signal over serial scans, either to explore the natural history of plaque vulnerability or in order to use this metric as a surrogate for therapeutic response.

Whilst quantitative measurements of 18F-fluoride activity have particular relevance to serial imaging studies, it is not clear that the numeric value of the TBR_{MAX} has direct correlation with plaque vulnerability. Indeed, this study found that amongst patients with acute myocardial infarction, the culprit plaques demonstrated proportionally lower TBR_{MAX} values than visually positive plaques in patients with clinically stable disease. Although somewhat counterintuitive, this finding is consistent with previous observations (Joshi, Vesey et al. 2014) and the relationship between TBR_{MAX} and risk of future clinical events remains to be determined in large-scale prospective trials, such as the PRE^{18}FFIR trial (NCT02278211). It should be remembered that 18F-fluoride uptake correlates with microcalcification and is a marker of calcification activity (Joshi, Vesey et al. 2014). While it identifies high-risk plaque with a necrotic core, the magnitude of uptake may reflect different stages of the calcification process and it may be the presence rather than the magnitude of

uptake that is most important. For example, high 18F-fluoride uptake may represent advanced calcification activity with rapidly developing macrocalcification which is stabilising the plaque and making it less prone to rupture. Conversely, relatively lower levels of 18F-fluoride uptake may represent the immediate response to a recently developed unstable plaque with a necrotic core that has yet to develop demonstrable macrocalcification and has only nascent calcification activity.

This study has demonstrated good reliability for visual assessment alone in the identification of culprit plaques following recent acute coronary syndrome. Perhaps unsurprisingly, the inter-observer and scan-rescan agreement for the classification of 18F-fluoride positivity within a coronary segment increased inline with the TBR_{MAX} and was greatest for coronary segments with maximum standardized uptake values >1.1 times the blood pool SUV_{MEAN}. In this regard, a recent cohort study has demonstrated that coronary TBR_{MAX} ≥1.28 stratified individuals at increased risk of plaque rupture (Kitagawa, Yamamoto et al. 2018). Whilst this higher patient-level threshold identified individuals at risk of late coronary revascularisation, at the plaque-level 45% of culprit plaques (n=5/11) did not meet this threshold (Kitagawa, Yamamoto et al. 2018). This observation is in keeping with the finding that culprit plaque 18F-fluoride activity, whilst readily identifiable, is often at a lower intensity than blood pool which future studies may need to account for. The identification of low intensity 18F-fluoride activity needs to be prospectively evaluated in future studies of repeated imaging following an acute coronary syndrome.

4.5.1 Limitations

This study has a number of limitations. It was undertaken in a single centre with extensive experience in cardiac 18F-fluoride PET-CCTA imaging and scans were

performed using a single PET-CCTA scanning system. It is important to acknowledge that many operator and system-dependent variables can influence final image quality and these will necessitate careful consideration when applying our findings in different settings. A number of limitations of our study are inherent to coronary PET imaging, and include the challenges of non-specific binding, cardiac motion, partial voluming and relatively low signal-to-noise ratios. We chose to use 18F-fluoride as our PET tracer as there is low physiological activity within the myocardium reducing the chance for 'spill-in' activity. Furthermore, data from our group have previously established that the problem of cardiac motion can be overcome through ECG-gating in a similar manner to that employed in coronary computed tomography angiography (Pawade, Cartlidge et al. 2016). Although restricting the analysis of the PET signal to one quarter of the cardiac cycle reduces the signal-to-noise ratio, this can be compensated for by increasing tracer dose, increasing scan duration, and applying advanced image reconstruction algorithms including time-of-flight reconstruction with point spread function modelling. In combining these incremental gains, this study has derived a semi-quantitative measure of plaque pathophysiology that is highly reproducible on interval scanning and is well placed for observing dynamic changes in activity over time.

4.6 Conclusion

In conclusion, 18F-fluoride PET-CCTA imaging is highly reproducible over repeated scans and between multiple observers. A semi-quantitative approach achieves repeatable metrics than can now be assessed to determine their clinical significance. This approach to image acquisition and analysis provides strong support for the ongoing clinical studies investigating the value of 18F-fluoride PET-CCTA to inform cardiovascular prognostic assessment and guide novel therapeutic strategies.

CHAPTER 5

Ex vivo 18F-fluoride uptake in human coronary atherosclerosis

5.1 Summary

Objectives

18F-Fluoride positron emission tomography is a sensitive imaging biomarker that identifies microcalcification in atherosclerotic plaque. Coronary plaques with early microcalcification have an increased propensity to rupture and are associated with acute myocardial infarction. The objective of this study was to characterise and define 18F-fluoride uptake in human coronary atherosclerotic plaques.

Methods

Fresh frozen post-mortem human specimens of left coronary artery were imaged using 18F-fluoride micro-positron emission tomography-computed tomography prior to fixation in 10% buffered formalin. Histology, fluorescein-bisphosphonate immunofluorescence and Raman spectroscopy were performed to identify specific regions of hydroxyapatite deposition. Immunohistochemical analysis was undertaken in regions of high 18F-fluoride uptake using markers of tissue mineralisation.

Results

Compared with low levels of non-specific binding in the myocardium, 18F-fluoride demonstrated a high signal to noise ratio in both calcified (median 149.8, interquartile range [IQR] 85.3 to 207.3 kBq/mL) and non-calcified (median 158.1, IQR 121.79 to 234.8 kBq/mL) coronary atherosclerotic plaque. High intensity 18F-fluoride (157 kBq/mL) had a Raman signal at 963 cm^{-1} corresponding to hydroxyapatite. Areas of enhanced osteopontin and Runt-related transcription factor 2 staining were associated with increased coronary 18F-fluoride uptake (increases

of 50.5 [95% confidence interval 28.1 to 72.9] kBq/mL ($p<0.0001$) and 37.2 [95% confidence interval 12.6 to 61.8] kBq/mL ($p=0.0043$) respectively).

Conclusions

18F-Fluoride uptake in human coronary atherosclerosis identifies early microcalcification in the form of hydroxyapatite. Coronary plaques with high 18F-fluoride uptake are associated characteristic histologic markers of active mineralisation and atherosclerosis.

5.2 Introduction

Coronary atherosclerosis is an inflammatory disease that results in the formation of intimal plaque with an increased propensity to rupture. Microscopic calcification is a key feature of ruptured atherosclerotic plaques and the identification of coronary microcalcification is closely linked to coronary thrombotic events (Joshi, Vesey et al. 2014). However, the *in vivo* mechanisms governing the accumulation of early microscopic calcification within the coronary vasculature are poorly understood. Pre-clinical studies have proposed atherosclerotic inflammation to be an initiator of plaque calcification through the extrusion and response to calcifying extracellular vesicles (Hutcheson, Blaser et al. 2017, Hutcheson, Goettsch et al. 2016). Additionally, *in vitro* models of intimal plaque microcalcification have demonstrated that spherical or ellipsoidal micro-calcifying vesicles aggregate within plaques and coalesce to form larger plates of macrocalcification (Hutcheson, Goettsch et al. 2016). Whilst the transition from microcalcification to macrocalcification in the vast majority of plaques is thought to confer stability, the presence of micro-calcifying vesicles in the tunica intima has the potential to reduce the structural integrity of thin-capped fibroatheroma, resulting in plaque rupture (Kelly-Arnold, Maldonado et al. 2013, Mori, Torii et al. 2018).

Recently, studies have demonstrated that increased 18F-sodium fluoride (18F-fluoride) positron emission tomography (PET) uptake is observed in culprit plaques following myocardial infarction and in plaques with multiple adverse features in patients with stable disease (Joshi, Vesey et al. 2014, Dweck, Chow et al. 2012, Kitagawa, Yamamoto et al. 2018). 18F-Fluoride preferentially binds to exposed hydroxyl groups on the surface of nanocystalline hydroxyapatite. We have

previously demonstrated that the signal intensity of 18F-fluoride in carotid endarterectomy specimens increases as the size of the calcifications decrease, such that 18F-fluoride is an imaging biomarker of unbound microscopic calcification (Creager, Hohl et al. 2019, Irkle, Vesey et al. 2015). However, there are important differences between carotid and coronary atherosclerotic plaque progression, predominantly attributed to plaque composition. Compared with carotid plaques, vulnerable coronary plaques are more prone to rupture owing to thinner fibrous caps (<65 μm versus <200 μm) and a reduction in smooth muscle cells in the tunica media. To address these differences in pathophysiology and to fully understand the mechanisms of 18F-fluoride binding in coronary atherosclerotic plaque, direct histological examination of coronary artery tissue is warranted (Salarian, Sadeghi et al. 2019). In this study, we performed an *ex vivo* histological validation of 18F-fluoride binding to calcium derivatives and osteogenic proteins involved in human coronary atherosclerotic calcification.

5.3 Methods

5.3.1 18F-Fluoride micro-positron emission tomography computed tomography

Calcium derivative phantoms and coronary artery specimens underwent micro-positron emission tomography computed tomography followed by specimen histology and Raman spectroscopy as described in Chapter 2.

5.3.2 Statistical analysis

Categorical variables are reported as number (%) and continuous variables as mean ± standard deviation for parametric or median and interquartile range for non-parametric data. Normality was tested for using the D'Agostino and Pearson test. Continuous unpaired variables were compared using Student's T-test with Welch's correction when two samples had unequal variances and/or unequal sample sizes. Non-parametric data was compared between two categories using Mann-Witney U Test or using Kruskal-Wallis Test for multiple categories. Statistical analysis was undertaken using PRISM for OS X, version 8.1.1. (GraphPad Software, San Diego, California, USA). Statistical significance was considered as a two-sided p value <0.05.

5.4 Results

5.4.1 Selectivity of 18F-fluoride for hydroxyapatite

18F-Fluoride had favourable equilibrium kinetics (Bmax 9.8 kBq/mL, K_d 58.14 kBq) for hydroxyapatite with binding equilibrium occurring within 20 min (***Figure 5.1***). To achieve target saturation, 100 kBq of 18F-fluoride was used for subsequent *ex vivo* experiments. There was high selectivity of 18F-fluoride for hydroxyapatite in comparison with other calcium-phosphate derivatives (calcium bisphosphate, $p<0.01$; calcium pyrophosphate $p<0.001$) (***Figure 5.1***). Very low activity was observed in calcium oxalate samples incubated with 18F-fluoride ($p<0.001$).

5.4.2 Study population

Between 2016 and 2017, coronary artery samples were obtained at autopsy from 13 victims of sudden death. The majority were male (n=10, 76.9%) with a median age of 51 (range 40-71) years. Ten deaths (76.9%) were adjudicated as related to ischemic heart disease, one death was attributed to haemopericardium from thoracic aortic dissection and two deaths were related to non-cardiac causes (suffocation and alcohol toxicity) (***Table 5.1***). None of the coronary artery specimens represented culprit or ruptured plaque directly related to the sudden death.

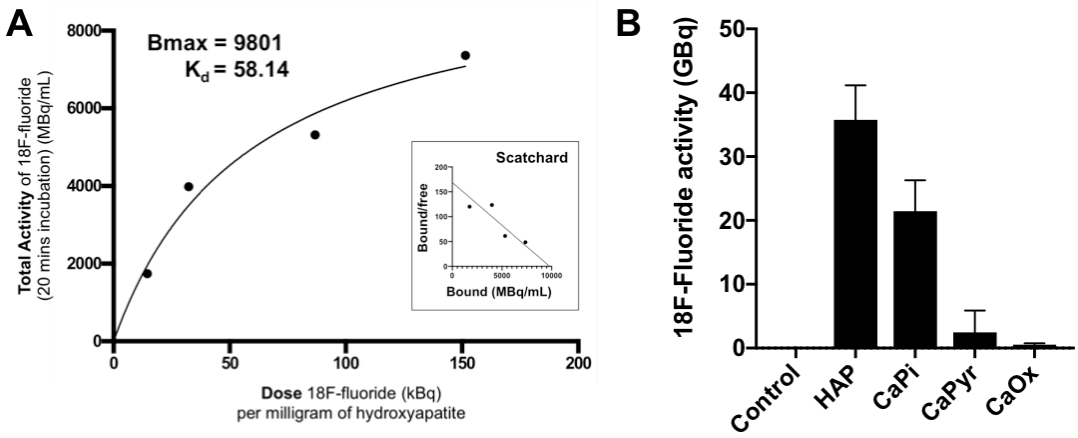

Figure 5.1 18F-Fluoride activity in calcium derivative phantoms.

(A) Total activity of 18F-fluoride (MBq/mL) following 20 min incubation in hydroxyapatite plotted against dose of 18F-fluoride (kBq) per milligram of hydroxyapatite. Scatchard plot of bound/free versus bound 18F-fluoride (inset). (B) Hydroxyapatite and other calcium-derived minerals were incubated with 18F-fluoride for 20 minutes after which unbound supernatant was removed and the solid particles were analysed by micro positron emission tomography. Data shown is from at least three replicates and shown as the mean ± standard deviation.

Coronary sample	Age	Sex	Cause of death	Plaque type - Macro-calcified/ Non-calcified (n = plaques)
1	46	M	Ischaemic heart disease	Macro-calcified (6)
2	57	M	Ischaemic heart disease	Macro-calcified (2)
3	49	M	Ischaemic heart disease	Macro-calcified (1)
4	49	F	*Complications of alcohol toxicity*	Non-calcified (1)
5	71	F	Ischaemic heart disease	Macro-calcified (4)
6	57	M	Ischaemic heart disease	Non-calcified (3)
7	69	M	Ischaemic heart disease	Non-calcified (3)
8	71	F	*Suffocation*	Macro-calcified (1)
9	51	M	Ischaemic heart disease	Non-calcified (2)
10	50	M	Thoracic aortic dissection	Macro-calcified (1)
11	67	M	Ischaemic heart disease	Macro-calcified (2)
12	48	M	Ischaemic heart disease	Macro-calcified (1)
13	40	M	Ischaemic heart disease	Non-calcified (4), Macro-calcified (1)

Table 5.1 Cause of death

5.4.3 18F-Fluoride co-localisation with hydroxyapatite

Within tissue sections from the 13 patients, 32 plaques were identified. 18F-Fluoride binding was observed in plaques both with (n=19) and without (n=13) areas of macroscopic calcification as determined on micro-CT (***Figure 5.2***). Total plaque 18F-fluoride binding (median 157.5 [IQR 103.9 to 216.9] kBq/mL) was more than 10-fold greater than non-specific binding in the surrounding myocardium (median 14.9 [IQR 9.6 to 27.4] kBq/mL, $p<0.0001$) and more than 500-fold greater than background regions (median 0.3 [IQR 0.09 to 1.3] kBq/mL, $p<0.0001$) (***Figure 5.2***). 18F-fluoride activity in coronary plaques without macroscopic calcification (median 158.1 [IQR 121.7 to 234.8] kBq/mL) was higher than plaque with macrocalcification (median 149.8 [IQR 85.3 to 207.3] kBq/mL; $p=0.0469$). Even in plaques with macrocalcification 18F-Fluoride occurred in distinct regions remote from larger macrocalcific deposits identified on micro-computed tomography (***Figure 5.3***). In these regions, 18F-fluoride colocalised with histological markers of microcalcification (von Kossa, Alizarin Red S). Moreover the microcalcification observed in areas of 18F-fluoride binding was specifically classified as hydroxyapatite using a highly selective immunofluorescence probe, Fluorescein-bisphosphonate (***Figure 5.3***).

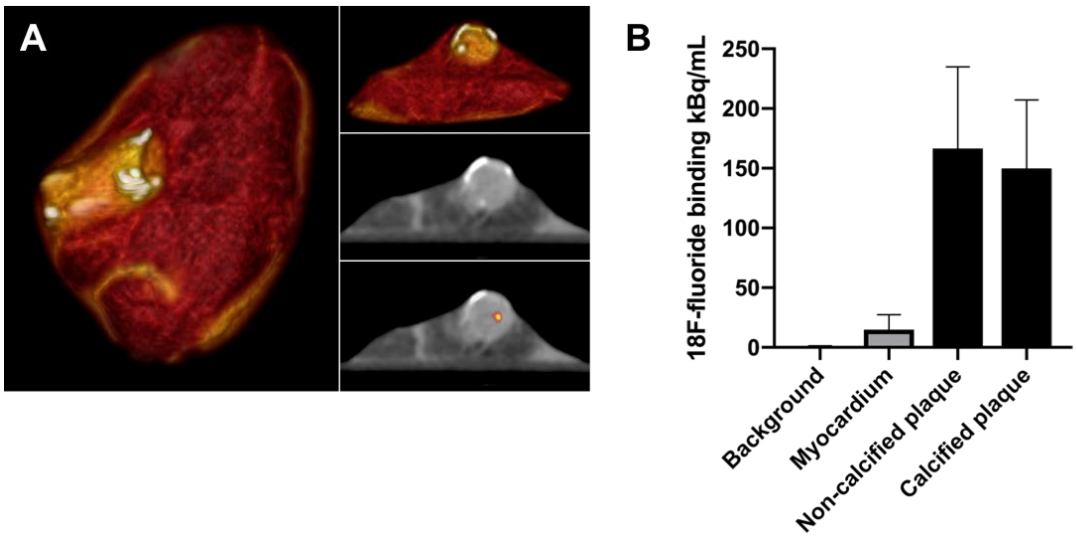

Figure 5.2 18F-Fluoride binding in ex vivo coronary artery specimens.

(A) Volume rendered images micro-positron emission tomography-computed tomography of left anterior descending artery segments were reconstructed to provide axial alignment of coronary arteries for quantitative analysis. Micro-computed tomography defined regions of myocardium, non-calcified plaque and calcification in coronary arteries with PET quantification on hybrid images. (B) Non-specific binding in the surrounding myocardium was higher than background activity (median 14.9 [interquartile range 9.6 to 27.4] versus 0.30 [interquartile range, 0.09 to 1.3] kBq/mL respectively, $p<0.0001$). Signal in coronary artery segments was 10-fold higher ($p<0.0001$) than myocardium (non-calcified plaque median 158.1 [interquartile range, 121.7 to 234.8] kBq/mL and calcified plaque median 149.8 [interquartile range, 85.3 to 207.3] kBq/mL).
CaPi, calcium bisphosphate, CaPyr, calcium pyrophosphate, CaOx, calcium oxalate, HAP, hydroxyapatite.

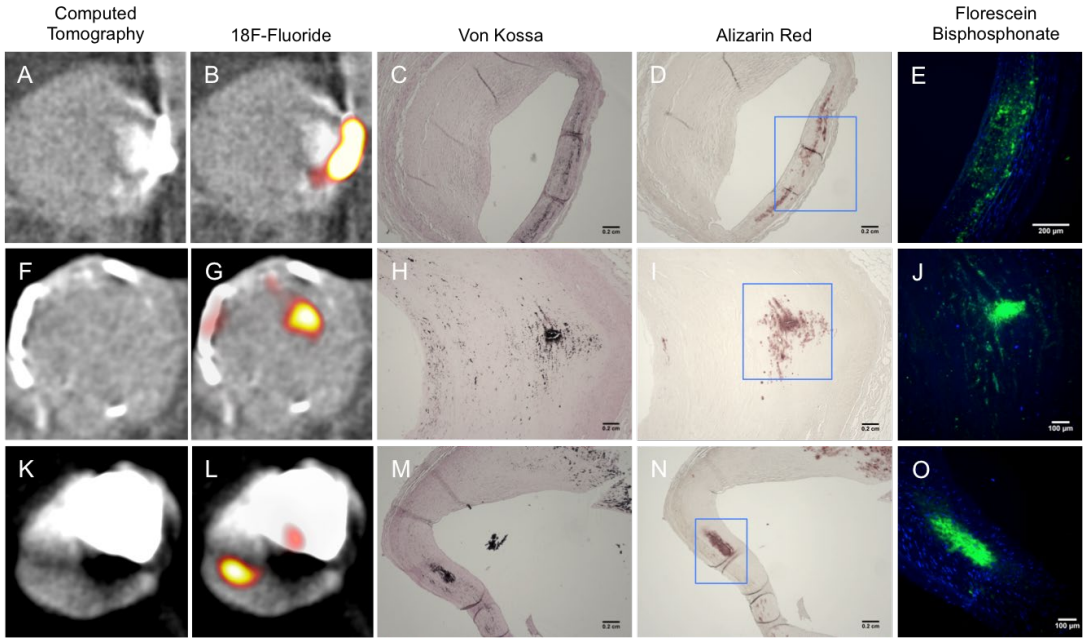

Figure 5.3 18F-Fluoride, coronary microcalcification and hydroxyapatite deposition.

Coronary artery specimens had focal (**A**), circumferential (**F**) or large regions (**K**) of macrocalcification on microcomputed tomography. 18F-Fluoride binding occurred in regions remote from macrocalcification in intimal fibroatheromatous plaque (**B, G, L**) and colocalised with histological markers of tissue mineralisation (Von Kossa, **C, H, M**), microcalcification (Alizarin Red, **D, I, M**) and a hydroxyapatite-specific bisphosphonate probe (Fluorescein-Bisphosphonate [green], **E, J, O**).

5.4.4 Raman spectroscopy and 18F-fluoride intensity

Raman spectroscopy imaging of selected regions with high and low intensity 18F-fluoride binding was performed in eight samples (***Figure 5.4***). The characteristic cell Raman signal was observed in all these samples at 1004 cm^{-1} corresponding to phenylalanine. In a control sample, no Raman signal was observed in the range between 940 and 1000 cm^{-1} (***Figure 5.4***). Samples containing microcalcification identified by high intensity 18F-fluoride (157 kBq/mL) had a Raman signal at 963 cm^{-1} corresponding to hydroxyapatite (***Figure 5.4***). In macrocalcified specimens with low 18F-fluoride intensity (30 kBq/mL), Raman signal with an asymmetrical v1 stretching band appeared at 973 cm^{-1} corresponding to whitlockite (***Figure 5.4***). As there was an asymmetrical peak to signal in these macrocalcified specimens, further analysis of the area under the whitlockite peak revealed two overlapping peaks attributable to hydroxyapatite and whitlockite at a ratio of 30:70 (***Figure 5.5***).

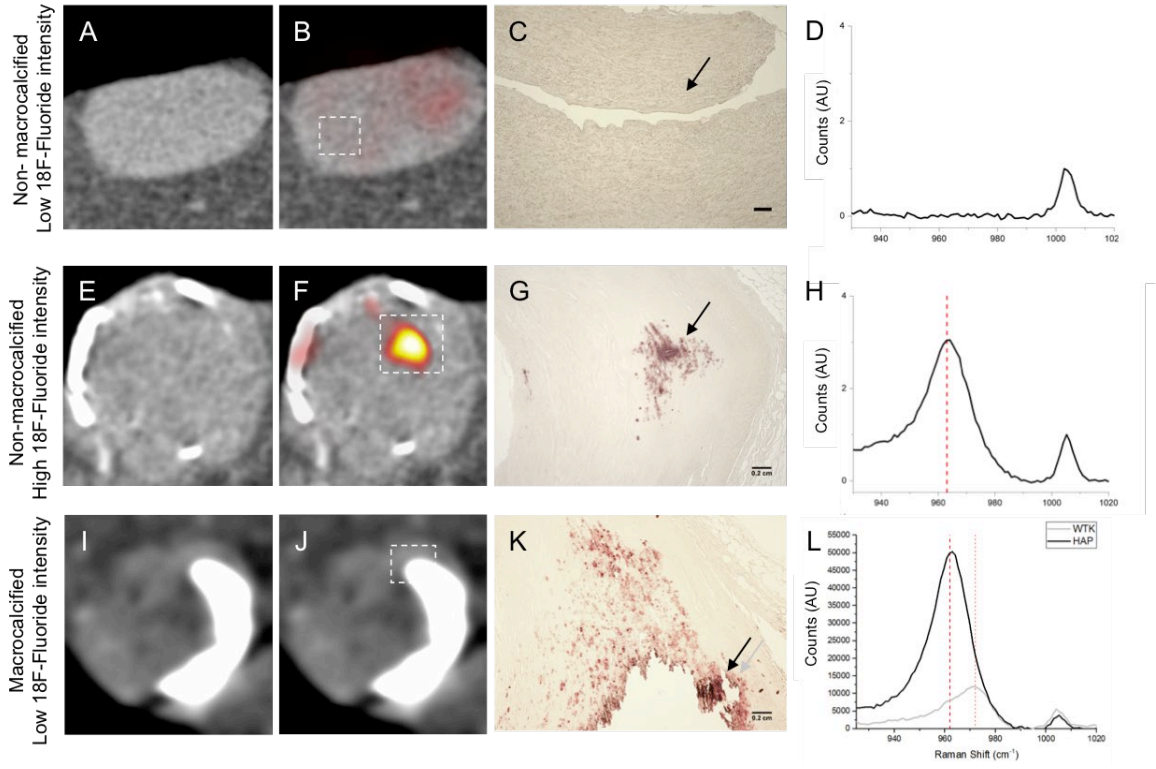

Figure 5.4 18F-Fluoride with Raman spectroscopy for hydroxyapatite and whitlockite.

Coronary artery specimens with high 18F-fluoride binding and low 18F-fluoride binding underwent Raman spectroscopy analysis to differentiate mineral composition (n=8). Non-macrocalcified specimens with low 18F-fluoride intensity (control, n=1) had a single spectra peak at 1004 cm^{-1} corresponding to phenylalanine (**A-D**). Focal regions with no macrocalcification and high 18F-fluoride intensity (n=3) had a Raman spectra peak at 963 cm^{-1}, hydroxyapatite (**E-H**). Macrocalcified regions with low 18F-fluoride intensity had a Raman spectra peaks at 975 cm^{-1}, whitlockite (**I-L**). Raman Shift: Hydroxyapatite, 963cm^{-1}, Whitlockite, 973 cm^{-1}, Phenylalanine, 1004 cm^{-1}.

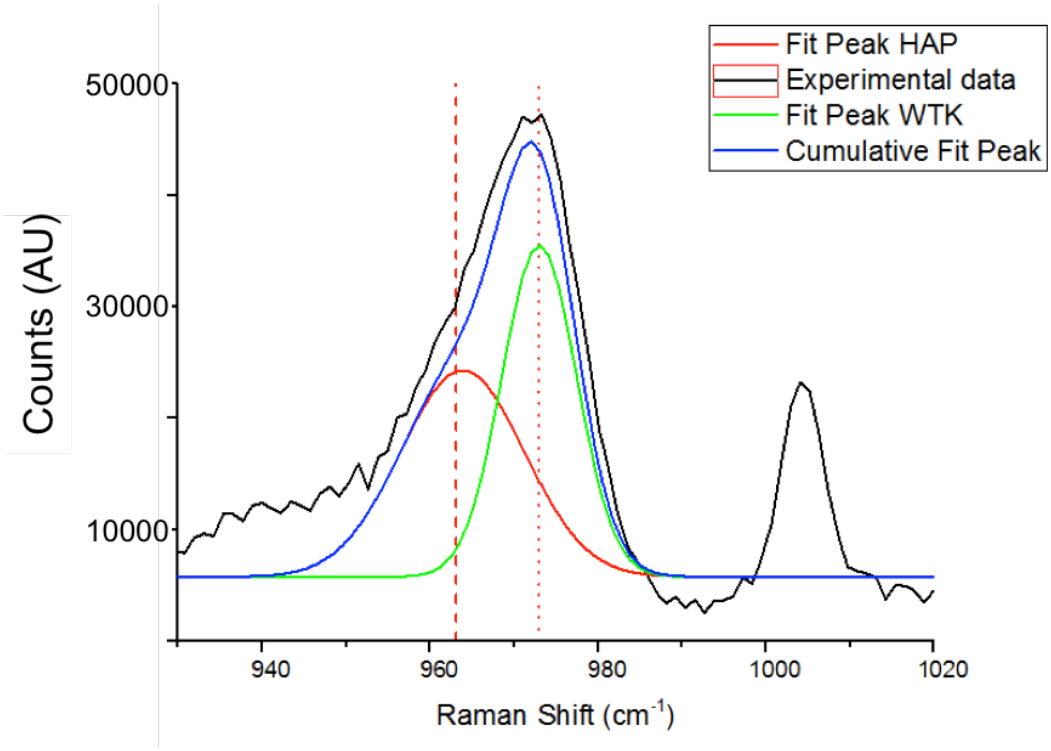

Figure 5.5 Raman spectra for macrocalcification with low 18F-fluoride intensity.

Peak fitted analysis of Raman spectra in regions with macrocalcification and low 18F-fluoride intensity. Analysis of the area under the whitlockite peak reveals the merging of two peaks corresponding to hydroxyapatite and whitlockite in a 30:70 ratio. HAP, hydroxyapatite, WTK, Whitlockite.

5.4.5 18F-Fluoride co-localisation with markers of osteogenic activity in coronary arteries

Detailed analysis of coronary artery specimens revealed that 18F-fluoride binding was predominantly observed within the tunica intima in areas of plaque formation (***Figure 5.6***). Little or no binding was observed in the tunica media. In coronary atherosclerotic plaques without macrocalcification, there was no intense staining for alkaline phosphatase (weakly positive) despite high 18F-fluoride activity (***Figure 5.6***). However, these regions of high 18F-fluoride activity co-localised with the increased expression of osteopontin (***Figure 5.6***). Osteopontin-positive plaques had higher 18F-fluoride activity compared to those without (mean 145 versus 94.5 kBq/mL respectively: difference in means 50.5 [95% confidence interval 28.1 to 72.9] kBq/mL, p<0.0001) (***Figure 5.7***). Similarly, Runt-related transcription factor 2 (Runx2) positive plaques had higher 18F-fluoride activity compared to those without (mean 139.8 versus 102.6 kBq/mL respectively; difference in means 37.2 [95% confidence interval 12.6 to 61.8] kBq/mL, p=0.0043) (***Figure 5.7)***. Staining for transforming growth factor beta 1 and caspase 3 was evident in these plaques, particularly in regions of macrocalcification. However, 18F-fluoride activity did not correlate with increased staining for transforming growth factor beta 1 (TGFβ1, p=0.1042), wingless/integrated 3a (WNT3A, p=0.8732) or caspase 3 (p=0.5476).

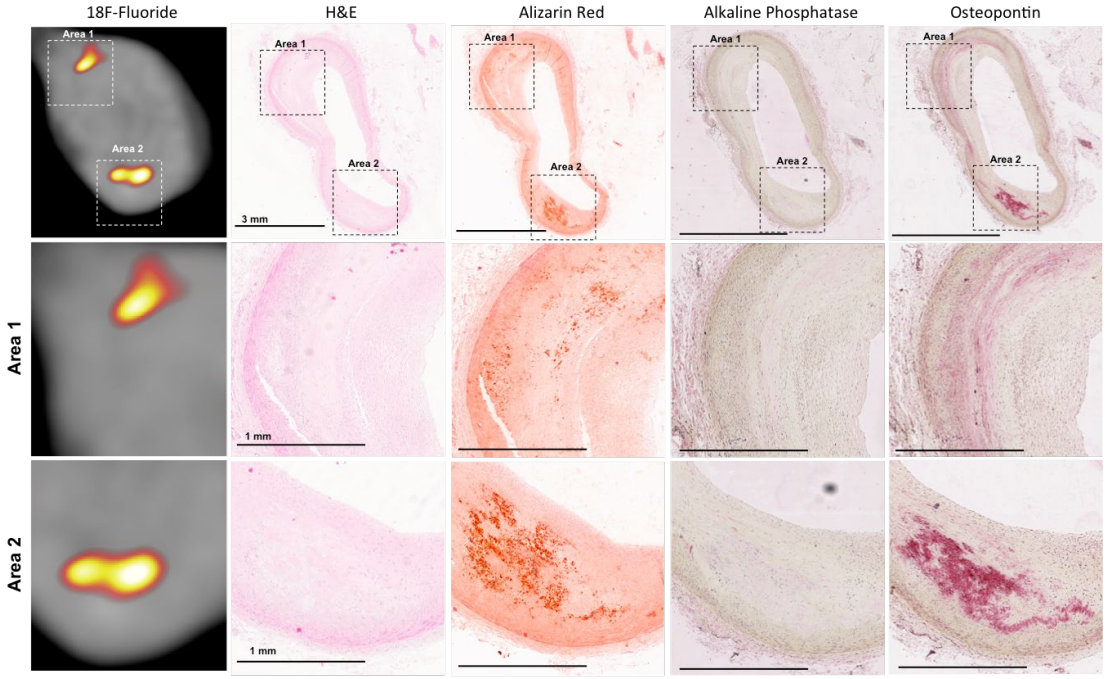

Figure 5.6 Intimal 18F-fluoride plaque intensity and markers of osteogenic activity.

Fibroatheromatous plaques had an abundance of microcalcification (Alizarin Red S) in regions of high 18F-fluoride signal. The distribution of the biomineralisation glycophosphoprotein osteopontin colocalised with microcalcification in the intimal layer.

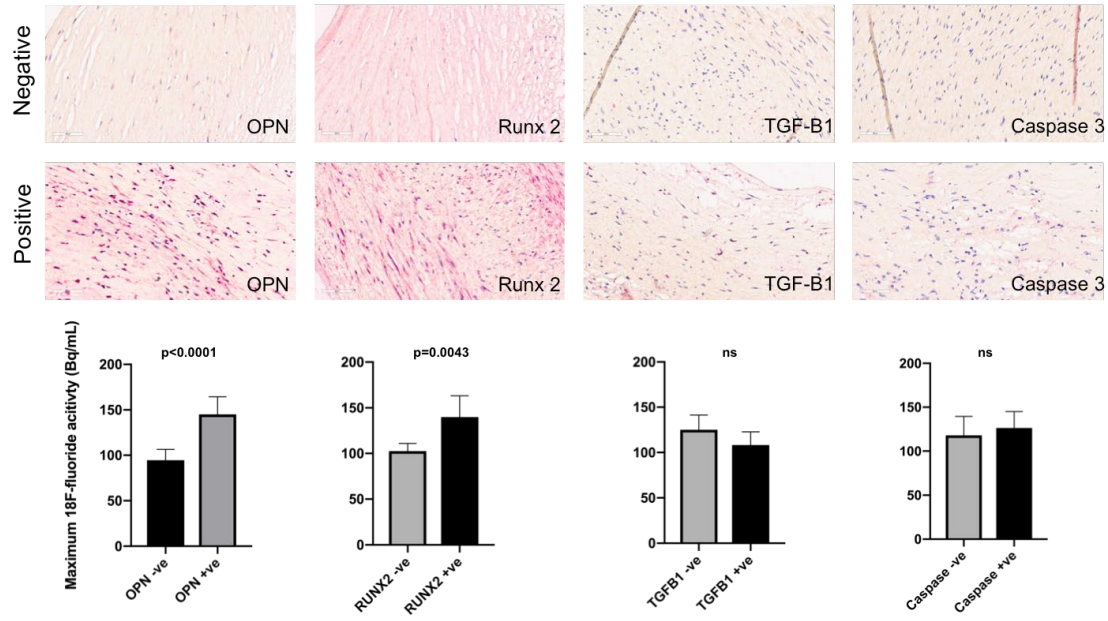

Figure 5.7 18F-Fluoride and transcription factors associated with atherosclerotic mineralisation.

High 18F-fluoride activity was associated with markers of inflammatory mediated mineralization (Osteopontin: positive 145.0 kBq/mL versus negative 94.5 kBq/mL, difference in means 50.5 [95% confidence interval 28.1 to 72.9] kBq/mL, p<0.0001; Runt-related transcription factor 2: positive 139.8 kBq/mL versus negative 102.6 kBq/mL, difference in means 37.2 [95% confidence interval 12.6 to 61.8] kBq/mL, p=0.0043). No difference in 18F-fluoride activity was observed for TGFβ1 (p=0.1042) or Caspase 3 (p=0.5476).
OPN, Osteopontin, RUNX-2, Runt-related transcription factor 2, TGFβ1, Transforming growth factor-beta1.

5.5 Discussion

In this *ex vivo* imaging study of coronary atherosclerosis, we have demonstrated for the first time that 18F-fluoride is a selective marker of intimal hydroxyapatite deposition in human coronary atherosclerotic plaques. Similar to other disease states it preferentially binds in areas of microcalcification rather than macrocalcification. 18F-Fluoride has a high affinity for hydroxyapatite, which is more abundant in regions of microcalcification compared with larger macrocalcified deposits. Importantly, high 18F-fluoride signal co-localises with the distribution of osteopontin and Runx 2, established markers of early calcification activity and adverse plaque formation. This histological validation supports the use of 18F-fluoride positron emission tomography as a marker of developing microcalcification and plaque activity in patients with coronary artery disease.

Whilst there has been histological confirmation of 18F-fluoride binding in carotid atheroma, studies demonstrating increased 18F-fluoride activity in the coronary arteries (Joshi, Vesey et al. 2014, Dweck, Chow et al. 2012) have been called into question due to the limited spatial resolution of clinical positron emission tomography, with some investigators questioning whether 18F-fluoride binding actually occurs in coronary arteries (Demer, Tintut et al. 2017). In this regard, the confirmation of high intensity 18F-fluoride binding in the intimal layer of coronary plaques compared to background and adjacent myocardium is of considerable importance. We have also confirmed that 18F-fluoride binding occurs in plaques both with and without macroscopic calcium observed on CT, and that binding appears to occur preferentially in regions of developing microcalcification. This strongly supports 18F-fluoride PET as a marker of calcification activity and developing microcalcification in the coronary arteries and is consistent with previous

observations in coronary artery disease as well the data in carotid atheroma and other cardiovascular disease states (Creager, Hohl et al. 2019, Irkle, Vesey et al. 2015, Forsythe, Dweck et al. 2018, Dweck, Jenkins et al. 2014, Cartlidge, Doris et al. 2019).

Of particular interest is the potential for 18F-fluoride to discriminate hydroxyapatite deposition above other calcium derivatives in regions of active mineralisation (Aikawa, Nahrendorf et al. 2007). Of the many calcium derivatives, nanocrystalline hydroxyapatite is the central component of microcalcification in atherosclerotic coronary plaques (Aikawa, Nahrendorf et al. 2007). We have here confirmed the preferential binding of 18F-fluoride for microcalcification and for hydroxyapatite based upon the binding of a specific optical probe and Raman spectroscopy. At later stages in the calcification process, other calcium derivatives, such as whitlockite, become more abundant in calcified vascular tissue, particularly within large vessel atherosclerosis where there is often a high whitlockite to hydroxyapatite ratio (You, Bergholt et al. 2017). The phase transformation of hydroxyapatite to whitlockite may occur in the hypoxic or acidic conditions within necrotic cores where magnesium ions are incorporated onto the surface and prevent further growth of hydroxyapatite crystals (Jang, Jin et al. 2014). Traditionally surface area effects have been used to explain the preferential binding of 18F-fluoride for microcalcification. However, the specificity of 18F-fluoride for hydroxyapatite provides an additional explanation for why high 18F-fluoride activity is not observed in areas macrocalcification and why it provides different information to CT (Creager, Hohl et al. 2019).

We also observed a close relationship between the coronary 18F-fluoride signal and both osteopontin and Runx-2 expression, established markers of early calcification

activity and adverse coronary plaque. High concentrations of osteopontin accumulate in coronary atheroma exposed to hypoxia and endothelial injury (O'Brien, Garvin et al. 1994). Of note, inflammatory signalling within metabolically active coronary plaques stimulates macrophage-derived foam cells to express high levels of osteopontin (Shanahan, Cary et al. 1994). In comparison, low levels of osteopontin mRNA are found in vascular smooth muscle cells often regarded as the cell type responsible for initiating plaque calcification (Newman, Bruun et al. 1995). Importantly, from a clinical perspective, high plasma osteopontin levels are associated with adverse clinical events in patients with both stable and unstable coronary artery disease (Minoretti, Falcone et al. 2006, Bjerre, Pedersen et al. 2013). Combined with high-sensitivity C reactive protein, osteopontin had a two-fold increased risk of recurrent myocardial infarction in patients presenting with ST elevation myocardial infarction (Bjerre, Pedersen et al. 2013). The role of osteopontin in mediating plaque activity is noted by the beneficial effect of statins in reducing osteopontin levels and thereby reduce the risk of plaque rupture (Kadoglou, Kottas et al. 2014). The relationship between 18F-fluoride uptake and osteopontin therefore supports its role as a marker of early calcification activity and adverse plaque. However, ultimately data are required to investigate whether 18F-fluoride predicts future myocardial infarction and therefore might provide important clinical information. In this regard, to determine whether coronary 18F-fluoride has clinical utility, prognostic observation studies in patients with recent myocardial infarction are ongoing (NCT02278211).

5.5.1 Limitations

There are some limitations to this study. Legislation regarding the regulation of tissue in victims of sudden death meant that only left main and proximal left anterior

descending coronary artery specimens could be obtained for detailed research analysis. These specimens did not include sections of culprit coronary plaque rupture with thrombus formation and therefore extrapolation of these findings to ruptured atherosclerotic plaques cannot be made. Ante-mortem demographics regarding risk factors such as diabetes mellitus and renal disease which influence atherosclerotic calcification were unavailable. However, the majority of cases in this study were adjudicated by a forensic pathologist who determined a cause of death attributed to ischemic heart disease independent from the study investigators. This provides further evidence of the high prevalence of 18F-fluoride binding in coronary arteries in a high-risk cohort. Although the significance of the high frequency of sudden cardiac death (77%) in this study population is uncertain, further studies exploring the utility of coronary 18F-fluoride imaging in victims of sudden death are worth pursuing.

5.6 Conclusion

In this *ex vivo* study of coronary atherosclerotic plaques, 18F-fluoride binding was highly selective for unbound hydroxyapatite deposition. High 18F-fluoride intensity was associated with intimal microcalcification in regions of osteopontin and Runx-2 expression. This study provides further evidence to support the use of 18F-fluoride positron emission tomography as a marker of plaque vulnerability in patients with coronary artery disease.

CHAPTER 6

Ticagrelor to reduce myocardial injury in patients with high-risk coronary artery plaque

Moss AJ, Dweck MR, Doris MK, Andrews JPM, Bing R, Forsythe RO, Cartlidge TR, Pawade TA, Daghem M, Raftis JB, Williams MC, van Beek EJR, Forsyth L, Lewis SC, Lee RJ, Shah ASV, Mills NL, Newby DE, Adamson PD.
Ticagrelor to reduce myocardial injury in patients with high-risk coronary artery plaque
JACC: Cardiovasc Imaging. 2019. Doi: 10/1016/j.jcmg.2019.05.023

6.1 Summary

Objectives

High-risk coronary atherosclerotic plaque is associated with higher plasma troponin concentrations suggesting ongoing myocardial injury that may be a target for dual antiplatelet therapy. To determine whether ticagrelor reduces high-sensitivity troponin I concentrations in patients with established coronary artery disease and high-risk coronary plaque.

Methods

In a randomised double-blind placebo-controlled trial, patients with multivessel coronary artery disease underwent coronary 18F-fluoride positron emission tomography-computed tomography and measurement of high-sensitivity cardiac troponin I and were randomized (1:1) to ticagrelor 90 mg twice daily or matched placebo. The primary endpoint was troponin I concentration at 30 days in patients with increased coronary 18F-fluoride uptake.

Results

In total, 202 patients were randomised and 191 met the pre-specified criteria for inclusion in the primary analysis. In patients with increased coronary 18F-fluoride uptake (n=120/191) there was no evidence that ticagrelor had an effect on plasma troponin concentrations at 30 days (ratio of geometric means for ticagrelor *versus* placebo, 1.11, [95% confidence interval 0.90 to 1.36], p=0.32). Over 1 year, ticagrelor had no effect on troponin concentrations in patients with increased coronary 18F-fluoride uptake (ratio of geometric means, 0.86, 95% confidence interval 0.63 to 1.17, p=0.33).

Conclusions

Dual antiplatelet therapy with ticagrelor does not reduce plasma troponin concentrations in patients with high-risk coronary plaque, suggesting that subclinical plaque thrombosis does not contribute to ongoing myocardial injury in this setting.

Clinical Trial Registration Information

Clinical Trials.gov Study ID: NCT02110303

6.2 Introduction

Coronary plaque rupture is the commonest cause of acute coronary thrombosis and myocardial infarction (Libby, 2013). Patients who have an increased risk of recurrent plaque rupture events may benefit from intensification of secondary prevention therapy (Fox, Carruthers et al. 2010). In this regard, the addition of a $P2Y_{12}$ receptor antagonist to low-dose aspirin reduces the risk of cardiovascular death, myocardial infarction and stroke in patients with recent (Wallentin, Becker et al. 2009) or prior (Bonaca, Bhatt et al. 2015) myocardial infarction. Ticagrelor is an oral reversible antagonist of the platelet adenosine diphosphate $P2Y_{12}$ receptor. It provides faster, more potent and more consistent $P2Y_{12}$ inhibition than clopidogrel (Gurbel, Bliden et al. 2009). In the PLATelet inhibition and patients Outcomes (PLATO) trial of 18,624 patients presenting with acute coronary syndrome, ticagrelor was superior to clopidogrel for the prevention of cardiovascular events and death (3) (Wallentin, Becker et al. 2009). Moreover, the prolonged use of dual antiplatelet therapy following myocardial infarction continues to reduce cardiovascular events, albeit at the expense of increased rates of major bleeding (Bonaca, Bhatt et al. 2015). Thus, there is a clinical need to improve the risk stratification of patients to enable physicians to better select ‘vulnerable’ patients who may benefit from extended duration of dual antiplatelet therapy.

A novel approach for assessing patients at high-risk of coronary plaque rupture is using positron emission tomography and coronary computed tomography angiography (PET-CCTA). This technique uses the radiotracer 18F-fluoride to identify regions of increased disease activity in coronary artery plaques. Previous studies have demonstrated that coronary 18F-fluoride uptake correlates with a high-risk cardiovascular profile and identifies ruptured coronary plaques in patients with

recent myocardial infarction (Dweck, Chow et al. 2012, Joshi, Vesey et al. 2014). Importantly, we have previously reported an association between increased coronary 18F-fluoride uptake and higher plasma high-sensitivity cardiac troponin I concentrations in patients with stable coronary artery disease (Joshi, Vesey et al. 2014). Silent plaque rupture is common and subclinical plaque thrombus formation is a frequent incidental post-mortem finding in patients with multivessel coronary artery disease who have died from non-cardiovascular causes (Mann, Davies, 1999). This suggests that coronary 18F-fluoride uptake may identify high-risk plaque that is associated with thrombus formation and subclinical myocardial injury from microemboli. If correct, this would potentially be modifiable with intensive dual antiplatelet therapy.

In this study, coronary 18F-fluoride activity was used to identify patients with stable multivessel coronary artery disease who respond favorably to ticagrelor as assessed by a reduction in high-sensitivity cardiac troponin I concentrations.

6.3 Methods

6.3.1 Study Design

This was an investigator-initiated double-blind randomised parallel-group placebo-controlled trial conducted at a single centre in Edinburgh, UK. The study was approved by the local institutional review board, the Scottish Research Ethics Committee (REC reference: 14/SS/0089), Medicines and Healthcare products Regulatory Agency, and the United Kingdom (UK) Administration of Radiation Substances Advisory Committee. It was performed in accordance with the Declaration of Helsinki. All patients provided written informed consent prior to any study procedures.

6.3.2 Study Population

Patients were recruited between March 2015 and March 2017. Patients were included if they met the following criteria: age ≥40 years and already receiving aspirin therapy with angiographically proven multivessel coronary artery disease defined as at least two major epicardial vessels with any combination of either (a) >50% luminal stenosis, or (b) previous revascularization (percutaneous coronary intervention or coronary artery bypass graft surgery). Patients were excluded if they had any of the following criteria: an acute coronary syndrome within the last 12 months, any ongoing indication for dual anti-platelet therapy, or concurrent thienopyridine (clopidogrel or prasugrel) or oral anticoagulant therapy, or percutaneous coronary intervention or coronary artery bypass graft surgery within the last 3 months.

6.3.3 Study Procedures

All patients underwent a baseline assessment to confirm eligibility and measurement of plasma high-sensitivity cardiac troponin I concentration and platelet-monocyte aggregates. An electrocardiogram (ECG) gated 18F-fluoride PET-CCTA was performed after patients had received 50-100 mg of oral metoprolol if their resting heart rate was >65 beats/min prior to the intravenous administration of 250 MBq 18F-fluoride. After 60 min, patients were imaged with a hybrid PET-CT scanner (64-multidetector Biograph mCT, Siemens Medical Systems, Erlangen, Germany). Attenuation correction CT scans were performed prior to the acquisition of ECG-gated list-mode PET data using a single 30-min bed position centred on the heart. Finally, an ECG-gated CCTA was performed in mid-diastole during held expiration following sublingual glyceryl trinitrate.

6.3.4 Statistical Analysis

Categorical data are presented using counts and percentages, whilst continuous variables are presented using mean, standard deviation (SD), median, interquartile range, minimum, maximum, and number of patients. Participants were removed from formal statistical analysis where data were missing for that outcome variable. All (except safety) analyses were performed on a per-protocol population that excluded participants without a blood sample, or whose compliance was <80% for the study medication, at the 30-day visit. For the primary analysis, the change in troponin I concentration from baseline to 30 days was compared between the two treatment groups (ticagrelor and placebo) using linear regression, adjusting for the minimisation variables in patients with increased coronary 18F-fluoride uptake. Prior to analysis, tests for normality were undertaken and, where data were skewed, logarithmic transformation was performed. Central estimates and 95% confidence intervals (CI) were calculated. Similar analyses were performed for secondary

outcomes. In post-hoc testing, comparison was made of baseline troponin concentrations between patients with and without evidence of coronary 18F-fluoride activity and also confirmed treatment efficacy by comparison of ADP-stimulated platelet activation between the two trial intervention groups (ticagrelor *versus* placebo). For 1-year evaluation of changes in cardiac troponin I concentrations, an adjusted linear regression model (adjusted for the minimisation variables) was generated and descriptive statistics were presented for the area under the curve. Where there were missing values, the value was imputed linearly from adjacent measurements. Adjustment for age was performed as a linear term. To determine whether there was efficacy of ticagrelor using a baseline troponin I concentration ≥5 ng/L, a post-hoc comparison was made between groups using the method described in the primary analysis. For all analyses, a two-sided $p<0.05$ was taken as statistically significant. Statistical analysis was performed using SAS (Software 9.4, North Carolina) with the primary analysis validated by a second statistician in Edinburgh Clinical Trials Unit. Post-hoc analyses were performed separately from the primary statistical analysis plan using R version 3.4.0 (R Foundation for Statistical Computing, Vienna, Austria).

6.4 Results

6.4.1 Study Population

A total of 361 patients were screened and 202 patients were randomized following the baseline coronary 18F-fluoride PET-CCTA (***Figure 6.1***). Eleven patients discontinued the study early due to withdrawal of consent (n=1), a new diagnosis of malignancy on baseline PET-CCTA (n=1), <80% compliance with study medication at 30 days (n=8), and a sudden unexpected death prior to receiving study medication (n=1). The randomized groups were well matched for the presence of cardiovascular risk factors and represented a high-risk cohort with 70% having a history of acute coronary syndrome (median 2.25 years prior to study enrolment) (***Table 6.1***). A per-protocol population of 191 patients (mean age 65.9, SD 8.3 years, 80% male) had both blood sampling at 30 days and ≥80% compliance with the study medication, comprising 94 patients in the ticagrelor group and 97 patients in the placebo group. One hundred and twenty (62.8%) patients had evidence of coronary 18F-fluoride activity in at least one epicardial vessel (***Table 6.2, Figure 6.2***).

The geometric mean troponin I concentration at baseline was 3.8 (Geometric SD 2.9) ng/L in patients with increased coronary 18F-fluoride activity compared with 2.5 (Geometric SD 2.6) ng/L in those without uptake (p=0.004; ***Table 6.3***).

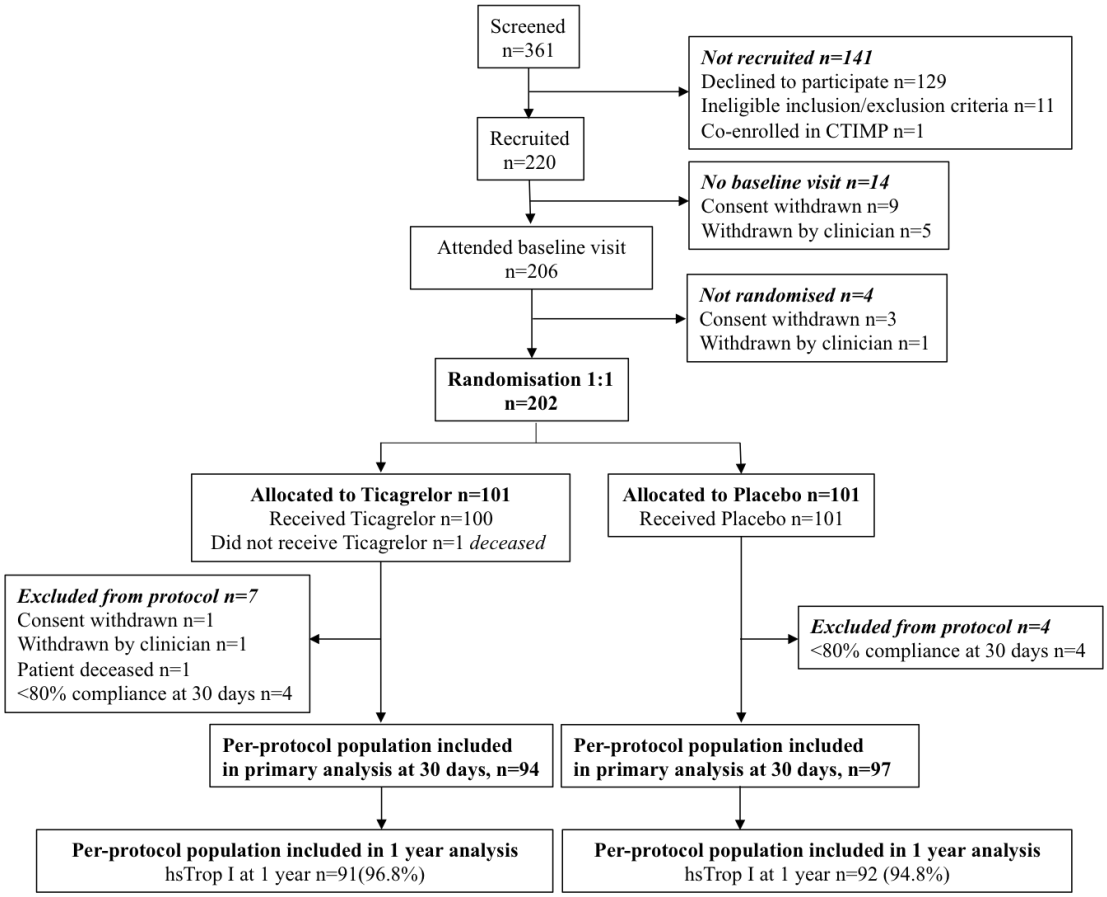

Figure 6.1 CONSORT Diagram of DIAMOND trial.

Flow diagram of the progress through the phases of the randomised trial between ticagrelor and placebo groups.

	Total Randomised Population (n=202)	Per Protocol population (n=191)	Ticagrelor (n=94)	Placebo (n=97)	P value (ticagrelor versus placebo)
Age, years	65.9±8.2	65.9±8.3	65.5±8.4	66.3±8.1	0.504
Male	162 (80)	152 (80)	74 (79)	78 (80)	0.912
Body Mass Index, kg/m^2	29.8±5.2	29.7±5.0	30.0±5.2	29.4±4.9	0.413
Medical history					
History of acute coronary syndrome	143 (71)	134 (70)	65 (69)	69 (71)	0.887
Days between ACS and randomisation*	821 (620, 1056)	821 (625, 1037)	800 (620, 970)	861 (646,1081)	
Percutaneous Coronary Intervention	163 (81)	154 (81)	75 (80)	79 (81)	0.915
Coronary Artery Bypass Grafting	40 (20)	38 (20)	18 (19)	20 (21)	0.942
Hypertension	113 (56)	105 (55)	52 (55)	53 (55)	1.000
Hypercholesterolaemia	195 (97)	185 (97)	93 (99)	92 (95)	0.228
Diabetes Mellitus	39 (19)	36 (19)	19 (20)	17 (18)	0.772
Prior Stroke/Transient Ischaemic Attack	4 (2)	4 (2)	2 (2)	2 (2)	1.000
History of Atrial Fibrillation	5 (2)	5 (3)	4 (4)	1 (1)	0.346
Peripheral Vascular Disease	8 (4)	7 (4)	1 (1)	6 (6)	0.134
Medications					
Aspirin	202 (100)	191 (100)	94 (100)	97 (100)	NA
Statin	192 (95)	182 (95)	92 (98)	90 (93)	0.188
Beta-Blocker	138 (68)	130 (68)	66 (70)	64 (66)	0.637
Angiotensin Converting Enzyme Inhibitor/Angiotensin II Receptor Blocker	155 (77)	145 (76)	68 (72)	77 (79)	0.333
Haemoglobin, g/dL	14.0±1.3)	14.0±1.3	14.2±1.2	13.8±1.3	0.034
Estimated Glomerular Filtration Rate, mL/min/1.73m^2					0.547
31-60	23 (11)	22 (12)	9 (10)	13 (13)	
>60	179 (89)	169 (88)	85 (90)	84 (87)	
Total Cholesterol, mg/dL	162±39	162±39	162±39	162±35	0.852
High density lipoprotein, mg/dL	46±12	46±12	43±15	46±12	0.128
Low density lipoprotein, mg/dL	89 ±31	89±31	85±35	89±27	0.377
Triglycerides, mg/dL	159±97	151±97	159±106	151±80	0.556

Table 6.1 Baseline characteristics of the DIAMOND population.

Values are n (%) or mean ± standard deviation* median (interquartile range) analysis

	OVERALL (N=191)	**TICAGRELOR (N=94)**	**PLACEBO (N=97)**	**P-VALUE**
CORONARY 18F-FLUORIDE UPTAKE				
N	120	59	61	
BASELINE	3.8±2.9	4.2±2.9	3.5±3.0	0.197
30 DAYS	3.6±2.7	4.1±2.5	3.2±2.9	0.072
RATIO OF 30 DAYS TO BASELINE	0.95±1.87	0.97±2.13	0.93±1.59	0.907
NO CORONARY 18F-FLUORIDE UPTAKE				
N	71	35	36	
BASELINE	2.5±2.6	2.5±2.8	2.4±2.4	0.872
30 DAYS	2.4±2.7	2.4±2.8	2.3±2.6	0.877
RATIO OF 30 DAYS TO BASELINE	0.97±1.68	0.97±1.77	0.96±1.59	

Table 6.2 Plasma high-sensitivity cardiac troponin I concentration (ng/L) in the per-protocol population.

Geometric mean and geometric standard deviation, back transformed from log transformed values.

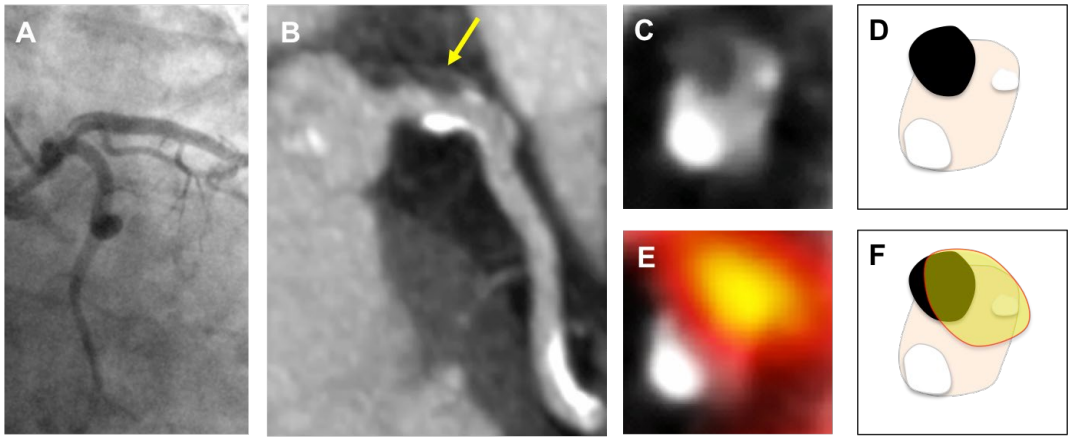

Figure 6.2 Intracoronary thrombus and coronary 18F-fluoride activity.

A 72-year-old female with intracoronary thrombus in the left main stem (A, B arrow). Axial reconstructions demonstrate a non-obstructive intracoronary thrombus at 11 o'clock with coronary calcification at 2 o'clock and 7 o'clock (C and D, schematic). 18F-Fluoride activity was present in the coronary plaque (E and F, schematic).

6.4.2 Effect of ticagrelor on platelet function

Baseline platelet and monocyte reactivities were well balanced between treatment arms. Consistent with its known pharmacological action, ticagrelor markedly inhibited platelet P-selectin expression and reduced the formation of platelet-monocyte aggregates following *ex vivo* stimulation with ADP (***Figure 6.3,*** $p<0.001$ for all). Ticagrelor had no effect on 30-day unstimulated platelet activation ($p>0.05$ for all). These results were derived from post-hoc analysis.

	Adjusted Geometric Mean (GSE)		**Ratio of Geometric Means**	
	Ticagrelor	**Placebo**	**(95% CI)**	**p-valve**
Cardiac troponin I, ng/L (*18F-fluoride activity*)	3.8 (1.1)	3.4 (1.1)	1.11 (0.90 to 1.36)	0.32
Cardiac Troponin I, ng/L (*No 18F-fluoride activity*)	2.4 (1.1)	2.3 (1.1)	1.02 (0.80 to 1.31)	0.87

Table 6.3 Plasma high-sensitivity cardiac troponin I concentration (ng/L) at 30 days for the per-protocol population.

Estimates are back transformed estimates from analysis of log transformed values at 30 days adjusting for age, sex and log transformed baseline troponin. Ratio of geometric means is Ticagrelor divided by Placebo. GSE, geometric standard error

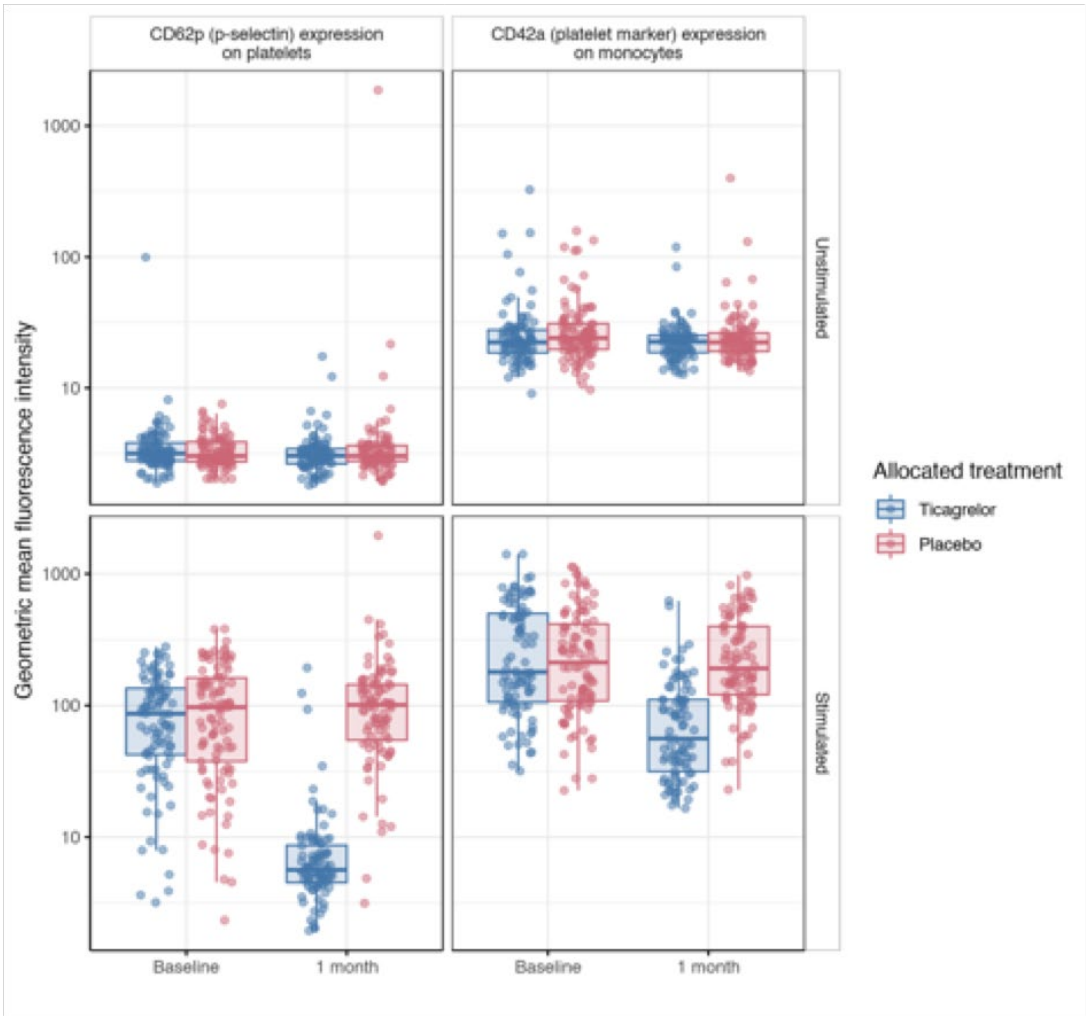

Figure 6.3 Flow cytometry assessment of platelet activation at baseline and 30 days.

Unstimulated (upper panels) and adenosine diphosphate (20 μmol/L) stimulated (lower panels) levels of (a) platelet activation (P-selectin expression) and (b) platelet-monocyte aggregates.

6.4.3 Effect of ticagrelor on high-sensitivity troponin I at 30 days

For the primary endpoint, there was no effect of ticagrelor on troponin I at 30 days in patients who had increased coronary 18F-fluoride activity (ratio of geometric means ticagrelor *versus* placebo 1.11, 95% CI 0.90 to 1.36; p=0.32) (***Table 6.3***). Similarly, amongst the 71 (37.2%) patients without discernible coronary 18F-fluoride activity, there was no difference in the 30-day troponin I concentration between ticagrelor and placebo (ratio of geometric means 1.02, 95% CI 0.80 to 1.31; p=0.87) (***Table 6.3***).

Secondary endpoints explored whether a reduction in cardiac troponin I could be demonstrated over twelve months. Twelve-month troponin I concentrations were measured in 183 (95.8%) patients, comprising of 91 (96.8%) patients in the ticagrelor group and 92 (94.8%) patients in the placebo group. There was no difference in area under the concentration curve of troponin I over twelve months between the ticagrelor and placebo groups (ratio of geometric means 0.92, 95% CI 0.74 to 1.13; p=0.42) (***Figure 6.4***) (***Table 6.4***). Post-hoc analysis of the subset of patients with a baseline troponin I concentration ≥5 ng/L (ticagrelor n=34, baseline geometric mean 10.3 ng/L; placebo n=33, baseline geometric mean 8.7 ng/L), found there was no change in troponin I concentration at 30 days (p=0.89) or twelve months (p=0.86). (***Figure 6.5, Table 6.5***).

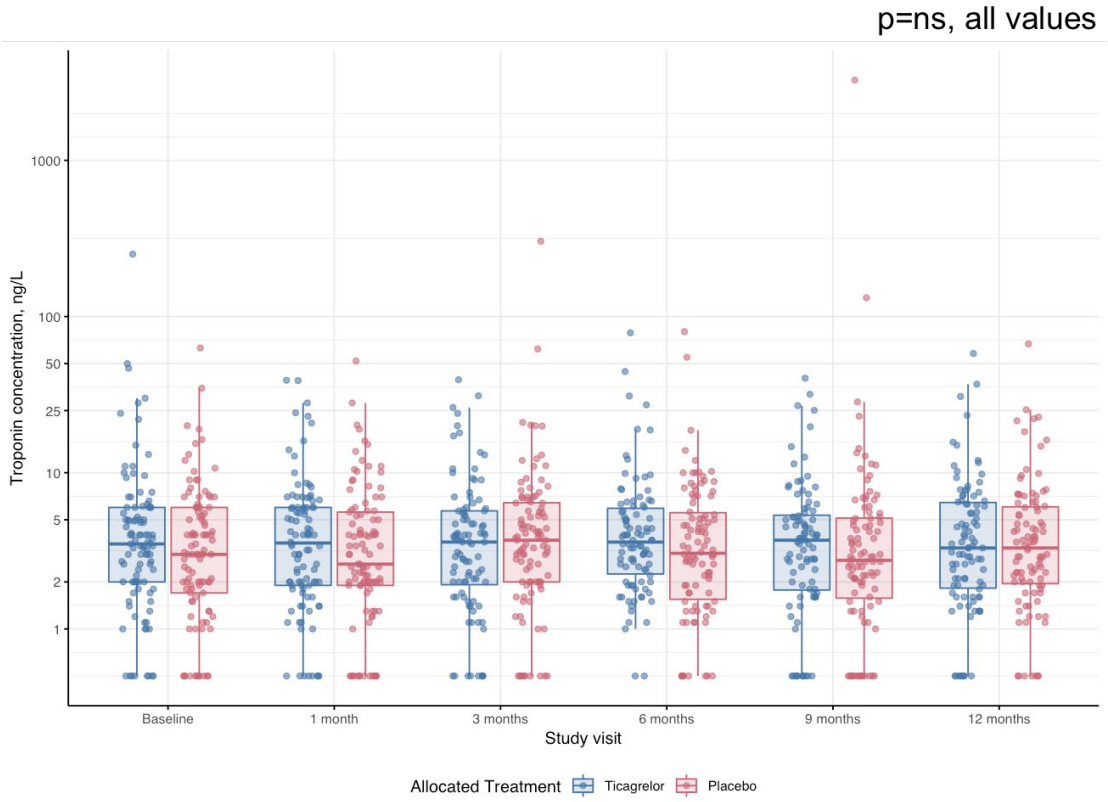

Figure 6.4 Plasma high-sensitivity cardiac troponin I concentration over 1 year.

Box-whisker plot of individual patient-level plasma high-sensitivity troponin I concentration (ng/L) in ticagrelor (blue) and placebo (red) groups at baseline, 1, 3, 6, 9 and 12 months. Median and interquartile range for each time point.

	Adjusted Geometric Mean (GSE)		**Ratio of Geometric Means**	
	Ticagrelor	**Placebo**	**(95% CI)**	**p-valve**
AUC from 30 days to 1 year (*18F-fluoride activity*)	3.7 (1.1)	4.4 (1.1)	0.86 (0.63 to 1.17)	0.33
AUC from 30 days to 1 year (*No 18F-fluoride activity*)	2.4 (1.1)	2.3 (1.1)	1.04 (0.84 to 1.28)	0.70

Table 6.4 Plasma high-sensitivity cardiac troponin I concentration over 1 year for participants in per-protocol population.

Estimates are back transformed estimates from analysis of log transformed values area under curve from 30 days to 1 year adjusting for age, sex and log transformed baseline troponin. Ratio of geometric means is Ticagrelor divided by Placebo. AUC, area under curve, ng/L, GSE, geometric standard error.

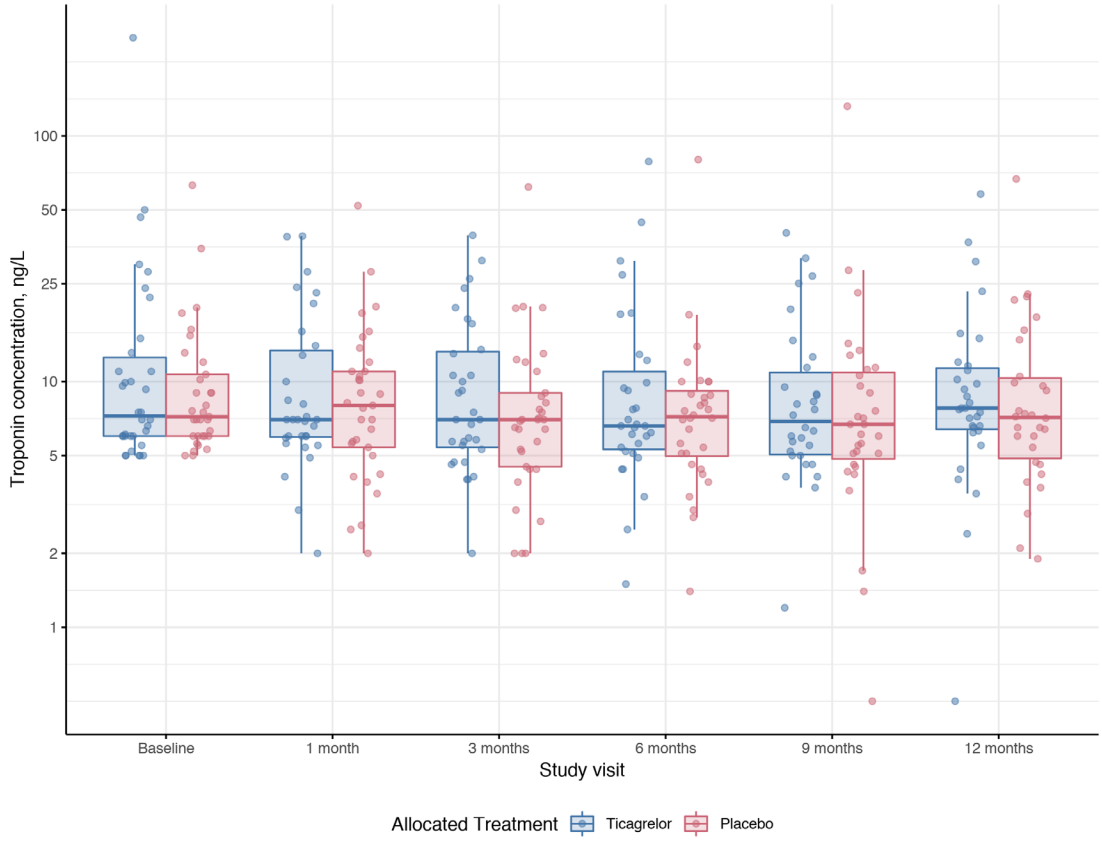

Figure 6.5 Plasma high-sensitivity cardiac troponin I concentration (stratified population with troponin I >5ng/L at baseline) over 1 year.

Box-whisker plot of individual patient-level plasma high-sensitivity troponin I concentration (ng/L) in ticagrelor (blue) and placebo (red) groups at baseline, 1, 3, 6, 9 and 12 months (p=ns for all values). Median and interquartile range for each time point.

PLACEBO	Baseline 18F-fluoride uptake on PET-CT			
	Negative	Negative	Positive	Positive
	Baseline hs-cTnI <5 ng/L	Baseline hs-cTnI ≥5 ng/L	Baseline hs-cTnI <5 ng/L	Baseline hs-cTnI ≥5 ng/L
Baseline hs-cTnI, geometric mean (95% CI)	1.8 (1.4 to 2.3)	7.7 (5.9 to 10.1)	1.8 (1.4 to 2.3)	9.3 (7.2 to 12.1)
30 day hs-cTnI, geometric mean (95% CI)	1.7 (1.3 to 2.3)	7.1 (4.1 to 12.1)	1.8 (1.4 to 2.3)	8.3 (6.1 to 11.2)

TICAGRELOR	Baseline 18F-fluoride uptake on PET-CT			
	Negative	Negative	Positive	Positive
	Baseline hs-cTnI <5 ng/L	Baseline hs-cTnI >5 ng/L	Baseline hs-cTnI <5 ng/L	Baseline hs-cTnI >5 ng/L
Baseline hs-cTnI, geometric mean (95% CI)	1.8 (1.4 to 2.3)	8.7 (4.7 to 16.3)	2.3 (1.9 to 2.9)	10.3 (7.6 to 15.8)
30 day hs-cTnI, geometric mean (95% CI)	1.7 (1.3 to 2.2)	10.2 (5.2 to 20.1)	2.7 (2.1 to 3.4)	8.3 (6.1 to 11.2)

Table 6.5 Efficacy of Ticagrelor in patients with troponin I concentration ≥ *5 ng/L.*

6.4.4 Safety outcomes

There were no suspected unexpected serious adverse reactions over the course of this study. Serious adverse events occurred in 7/100 (7%) patients who received at least one single dose of ticagrelor and 15/101 (11.9%) patients who were administered placebo (***Table 6.6***). There were no reported major life-threatening or other major bleeding events over the course of this study. Minimal bleeding events (bruising) were reported in 64 (64.0%) patients in the ticagrelor group and 12 (11.9%) patients in the placebo group (***Table 6.7***). Dyspnoea episodes occurred in 24 (24%) patients in the ticagrelor group compared with 8 (7.9%) patients in the placebo group at one year.

		Ticagrelor n=100		Placebo n=101		Overall n=201	
		Number of Events	**Number of Patients**	**Number of Events**	**Number of Patients**	**Number of Events**	**Number of Patients**
Any serious adverse event		10	7 (7%)	15	12 (11.9%)	25	19 (9.5%)
Outcome	Resolved	10	7 (7%)	15	12 (11.9%)	25	19 (9.5%)
Causality	Unrelated to IMP & NIMP	9	7 (7%)	14	11 (10.9%)	23	18 (9%)
	Unrelated to IMP	1	1 (1%)	1	1 (1%)	2	2 (1%)
Expectedness	Expected	0	0 (0%)	0	0 (%)	0	0 (0%)
	Unexpected	10	7 (7%)	15	12 (11.9%)	25	19 (9.5%)
Severity	Mild	5	5 (5%)	5	4 (4%)	10	9 (4.5%)
	Moderate	5	3 (3%)	9	9 (8.9%)	14	12 (6%)
	Severe	0	0 (0%)	1	1 (1%)	1	1 (0.5%)

Table 6.6 Serious adverse events for safety population.

		Ticagrelor n=100		Placebo n=101		Overall n=201	
		Number of Events	**Number of Patients**	**Number of Events**	**Number of Patients**	**Number of Events**	**Number of Patients**
Any bleeding event		88	64 (64%)	14	12 (11.9%)	102	76 (37.8%)
PLATO classification	Minimal	87	64 (64%)	14	12 (11.9%)	101	76 (37.8%)
	Minor	1	1 (1%)	0	0 (0%)	1	1 (0.5%)
	Major	0	0 (0%)	0	0 (0%)	0	0 (0%)
	Major life threatening	0	0 (0%)	0	0 (0%)	0	0 (0%)
Dyspnoea	At 1 year	27	24 (24%)	8	8 (7.9%)	35	32 (15.9%)

Table 6.7 Bleeding and dyspnoea events for safety population.

6.5 Discussion

In this randomised placebo-controlled trial, this study found no evidence that ticagrelor 90 mg twice daily reduces plasma high-sensitivity cardiac troponin I concentrations in patients with high-risk plaque and established multivessel coronary artery disease. This suggests that, in patients with high-risk coronary plaque, plasma cardiac troponin I concentrations are not attributable to subclinical myocardial injury from thrombotic microembolic injury.

This study has several important strengths. This is the first trial to use PET-CCTA imaging with 18F-fluoride to identify patients with high-risk coronary plaque who may be at heightened risk of future coronary events and thereby have the most to gain from potent dual antiplatelet therapies. It is also the largest trial to date employing coronary plaque PET imaging. Whilst previous PET studies have used 18F-fluorodeoxyglucose to visualise inflammation within the carotid arteries as a surrogate to guide intensification of atherosclerotic therapy (Tawakol, Fayad et al. 2013, Fayad, Mani et al. 2011), the coronary and cerebral vascular beds differ both with respect to their underlying molecular pathophysiology and also in response to the treatment effect using ticagrelor (Wallentin, Becker et al. 2009, Johnston, Amarenco et al. 2016). Second, the study design enabled high-risk patients with multivessel coronary disease and *in vivo* evidence of disease activity to be precisely phenotyped prior to randomization in a manner that can seldom be achieved in larger clinical outcome trials (Wallentin, Becker et al. 2009, Vranckx, Valgimigli et al. 2018). Finally, this is the first prospective randomised controlled trial to use high-sensitivity cardiac troponin I concentrations as a surrogate outcome measure for assessing future cardiovascular risk.

In trying to understand why $P2Y_{12}$ inhibition did not reduce cardiac troponin in this study, it is worth addressing some of the underlying assumptions in the trial design. Does coronary 18F-fluoride activity identify patients with high-risk plaque? Recent studies have found that 18F-fluoride holds potential in identifying culprit plaques in the coronary circulation by classifying patients who have a high-risk cardiovascular phenotype and culprit plaque rupture following type 1 myocardial infarction (Dweck, Chow et al. 2012, Joshi, Vesey et al. 2014). Histological validation indicates that 18F-fluoride preferentially binds to microcalcification in regions of plaque mineralisation, a key component of high-risk plaque (Irkle, Vesey et al 2015). Hydroxyapatite, the most common form of atherosclerotic microcalcification, is extruded from apoptotic macrophages, and accumulates within necrotic cores where it may destabilise the structural integrity of the fibrous cap (New, Goettsch et al. 2013, Hutcheson, Goettsch et al. 2016). The identification of abnormal material composition of the arterial wall has clinical relevance, as these regions may lead to atherosclerotic plaque rupture manifesting as myocardial infarction, stroke or aneurysm rupture (Joshi, Vesey et al. 2014, Vesey, Jenkins et al. 2017, Forsythe, Dweck et al. 2018). In this cohort, the frequency of 18F-fluoride activity (>60%) in stable coronary artery disease is similar to previous estimates in patients with a high burden of coronary artery disease and prior myocardial infarction (Dweck, Chow et al. 2012). This work confirms the high prevalence of coronary 18F-fluoride activity in stable patients with multivessel coronary artery disease in whom intensification of antiplatelet therapy may be considered.

A key question is whether troponin measurement below the 99th centile reflects subclinical plaque rupture with accompanying distal microvascular embolisation as has previously been posited (Oemraswingh, Cheng et al. 2017). In this regard,

some therapies directed at reducing the risk of atherosclerotic plaque rupture, such as pravastatin, both modify troponin concentrations and reduce the risk of myocardial infarction (Ford, Shah et al. 2016, Januzzi, Hahn et al. 2000). In contrast, strategies that have failed to demonstrate a reduction in cardiovascular events in the context of stable coronary artery disease, such as coronary revascularisation, attenuation of plaque inflammation and inhaled therapies for respiratory disease, have not correlated with a reduction in serial troponin concentration (Welsh, Tuckwell et al. 2016, Everett, Brooks et al. 2015, Adamson, Anderson et al. 2018). If subclinical plaque thrombosis is the dominant mechanism underlying detectable troponin I concentrations in patients with stable coronary artery disease, a reduction in troponin I concentration would be expected following the administration of potent antiplatelet therapy. The lack of response to ticagrelor in this study would suggest that other contributing mechanisms to myocardial injury should be considered. The emergence of newer therapies (such as sodium/glucose cotransporter 2 inhibition) that lower blood pressure may reduce troponin concentrations through an improvement in myocardial remodelling, further raising doubts over the subclinical plaque rupture hypothesis (Januzzi, Suchindran et al. 2018, Lohrke, Sibeneicher et al. 2017, McEnvoy, Chen et al. 2016). In this study, high-sensitivity cardiac troponin I concentrations were higher in patients with 18F-fluoride activity, albeit the differences were small and below the established risk stratification threshold of 5 ng/L (Shah, Anand et al. 2015, Ford, Shah et al. 2016, Januzzi, Suchindran et al. 2018). Therefore, it seems unlikely that troponin at these concentrations reflects subclinical plaque rupture and it is perhaps unsurprising that ticagrelor treatment did not result in an early or late reduction in troponin concentration.

Previous reports have suggested that there is a high incidence of subclinical intracoronary thrombus in patients with apparently stable coronary artery disease. Indeed, some have suggested that this occurs in as many as one in seven patients (Mann, Davies, 1999). If this is the case, it would appear that intracoronary thrombus does not track with troponin. This suggests we require better non-invasive markers of coronary thrombosis, such as novel PET tracers (Lohrke, Siebeneicher et al. 2017) or non-invasive imaging (Jansen, Perera et al. 2011), to use as biomarkers of cardiovascular risk and anti-thrombotic therapeutic efficacy.

6.5.1 Limitations

There are some study limitations that should be acknowledged. This study had a modest sample size to assess the impact of ticagrelor on a readily available plasma biomarker, and a larger study would be required to assess clinical outcomes of ticagrelor use in patients with stable coronary artery disease and coronary 18F-fluoride activity. The low baseline troponin I concentrations observed in this study may have limited power to demonstrate the benefit of ticagrelor in this population. Enrichment of the population by selecting patients with higher troponin I concentrations prior to study entry may need to be considered for future trials. It should also be acknowledged that this study was undertaken in a single centre with expertise in coronary 18F-fluoride imaging and the methods for analysing coronary 18F-fluoride activity are subject to a number of operator and scan-dependent variables. Whilst recent reports have suggested that coronary 18F-fluoride activity may hold prognostic value in stratifying high-risk populations (Kitagawa, Yamamoto, et al. 2018), larger prospective studies evaluating the prognostic utility of coronary 18F-fluoride activity in patients with cardiovascular disease are ongoing (NCT02278211).

6.6 Conclusion

In patients with multivessel coronary artery disease and *in vivo* coronary 18F-fluoride activity, this study found no evidence that intensification of antiplatelet therapy using ticagrelor 90 mg twice daily reduces plasma high-sensitivity cardiac troponin I concentration at 30 days or 1 year. These findings suggest that in this group of patients plasma high-sensitivity cardiac troponin I concentrations may not be a suitable marker to predict efficacy of $P2Y_{12}$ inhibition.

CHAPTER 7

Conclusions & Future Directions

Including adaptations from:

Moss AJ, Hutchison S, Dweck MR.
Gazing into smoldering volcanoes: precision cardiac imaging.
Future Sci OA. 2018;5:FSO294.

7.1 Summary of thesis findings

Clinicians routinely make intuitive decisions that aim to 'personalise' an individual's treatment. This is far from an exact science, and often results in clinicians oversimplifying the complexity of the underlying pathophysiology. In a time-pressured clinical environment, clinicians use intuitive decision-making to make fast and impulsive judgments that often attribute a patient's complaint to a single common phenotype leading to a "one size fits all" approach to treatment. This population-approach to the management of human coronary atherosclerosis has yielded better use of evidence-based therapies and promotion of lifestyle modifications to dramatically reduce early deaths from myocardial infarction over the past two decades. However, many patients fail to benefit from the widely advocated successes of a "one size fits all" approach either by sustaining harm from treatment or by remaining at increased risk of recurrent cardiovascular events despite optimal therapeutic interventions.

To influence long-term outcomes, a more considered approach is required. Precision medicine requires taking account of the heterogeneity of disease and an individual's variable response to treatment. A detailed insight into the biological continuum of disease will help unravel the complexity of why some individuals gain significant benefits from interventions whereas others do not. Whereas current strategies in coronary artery disease have focused on population-derived evidence-based therapies, precision imaging seeks to understand an individual's unique biological network to better stratify treatment.

The core aims of this thesis were to investigate whether the identification of vulnerable coronary plaques could refine the assessment of residual risk in

individual's with stable and unstable coronary artery disease and test it's use in stratifying high-risk individuals to intensified medical therapy.

7.1.1 Adverse plaque characterisation using coronary computed tomography angiography

In a sub-study of the Scottish Computed Tomography of the HEART (SCOT-HEART) trial, patients who were randomised to coronary computed tomography angiography for the assessment of stable chest pain underwent coronary plaque analysis to identify high-risk plaque features (positive remodelling, low attenuation plaque, spotty calcification, 'napkin ring' sign). For the purpose of this analysis, 1,769 patients had an interpretable coronary computed tomography angiography, of whom 608 (34%) patients had one of more features high-risk coronary plaque features. The primary outcome for this observational sub-study was a composite of fatal and non-fatal myocardial infarction at 5 years.

Patients with high-risk coronary plaque were at a three-fold increased risk of fatal and non-fatal myocardial infarction at 5 years compared to those without high-risk plaque features. When compared to patients with normal coronary arteries, the group at highest risk of fatal and non-fatal myocardial infarction included patients with a combination of both obstructive coronary artery disease and high-risk plaque (***Figure 7.1***). However, these associations were not independent of coronary plaque burden measured using the coronary artery calcium score. More specific methods of identifying high-risk plaque may be needed to select patients for more intensive medical therapy.

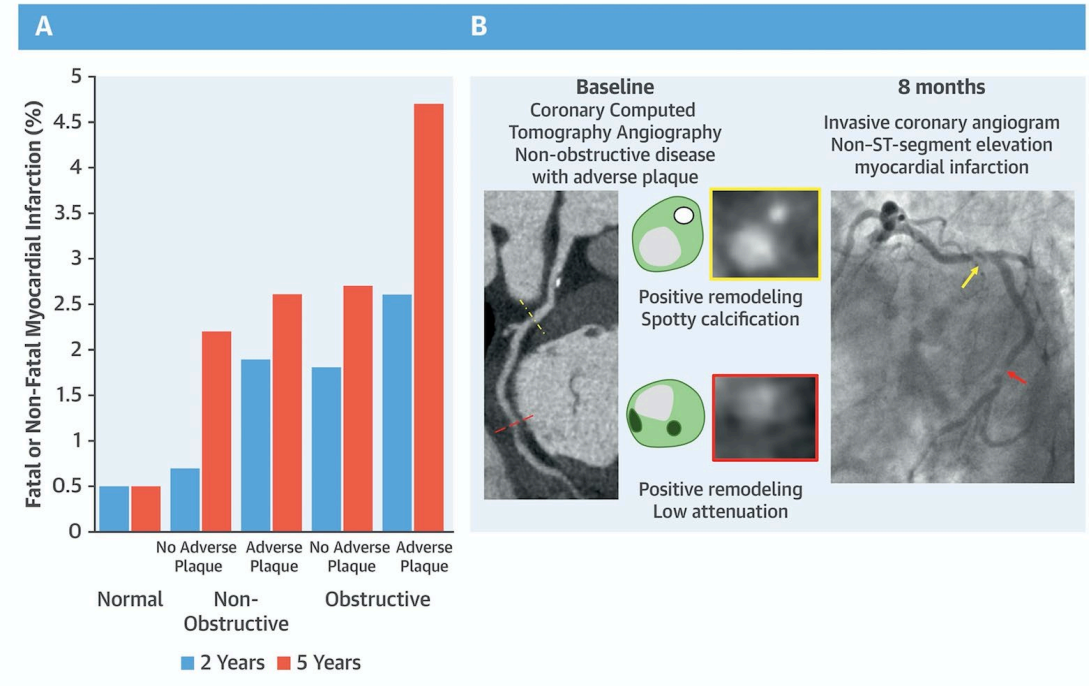

Figure 7.1 Adverse plaque features on coronary computed tomography angiography identifies patients at an increased risk of subsequent events.

(A) Bar graph of the frequency of coronary heart disease or nonfatal myocardial infarction at 2 and 5 years for patients with normal coronary arteries and non-obstructive or obstructive with and without adverse plaque. (B) Coronary computed tomography angiography and invasive coronary angiography images from a patient with non-obstructive coronary artery disease who had a subsequent non-ST segment elevation myocardial infarction. The red/yellow dotted lines and arrows correspond to the location of the plaques in the red/yellow boxes.
(Williams, Moss et al. 2019)

7.1.2 Reproducibility and optimisation of coronary 18F-Fluoride positron emission tomography imaging

Coronary positron emission tomography is a non-invasive imaging modality which has been used to detect high-risk coronary plaque. Microcalcification is a key feature of vulnerable plaques and can be readily identified with 18F-Fluoride. This radiotracer has been used to highlight regions of microcalcification in large vessel vascular beds, however technical challenges have limited the clinical translation of this technique to accurately identify plaque activity in coronary arteries. To establish the optimal methodology for quantifying and categorising 18F-fluoride uptake in the coronary vasculature, a prospective observational study was performed recruiting patients with stable and unstable multi-vessel coronary artery disease. Thirty patients with stable or recent acute coronary syndrome underwent scan-rescan imaging with coronary 18F-fluoride positron emission tomography within a two-week interval.

Twenty patients with stable coronary artery disease and ten patients with recent acute coronary syndrome had serial 250 MBq 18F-fluoride positron emission tomography scans. There was good agreement in the quantification and categorisation of plaque activity between observers and between scans. Coronary 18F-fluoride uptake is therefore a precise and reproducible metric in the coronary arteries and the analytic performance is sufficient to use this imaging biomarker in clinical trials.

7.1.3 Histological confirmation of 18F-fluoride binding in coronary artery specimens

The pathophysiological processes governing the deposition of microcalcification in coronary arteries are complex. In skeletal bone, 18F-fluoride binds to the exposed surface of hydroxyapatite to form fluoroapatite, however no previous study has demonstrated hydroxyapatite to be the substrate for 18F-fluoride binding in coronary arteries. In an *ex vivo* study using sections of human coronary arteries, regions of 18F-fluoride binding were evaluated for hydroxyapatite deposition using a selective immunofluorescence bisphosphonate probe and Raman spectroscopy. The expression of proteins and transcription factors associated with plaque mineralisation were analysed in regions of increased 18F-fluoride binding.

18F-Fluoride was highly selective for unbound hydroxyapatite deposition in coronary atherosclerotic plaques. In advanced atherosclerotic plaques, intimal hydroxyapatite identified using 18F-fluoride was associated with increased expression of osteopontin and Runt-related transcription factor 2 (***Figure 7.2***). These findings suggest that 18F-fluoride highlights regions of active atherosclerosis and may be used as a biomarker of disease activity.

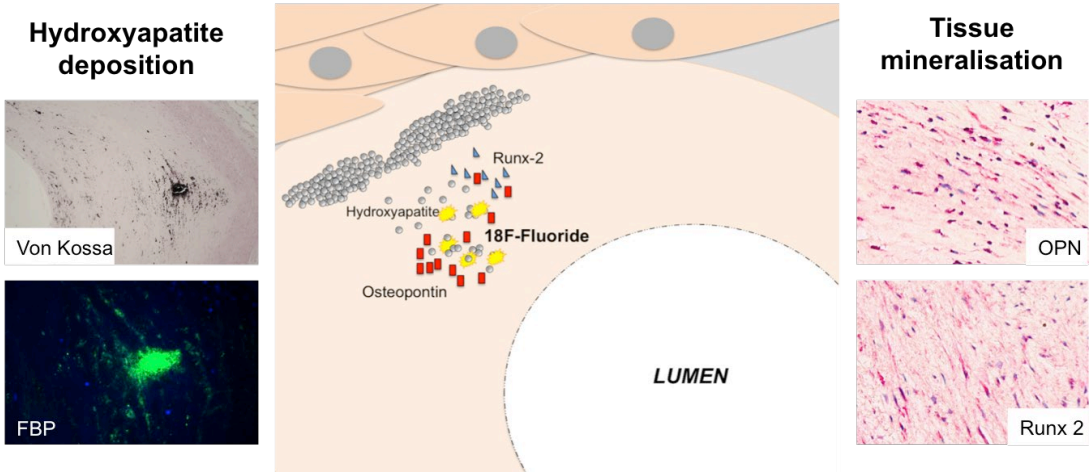

Figure 7.2 Histological analysis of 18F-fluoride binding in coronary artery specimens

Coronary 18F-fluoride uptake identifies regions of microscopic hydroxyapatite deposition in intimal atherosclerotic plaque. Intense 18F-fluoride uptake is associated with the intimal expression of osteopontin and Runt-related transcription factor 2, markers of plaque mineralization.
FBP, Fluorescein-Bisphosphonate, OPN, osteopontin, Runx-2, Runt-related transcription factor 2.

7.1.4 Identification of patients with high-risk plaque features to stratify treatment

Whilst high-risk plaque features are associated with an increased risk of cardiovascular events, it remains unknown whether intensified medical therapy should be used in these patients. To address whether patients with increased coronary 18F-fluoride uptake may benefit from the addition of P2Y12 inhibition with ticagrelor, a randomised, double-blind, placebo-controlled trial was performed. Patients with multi-vessel coronary artery disease were randomised (1:1) to either ticagrelor 90 mg twice daily or matched placebo and serial measurement of high-sensitivity cardiac troponin I was performed at 30 days and at 3-month intervals up to 1 year. The primary endpoint was a change in plasma troponin I concentration at 30 days in patients with increased coronary 18F-fluoride uptake.

Dual antiplatelet therapy using Ticagrelor did not reduce plasma troponin I concentration in patients with high-risk plaque features identified using coronary 18F-fluoride uptake (***Figure 7.3***). Despite a significant reduction in platelet reactivity in patients receiving ticagrelor, plasma troponin I concentration remained unchanged suggesting that subclinical coronary thrombosis does not contribute to subclinical troponin release in this setting.

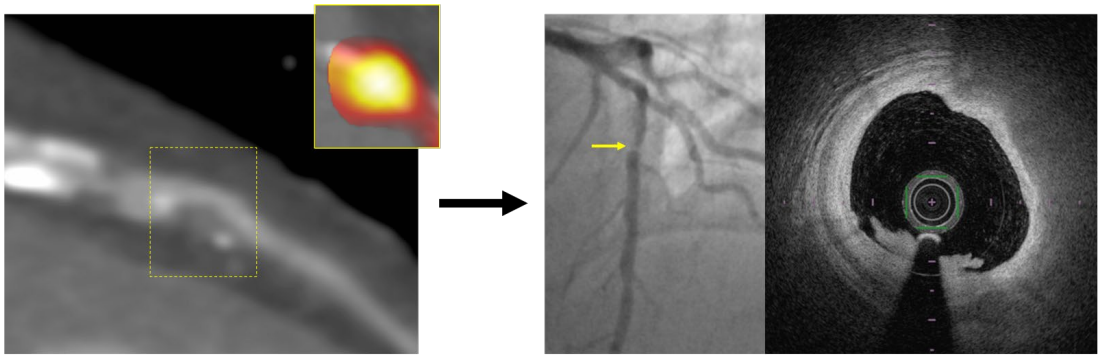

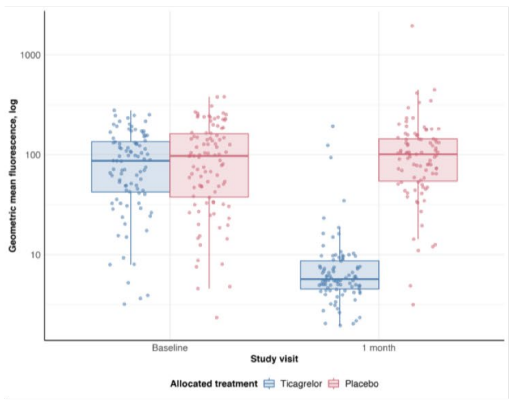

P-selectin expression on stimulated platelets at baseline and Day 30

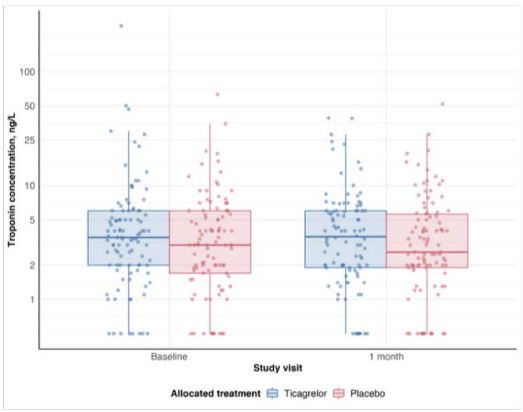

Baseline and Day 30 Troponin I concentration

Figure 7.3 Using coronary 18F-fluoride to identify patients who may benefit from intensified dual antiplatelet therapy.

Coronary 18F-fluoride positron emission tomography was used to identify high-risk coronary plaque in patients with stable multivessel coronary artery disease. Randomisation to intensified dual antiplatelet therapy with ticagrelor did not reduce plasma high-sensitivity cardiac troponin I concentrations at 30-days in patients with high-risk plaque.
(Moss, Doris et al. 2019)

7.2 Future Directions

The findings of this thesis raise important issues relevant to the application of vulnerable plaque detection in human coronary atherosclerosis. There is an unmet clinical need to improve clinical risk stratification in patients with coronary artery disease. As novel therapies targeting key components of the atherosclerotic pathway become more widely available for clinical use, selecting the appropriate patient for the appropriate treatment will remain a clinical priority. In this regard, cardiovascular imaging using hybrid positron emission tomography is an attractive tool, as it enables clinicians to phenotype coronary artery disease and monitor plaque activity. Ongoing clinical trials are exploring whether positron emission tomography may have prognostic clinical utility in the context of human coronary atherosclerosis.

7.2.1 Using 18F-fluoride imaging to predict future cardiovascular events

Following an acute myocardial infarction, one in five patients will have a recurrent event despite optimal medical therapy (Mills et al, 2011). Half of these recurrent myocardial infarctions occur at a site that was not deemed to be of clinical importance at the time of their initial presentation (Stone et al, 2011). The central hypothesis of the Prediction of Recurrent Events with 18F-Fluoride to Identify Ruptured and High-risk Coronary Artery Plaques in Patients with Myocardial Infarction, the PRE^{18}FFIR trial (NCT02278211), is that coronary 18F-fluoride uptake can identify high-risk and ruptured atherosclerotic plaque in patients with recent myocardial infarction and thereby assist in the diagnosis, risk stratification and management of patients with acute myocardial infarction. More targeted and

focused investigations and interventions have the potential to shorten hospital stay, to avoid the indiscriminate application of expensive therapies, and to focus and to maximize the impact of our current successful therapies to reduce recurrent major adverse cardiac events. The study rationale aims to confirm preliminary findings presented in this thesis in a broad range of patients across different centres throughout the United Kingdom. Specifically, this study is intended to confirm whether coronary 18F-fluoride uptake identifies high-risk or ruptured coronary atherosclerotic plaque, and to determine if coronary 18F-fluoride uptake is predictive of disease progression and clinical outcome.

7.2.2 Natural history of 18F-fluoride uptake in stable coronary artery disease and following recent myocardial infarction

Numerous studies have determined the predictive utility of features of vulnerability as determined by a variety of invasive and non-invasive imaging modalities. The majority of these investigations have focused on clinical endpoints following a single measurement rather than using serial imaging to detect temporal changes in plaque vulnerability. In this thesis, investigations using 18F-fluoride plaque characterisation have determined tracer uptake on a single positron emission tomography scan or within a two-week interval. In order to support more widespread adoption of this imaging method and better understand the natural history of plaque vulnerability, it is necessary to assess the temporal changes in 18F-fluoride radiotracer uptake by performing repeated imaging studies. A sub-study of the PRE^{18}FFIR trial, PRE^{18}FFIR-TIME – The Investigation of teMporal changE, will recruit 80 patients from the main study who will undergo an additional coronary 18F-fluoride positron emission tomography scan at 6 weeks, 12 weeks, 26 weeks and 52 weeks after

their baseline scan to determine how the pattern of coronary 18F-fluoride uptake change over the period of one year.

7.2.3 Correlation of 18F-fluoride with invasive imaging characteristics

The most comprehensively investigated diagnostic tools for assessing plaque vulnerability are invasive intravascular imaging using ultrasound (IVUS) and Fourier domain optical coherence tomography (OCT). In a pilot study, plaques with increased 18F-fluoride uptake correlated with high-risk features on intravascular imaging (Joshi, Vesey et al. 2014). Similar to findings that were observed in the adverse plaque sub-study of SCOT-HEART, necrotic core and positive remodelling identified using IVUS were the two plaque features which closely resembled plaques with increased 18F-fluoride uptake.

A recent development in intravascular imaging catheters has combined IVUS with near-infrared spectroscopy (NIRS) which allows the differing tissue characteristics of coronary plaques to be quantitatively measured with regards to light scatter and absorption, in particular, to detect cholesterol deposits. Accurate co-registration of invasive and non-invasive imaging datasets will provide more detailed information of plaque composition. By identifying individual culprit plaque rupture using intravascular imaging, the aim of the PRE^{18}FFIR – IMAGE sub-study is to determine whether coronary 18F-fluoride uptake is associated with culprit plaque rupture, luminal thrombosis and an increased lipid burden of cholesterol deposits.

7.2.4 Clinical trials using novel radiotracers to assess plaque rupture in coronary artery disease

Coronary plaque positron emission tomography imaging has focused on re-purposing oncological tracers for identifying plaque, however the potential exists to generate radiotracers which have specific ligands directly involved in atherosclerotic pathways. In this regard, the 18F-glycoprotein I (18F-GP1) is a novel fiban class ligand that binds with high affinity to the glycoprotein IIb/IIIa (GPIIb/IIIa) receptor on activated platelets. Following the activation of GPIIb/IIIa, the incorporation of fibrinogen results in cross-linking and thrombus formation. As a result, GPIIb/IIIa has been a therapeutic target in cardiology for many years, with inhibitors (tirofiban, abciximab and eptifibatide) commonly used in high-risk acute coronary syndromes upstream of, or during, percutaneous coronary intervention.

Kim *et al* performed a first-in-human investigational study of 18F-GP1 in patients with acute deep vein thrombosis or pulmonary embolism (Kim, Lee et al. 2018). The radiotracer was well tolerated with initial high uptake followed by rapid clearance in the spleen, kidneys and blood pool. 18F-GP1 PET-CT detected 89% of vessels with deep vein thrombosis and 60% with pulmonary embolism, and interestingly demonstrated increased uptake in 32 vessels that were not detected by conventional imaging (Lohrke, Sibeneicher et al. 2017). The mean standardised uptake value of thromboemboli to blood pool ratio was 4.9±1.4 and 3.7±1.5 for deep vein thrombosis and pulmonary embolism respectively; a signal to background ratio that is superior to 18F-fluoride. Recently, the first-in-human study of 18F-GP1 in arterial thrombosis (6 endovascular repair of abdominal aortic aneurysm, 1 bypass surgery and stent placement, 1 endarterectomy, 1 arterial dissection, and 1 acute cerebral infarction) has been reported (Chae, Kwon et al. 2019). The investigators

found uptake in arterial thrombus in all patients, again demonstrating a high mean standardised uptake value of thrombus to blood pool ratio. The favourable safety and radiation dosimetry profile of 18F-GP1 has been demonstrated and is comparable to other PET radiotracers (Lee, Chae et al. 2019). In light of these preliminary data, 18F-GP1 is a novel, highly promising radiotracer for coronary atherosclerosis imaging. The clinical applications of this specific thrombus tracer would be particularly useful in detecting subclinical plaque rupture events and distinguish type 1 from type 2 myocardial infarction. This will be addressed in the in-vivo Thrombus imaging with 18F-GP1 study, iThrombus (NCT03943966) which will determine whether the expression of GPIIb/IIIa receptor within thrombus can be detected in the arterial and venous circulation.

7.3 Clinical Perspective

Accurate risk prediction of future cardiovascular events in patients with coronary artery disease is a pertinent problem for frontline clinicians. Specifically in the current era of high-sensitivity troponin measurement, diagnosing the different types of myocardial infarction in patients in order to select the right treatment for the right individual is a vexing problem. The increasing prevalence of myocardial injury identified using high-sensitivity troponin assays in patients who present to the emergency department or outpatient clinic has made it more difficult to identify with sufficient certainty which patients are actually having a plaque rupture event. By using non-invasive imaging to unravel the complexity of the *in vivo* pathophysiological mechanisms at play in an individual, a more precise phenotype of coronary artery disease can be characterised.

There are number of clinical scenarios in which the identification of plaque rupture may have major clinical utility, for example, in populations where identifying high-risk individuals is a clinical priority. This would be the case for patients undergoing major non-cardiac surgery where the inappropriate initiation of medical therapy may confer more harm than benefit. This would also apply to individuals with a systemic inflammatory response due to a non-cardiac illness who are often diagnosed with a persistent troponin elevation attributed to chronic myocardial injury or type 2 myocardial infarction. Additionally, as targeted therapies using monoclonal antibodies and ribonucleic acid interference become more widely available, non-invasive imaging tools may be able to better stratify treatment in high-risk individuals. Moving away from a “one size fits all” approach in patients with coronary artery disease towards bespoke treatment algorithms based on the residual risk of a cardiac event is an important and necessary step.

In this thesis, the use of hybrid positron emission tomography computed tomography imaging to detect vulnerable plaques and stratify therapy has been shown to be both feasible and can be applied in the clinical trial setting. Whilst vulnerable plaque detection using coronary computed tomography angiography alone can be readily performed in clinical practice, coronary computed tomography angiography may lack the specificity needed to identify individuals who may benefit from intensified treatment to reduce their residual risk of future cardiovascular events. In this regard, coronary 18F-fluoride positron emission tomography has been shown to be a quantitative reproducible metric of plaque activity in the coronary vasculature. At the cellular level, it represents active mineralisation within coronary plaques and may serve to highlight coronary plaques at increased risk of rupture. The clinical utility of coronary 18F-fluoride positron emission tomography in identifying vulnerable plaques which contribute to future cardiovascular events will be more fully explored in the PRE^{18}FFIR study.

Relevant published papers during PhD period

Moss AJ, Dweck MR, Doris MK, Andrews JPM, Bing R, Forsythe RO, Cartlidge TR, Pawade TA, Daghem M, Raftis JB, Williams MC, van Beek EJR, Forsyth L, Lewis SC, Lee RJ, Shah ASV, Mills NL, Newby DE, Adamson PD. Ticagrelor to reduce myocardial injury in patients with high-risk coronary plaque. JACC Cardiovasc Imaging. 2019. Doi:10.1016/j.cmg.2019.05.023. Epub ahead of print.

Lassen ML, Kwiecinski J, Dey D, Cadet S, Germano G, Berman DS, Adamson PD, Moss AJ, Dweck MR, Newby DE, Slomka PJ. Triple-gated motion and blood pool clearance corrections improve reproducibility of coronary 18F-NaF PET. Eur J Nucl Med Mol Imaging. 2019;46:2610-2630.

Moss AJ, Doris MK, Andrews JPM, Bing R, Daghem M, van Beek EJR, Forsyth L, Shah ASV, Williams MC, Sellers S, Leipsic J, Dweck MR, Parker RA, Newby DE, Adamson PD. Molecular coronary plaque imaging using 18F-fluoride. Circ Cardiovasc Imaging. 2019;12:e008574.

Williams MC, Moss AJ, Dweck M, Adamson PD, Alam S, Hunter A, Shah ASV, Pawade T, Weir-McCall JR, Roditi F, van Beek EJR, Newby DE, Nicol ED. Coronary artery plaque characteristics associated with adverse outcomes in the SCOT-HEART study. J Am Coll Cardiol. 2019;73:291-301.

Creager MD, Hohl T, Hutcheson JD, Moss AJ, Schlotter F, Blaser MC, Park MA, Lee LH, Singh SA, Alcaide-Corral CJ, Tavares AAS, Newby DE, Kijewski MF, Aikawa M, Di Carli M, Dweck MR, Aikawa E. 18F-Fluoride signal amplification identifies microcalcifications associated with atherosclerotic plaque instability in positron emission tomography/computed tomography images. Circ Cardiovasc Imaging. 2019;12:e007835.

Kwiecinski J, Adamson PD, Lassen ML, Doris MK, Moss AJ, Cadet S, Jansen MA, Dey D, Lee SE, Yun M, Chang HJ, Dweck MR, Newby DE, Berman DS, Slomka PJ. Feasibility of coronary 18F-sodium fluoride positron-emission tomography assessment with the utilization of previously acquired computed tomography angiography. Circ Cardiovasc Imaging. 2018;11:e008325.

Sim AM, Rashdan NA, Cui L, Moss AJ, Nudelman F, Dweck MR, MacRae V, Hulme AN. A novel fluorescein-bisphosphonate based diagnostic tool for the detection of hydroxyapatite in both cell and tissue models. Sci Rep. 2018;8:17360.

References

Abdelbaky A, Corsini E, Figueroa AL *et al.* Focal arterial inflammation precedes subsequent calcification in the same location: a longitudinal FDG-PET/CT study. *Circ Cardiovasc Imaging*. 2013;6:747-754.

Adamson PD, Anderson JA, Brook RD *et al*. Cardiac troponin I and cardiovascular risk in patients with chronic obstructive pulmonary disease. *J Am Coll Cardiol*. 2018;72:1126-1137.

Agatston AS, Janowitz WR, Hildner FJ *et al*. Quantification of coronary artery calcium using ultrafast computed tomography. *J Am Coll Cardiol*. 1990;15:827–832.

Ahmadi A, Leipsic J, Blankstein R *et al*. Do plaques rapidly progress prior to myocardial infarction? The interplay between plaque vulnerability and progression. *Circ Res*. 2015;117:99-104.

Aikawa E, Nahrendorf M, Figueiredo JL *et al*. Osteogenesis associates with inflammation in early-stage atherosclerosis evaluated by molecular imaging in vivo. *Circulation*. 2007;116:2841-2850.

Alavi A, Werner TJ, Hoilund-Carlsen PF. What can be and what cannot be accomplished with PET to detect and characterize atherosclerotic plaques. *J Nucl Cardiol*. 2016;25:2012-2015.

Al-Mashhadi RH, Tolbod LP, Bloch LØ *et al*. 18-Fluorodeoxyglucose accumulation in arterial tissues determined by PET signal analysis. *J Am Coll Cardiol*. 2019;74:1220-1232.

Armani C, Catalani E, Balbarini A *et al*. Expression, pharmacology and functional role of somatostatin receptor subtypes 1 and 2 in human macrophages. *J Leukoc Bio.* 2007;8:845-855.

Austen WG, Edwards JE, Frye RL *et al*. A reporting system on patients evaluated for coronary artery disease. Report of the Ad Hoc Committee for Grading of Coronary Artery Disease, Council on Cardiovascular Surgery, American Heart Association. *Circulation*. 1975;51:5–40.

Battle MR, Goggi JL, Allen L *et al*. Monitoring tumor response to antiangiogenic sunitinib therapy with 18F-fluciclatide, an 18F-labeled αVbeta3-integrin and αVbeta5-integrin imaging agent. *J Nucl Med.* 2011;52:424-430.

Bertazzo S, Gentleman E, Cloyd KL, *et al*. Nano-analytical electron microscopy reveals fundamental insights into human cardiovascular tissue calcification. *Nat Mater*. 2013;12:576-583.

Bini J, Robson PM, Calcagno C *et al*. Quantitative carotid PET/MR imaging: clinical evaluation of MR-attenuation correction versus CT-attenuation correction in 18F-FDG PET/MR emission data and comparison to PET/CT. *Am J Nucl Med Mol Imaging.* 2015;5:293-304.

Bjerre M, Pedersen SH, Møgelvang R *et al.* High osteopontin levels predict long-term outcome after STEMI and primary percutaneous coronary intervention. *Eur J Prev Cardiol.* 2013;20:922-999.

Bonaca MP, Bhatt DL, Cohen M *et al*. Long-term use of Ticagrelor in patients with prior myocardial infarction. *N Engl J Med*. 2015;372:1791-800.

Braunwald E, Jones RH, Mark DB *et al*. Diagnosing and managing unstable angina. *Circulation*. 1994;90:613-622.

Bucerius J, Mani V, Moncrieff C *et al.* Optimizing 18F-FDG PET/CT imaging of vessel wall inflammation: the impact of 18F-FDG circulation time, injected dose, uptake parameters, and fasting blood glucose levels. *Eur J Nucl Med Mol Imaging.* 2014;41:369-383.

Budoff MJ, Dowe D, Jollis JG *et al*. Diagnostic performance of 64-multidector row coronary computed tomographic angiography for evaluation of coronary artery stenosis in individuals without know coronary artery disease. *J Am Coll Cardiol* 2008;52:1724-32.

Budoff MJ, Mayrhofer T, Ferencik M *et al*. Prognostic value of coronary artery calcium in the PROMISE Study (Prospective Multicenter Imaging Study for Evaluation of Chest Pain). *Circulation*. 2017;136:1993–2005.

Burke AP, Farb A, Malcolm GT *et al*. Coronary risk factors and plaque morphology in men with coronary disease who died suddenly. *N Eng J Med.* 1997;336(18):1276-1282.

Canat X, Carayon P, Bouaboula M *et al.* Distribution profile and properties of peripheral-type benzodiazepine receptors on human hemopoieitc cells. *Life Sci.* 1993;52:107-118.

Carayon P, Portier M, Dussossoy D *et al.* Involvement of peripheral benzodiazepine receptors in the protection of hematopoietic cells against oxygen radical damage. *Blood.* 1996;87:3170-3178.

Carrasco JL, Phillips BR, Puig-Martinez J *et al*. Estimation of the concordance correlation coefficient for repeated measures using SAS and R. *Comput Methods Programs Biomed*. 2013;109:293-304.

Cartlidge TRG, Doris MK, Sellers SL *et al*. Detection and prediction of bioprosthetic aortic valve degeneration. *J Am Coll Cardiol*. 2019;73:1107-1119.

Chae SY, Kwon T-W, Jin S *et al*. A phase 1, first-in-human study of 18F-GP1 positron emission tomography for imaging acute arterial thrombosis. *EJNMMI Res*. 2019;9:3. doi: 10.1186/s13550-018-0471-8.

Chang HJ, Lin FY, Lee SE *et al*. Coronary atherosclerotic precursors of acute coronary syndromes. *J Am Coll Cardiol*. 2018;71:2511-2522.

Cheng VY, Berman DS, Rozanski A *et al*. Performance of the traditional age, sex, and angina typicality-based approach for estimating pretest probability of angiographically significant coronary artery disease in patients undergoing coronary

computed tomographic angiography: results from the multinational coronary CT angiography evaluation for clinical outcomes: an international multicentre registry (CONFIRM). *Circulation*. 2011;124:2423-2432.

Cho I, Chang HJ, Sung JM *et al*. Coronary computed tomographic angiography and risk of all-cause mortality and nonfatal myocardial infarction in subjects without chest pain syndrome from the CONFIRM Registry (coronary CT angiography evaluation for clinical outcomes: an international multicentre registry). *Circulation*. 2012;126:304-13.

Chow BJ, Small G, Yam Y *et al*. Prognostic and therapeutic implications of statin and aspirin therapy in individuals with non-obstructive coronary artery disease: results from the CONFIRM (Coronary CT Angiography Evaluation for Clinical Outcomes: An International Multicenter Registry) Registry. *Arterioscler Thromb Vasc Biol.* 2015;35:981-89.

Conte E, Annoni A, Pontone G *et al*. Evaluation of coronary plaque characteristics with coronary computed tomography angiography in patients with non-obstructive coronary artery disease: a long-term follow-up study. *Eur Heart J Cardiovasc Imaging*. 2017;18:1170–1178.

Creager MD, Hohl T, Hutcheson JD *et al*. 18F-Fluoride signal amplification identifies microcalcifications associated with atherosclerotic plaque instability in positron emission tomography/computed tomography images. *Circ Cardiovasc Imaging*. 2019;12:e007835.

Criqui MH, Denenberg JO, Ix JH *et al.* Calcium density of coronary artery plaque and risk of incident cardiovascular events. *JAMA*. 2014;311:271-278.

Davies MJ. The pathophysiology of acute coronary syndromes. *Heart*. 2000;83:361–366.

Davies MJ, Thomas A. Thrombosis and acute coronary-artery lesions in sudden cardiac ischemic death. *N Engl J Med.* 1984;310:1127-1140.

Demer LL, Tintut Y, Nguyen KL *et al*. Rigor and Reproducibility in Analysis of Vascular Calcification. *Circ Res*. 2017;120:1240-1242.

Diamond GA, Forrester JS. Analysis of probability as an aid in the clinical diagnosis of coronary-artery disease. *N Engl J Med*. 1979;300:1350-1358.

Doris MK, Otaki Y, Krishnan SK *et al*. Optimization of reconstruction and quantification of motion-corrected coronary PET-CT. *J Nucl. Cardiol*. 2018. doi:10.1007/s12350-018-1317-5.

Douglas PS, Hoffman U, Patel MR *et al*. Outcomes of anatomical versus functional testing for coronary artery disease. *N Engl J Med*. 2015;372:1291-1300.

Douglas PS, Pontone G, Hlatky MA *et al*. Clinical outcomes of fractional flow reserve by computed tomographic angiography-guided diagnostic strategies vs. usual care in patients with suspected coronary artery disease: the prospective

longitudinal trial of FFRct: outcome and resource impacts study. *Eur Heart J*. 2015;36:3359-3367.

Dweck MR, Chow MW, Joshi NV *et al.* Coronary arterial 18F-sodium fluoride uptake: a novel marker of plaque biology. *J Am Coll Cardiol.* 2012;59:1539-1548.

Dweck MR, Khaw HJ, Sng GK *et al.* Aortic stenosis, atherosclerosis, and skeletal bone: is there a common link with calcification and inflammation? *Eur Heart J.* 2013;34:1567-1574.

Dweck MR, Jenkins WS, Vesey AT *et al*. 18F-Sodium fluoride uptake is a marker of active calcification and disease progression in patients with aortic stenosis. *Circ Cardiovasc Imaging*. 2014;7:371-378.

Dweck MR, Jones C, Joshi NV *et al.* Assessment of valvular calcification and inflammation by positron emission tomography in patients with aortic stenosis. *Circulation.* 2012;125:76-86.

Dweck MR, Williams MC, Moss AJ *et al*. Computed tomography and cardiac magnetic resonance in ischemic heart disease. *J Am Coll Cardiol*. 2016;68:2201-2216.

Elkhawad M, Rudd JHF, Sarov-Blat L *et al*. Effects of p38 mitogen-activated protein kinase inhibition on vascular and systemic inflammation in patients with atherosclerosis. *JACC Cardiovasc Imaging*. 2012:5:911-922.

Everett BM, Brooks MM, Vlachos HE *et al*. Troponin and cardiac events in stable ischemic heart disease. *N Engl J Med*. 2015;373:610-620.

Fayad ZA, Mani V, Woodward M *et al.* Rationale and design of dal-PLAQUE: a study assessing efficacy and safety of dalcetrapib on progression or regression of atherosclerosis using magnetic resonance imaging and 18F-fluorodeoxyglucose positron emission tomography/computed tomography. *Am Heart J*. 2011;162:214-221.

Fayad ZA, Mani V, Woodward M *et al*. Safety and efficacy of dalcetrapib on atherosclerotic disease using novel non-invasive multimodality imaging (dal-PLAQUE): a randomised clinical trial. *Lancet*. 2011;378:1547-1559.

Ferencik M, Mayrhofer T, Bittner DO *et al*. Use of high-risk coronary atherosclerotic plaque detection for risk stratification of patients with stable chest pain: a secondary analysis of the PROMISE randomized clinical trial. *JAMA Cardiol*. 2018;3:144–152.

Fihn SD, Blankenship JC, Alexander KP, et al. 2014 ACC/AHA/AATS/PCNA/SCAI/STS focused update of the guideline for the diagnosis and management of patients with stable ischemic heart disease: a report of the American College of Cardiology/American Heart Association Task Force on Practice Guidelines, and the American Association for Thoracic Surgery, Preventive Cardiovascular Nurses Association, Society for Cardiovascular Angiography and Interventions, and Society of Thoracic Surgeons. *J Am Coll Cardiol*. 2014;64:1929-1949.

Finn AV, Nakano M, Polavarapu R *et al.* Hemoglobin directs macrophage differentiation and prevents foam cell formation in human atherosclerotic plaques. *J Am Coll Cardiol.* 2012;59:166-177.

Folco EJ, Sheikine Y, Rocha VZ *et al.* Hypoxia but not inflammation augments glucose uptake in human macrophages. Implications for imaging atherosclerosis with 18Fluorine-labeled 2-deoxy-D-glucose positron emission tomography. *J Am Coll Cardiol.* 2011;58:603-614.

Ford I, Shah ASV, Zhang R *et al*. High-sensitivity cardiac troponin, statin therapy, and risk of coronary heart disease. *J Am Coll Cardiol*. 2016;25:2719-728.

Forsythe RO, Dweck MR, McBridge OMB *et al*. 18F-Sodium fluoride uptake in abdominal aortic aneurysms: the SoFIA3 study. *J Am Coll Cardiol*. 2018;71:513-523.

Fox KA, Carruthers KF, Dunbar DR *et al*. Underestimated and under-recognized: the late consequences of acute coronary syndrome (GRACE UK-Belgian Study). *Eur Heart J*. 2010;31:2755-64.

Gaemperli O, Shalhoub J, Owen DR *et al.* Imaging intraplaque inflammation in carotid atherosclerosis with 11C-PK11195 positron emission tomography/computed tomography. *Eur Heart J.* 2012;33:1902-1910.

Gallagher BM, Fowler JS, Gutterson NI *et al*. Metabolic trapping as a principle of oradiopharmaceutical design: some factors responsible for the biodistribution of [18F] 2-deoxy-2-fluoro-D-gluose. *J Nucl Med.* 1978;19:1154-1161.

Gaztanaga J, Farkouh M, Rudd JH *et al*. A phase 2 randomized, double-blind, placebo-controlled study of the effect of VIA-2291, a 5-lipoxygenase inhibitor, on vascular inflammation in patients after an acute coronary syndrome. *Atherosclerosis*. 2015;240:53-60.

Georgiadou P, Iliodromitis EK, Kolotathis F *et al.* Osteopontin as a novel prognostic marker in stable ischaemic heart disease: a 3-year follow-up study. *Eur J Clin Invest*. 2010;40:288-293.

Golestani R, Mirfeizi L, Zeebregts CJ *et al.* Feasibility of [18F]-RGD for ex vivo imaging of atherosclerosis in detection of $\alpha v \beta 3$ integrin expression. *J Nucl Cardiol.* 2015;22:1179-1186.

Greenwood JP, Maredia N, Younger JF *et al*. Cardiovascular magnetic resonance and single-photon emission computed tomography for diagnosis of coronary heart disease (CE-MARC): a prospective trial. *Lancet*. 2012;379:453-60.

Gurbel PA, Bliden KP, Butler K *et al*. Randomized double-blind assessment of the ONSET and OFFSET of the antiplatelet effects of ticagrelor versus clopidogrel in patients with stable coronary artery disease: the ONSET/OFFSET study. *Circulation*. 2009;120:2577-2585.

Harding SA, Din JN, Sarma J *et al*. Flow cytometric analysis of circulating platelet-monocyte aggregates in whole blood: Methodological considerations. *Thromb Haemost*. 2007;98:451-456.

Hawkins RA, Choi Y, Huang SC *et al.* Evaluation of skeletal kinetics of fluorine-18-fluoride ion with PET. *J Nucl Med.* 1992;33:663-642.

Hay AM, Pedersen SF, Christoffersen C *et al.* 18F-FDG PET imaging of murine atherosclerosis: association with gene expression of key molecular markers. *PLOS One*. 2012;7:e50908.

Hoffmann U, Ferencik M, Udelson JE *et al*. Prognostic value of noninvasive cardiovascular testing in patients with stable chest pain: insights from the PROMISE Trial (Prospective Multicenter Imaging Study for Evaluation of Chest Pain). *Circulation*. 2017;135:2320–2332.

Hutcheson JD, Blaser MC, Aikawa E. Giving calcification its due: recognition of a diverse disease: a first attempt to standardize the field. *Circ Res*. 2017;120:270-273.

Hutcheson JD, Goettsch C, Bertazzo S *et al.* Genesis and growth of extracellular-vesicle-derived microcalcification in atherosclerotic plaques. *Nat Mater*. 2016;15:335-343.

Irkle A, Vesey AT, Lewis DY *et al.* Identifying active vascular microcalcification by 18F-sodium fluoride positron emission tomography. *Nat Commun.* 2015;6:7495.

Izquierdo-Garcia D, Davies JR, Graves MJ *et al.* Comparison of methods for magnetic resonance-guided [18-F]Fluorodeoxyglucose positron emission tomography in human carotid arteries: reproducibility, partial volume correction, and correlation between methods. *Stroke*. 2009;40:86-93.

Jang HL, Jin K, Lee J *et al*. Revisiting whitlockite, the second most abundant biomineral in bone: nanocrystal synthesis in physiologically relevant conditions and biocompatibility evalution. ACS Nano. 2014;8:634-641.

Jansen CHP, Perera D, Makowski MR *et al*. Detection of intracoronary thrombus by magnetic resonance imaging in patients with acute myocardial infarction. *Circulation*. 2011;124:416-242.

Januzzi Jr JL, Butler J, Jarolim P *et al*. Effects of canagliflozin on cardiovascular biomarkers in older adults with type 2 diabetes. *J Am Coll Cardiol*. 2019;70:704-12.

Januzzi JL, Hahn SS, Chae CU *et al*. Effects of tirofiban plus heparin versus heparin alone on troponin I levels in patients with acute coronary syndromes. *Am J Cardiol*. 2000;86:713-717.

Januzzi JL Jr, Suchindran S, Coles A *et al*. High-sensitivity Troponin I and coronary computed tomography in symptomatic outpatients with suspected coronary artery disease: insights from the PROMISE trial. *JACC Cardiovasc Imaging*. 2019;73:251-260.

Jenkins WS, Vesey AT, Shah AS *et al.* Valvular (18)F-Fluoride and (18)F-Fluorodeoxyglucose Uptake Predict Disease Progression and Clinical Outcome in

Patients With Aortic Stenosis. *J Am Coll Cardiol.* 2015;66:1200-1201.

Jenkins WS, Vesey AT, Stirrat C *et al*. Cardiac alpha-V beta-3 integrin expression following acute myocardial infarction in humans. *Heart*. 2017;103:607-615.

Jenkins WS, Vesey AT, Vickers A *et al.* In vivo alpha-V beta-3 integrin expression in human aortic atherosclerosis. *Heart*. 2019;1868-1875

Jin C, Frayssinet P, Pelker R *et al.* NLRP3 inflammasome plays a critical role in the pathogenesis of hydroxyapatite-associated arthropathy. *Proc Natl Acad Sci USA*. 2011;108:14867-14872.

Johnston SC, Amarenco P, Albers GW *et al*. Ticagrelor versus aspirin in acute stroke or transient ischemic attack. *N Engl J Med*. 2016;375:35-43.

Joseph A, Ackerman D, Talley JD *et al*. Manifestations of coronary atherosclerosis in young trauma victims - an autopsy study. *J Am Coll Cardiol*. 1993;22:459–467.

Joshi FR, Ranjani NK, Abt M *et al.* Does vascular calcification accelerate inflammation?: a substudy of the dal-PLAQUE trial. *J Am Coll Cardiol*. 2016;67: 69-78.

Joshi NV, Toor I, Shah AS *et al.* Systemic atherosclerotic inflammation following acute myocardial infarction: Myocardial infarction begets myocardial infarction. *J Am Heart Assoc.* 2015:4:e001956.

Joshi NV, Vesey AT, Williams MC *et al.* 18F-fluoride positron emission tomography for identification of ruptured and high-risk coronary atherosclerotic plaques: a prospective clinical trial. *Lancet*. 2014;383:705-713.

Kadoglou MP, Kottas G, Lampropoulos S *et al*. Serum levels of fetuin-A, osteoprotegerin and osteopontin in patients with coronary artery diease: effects of statin (HMGCoA-reductase inhibitor) therapy. *Clin Drug Investig*. 2014;34:165-171.

Kato R, Momiyama Y, Ohmori R *et al.* Prognostic significance of plasma osteopontin levels in patients undergoing percutaneous coronary intervention. *Circ J*. 2009;73:152-157.

Kelly-Arnold A, Maldonado N, Laudier D *et al*. Revised microcalcification hypothesis for fibrous cap rupture in human coronary arteries. *Proc Natl Acad Sci USA*. 2013;110:10741-10746.

Kietselaer BL, Reutelingsperger CP, Heidendal GA *et al.* Noninvasive detection of plaque instability with use of radiolabeled annexin A5 in patients with carotid-artery atherosclerosis. *N Engl J Med.* 2004;350:1472-1473.

Kim C, Lee JS, Han Y *et al*. Glycoprotein IIb/IIIa receptor imaging with (18)F-GP1 positron emission tomography for acute venous thromboembolism: an open-label, non-randomized, first-in-human phase 1 study. *J Nucl Med*. 2018. Doi:10.2967/jnumed.118.212084.

Kitagawa T, Yamamoto H, Nakamoto Y *et al*. Predictive value of 18F-fluoride positron emission tomography in detecting high-risk coronary artery disease in combined with computed tomography. *J Am Heart Assoc*. 2018;16;7:e010224.

Knuuti J, Wijns W, Saraste A *et al*. 2019 ESC guidelines for the diagnosis and management of chronic coronary syndromes. *Eur Heart J*. 2019. Doi:10/1093/eurheartj/ehz425.

Kolodgie FD, Gold HK, Burke AP *et al.* Intraplaque hemorrhage and progression of coronary atheroma. *N Engl J Med.* 2003;349:2316-2325.

Kolodgie FD, Petro A, Virmani R *et al.* Targeting of apoptotic macrophages and experimental atheroma with radiolabeled Annexin V. A technique with potential for noninvasive imaging of vulnerable plaque. *Circulation.* 2003;108:3134-3139.

Krohn KA, Link JM, Mason RP. Molecular imaging of hypoxia. *J Nucl Med.* 2008;49:129S-148S.

Kwiecinski J, Berman DS, Lee SE *et al*. Three-hour delayed imaging improves assessment of coronary 18F-sodium fluoride PET. *J Nucl Med*. 2019;60:530-535.

Lee N, Oh I, Chae SY *et al*. Radiation dosimetry of [18F]GP1 for imaging activated glucoprotein IIb/IIIa receptors with positron emission tomography in patients with acute thromboembolism. *Nucl Med Biol*. 2019;10:72-73:45-48.

Lee SE, Chang HJ, Sung JM *et al*. Effects of statins on coronary atherosclerotic plaques: The PARADIGM (Progression of AtheRosclerotic PlAque DetermIned by Computed TomoGraphic Angiography Imaging) Study. *JACC Cardiovasc Imaging.* 2018;11:1475-1484.

Lee SJ, Quach CHT, Jung KH *et al.* Oxidized low-density lipoprotein stimulates macrophage 18F-FDG uptake via hypoxia-inducible factor-1alpha activation through Nox2-dependent reactive oxygen species generation. *J Nucl Med.* 2014;55:1699-1705.

Lehner S, Todica A, Vanchev Y *et al.* In vivo monitoring of parathyroid hormone treatment after myocardial infarction in mice with [68Ga]annexin A5 and [18F]fluorodeoxyglucose positron emission tomography. *Mol Imaging.* 2014;13. Doi:10.2310/7290.2014.00035.

Lehrer-Graiwer J, Singh P, Abdelbaky A *et al*. FDG-PET imaging for oxidized LDL in stable atherosclerotic disease: a phase II study of safety, tolerability, and anti-inflammatory activity. *JACC Cardiovasc Imaging*. 2015;8:493-494.

Leipsic J, Abbara S, Achenbach S *et al*. SCCT guidelines for the interpretation and reporting of coronary CT angiography: a report of the Society of Cardiovascular Computed Tomography Guidelines Committee. *J Cardiovasc Comput Tomogr*. 2014;8:342-358.

Le Meunier L, Slomka PJ, Dey D *et al.* Motion frozen (18)F-FDG cardiac PET. *J Nucl Cardiol*. 2011;18:259-266.

Lendon CL, Davies MJ, Born GV *et al*. Atherosclerotic plaque caps are locally weakened when macrophages density is increased. *Atherosclerosis.* 1991;87:97-90.

Libby P. Mechanisms of acute coronary syndromes and their implications for therapy. *N Engl J Med*. 2013;368:2004-2013.

Lohrke J, Siebeneicher H, Berger M *et al*. 18F-GP1, a novel PET tracer designed for high-sensitivity, low-background detection of thrombi. *J Nucl Med*. 2017;58:1094-99.

MacAskill MG, Walton T, Williams L *et al*. Kinetic modelling and quantification bias in small animal PET studies with [18F]AB5186, a novel 18kDa translocator protein radiotracer. *PLoS One*. 2019;14:e0217515.

Maddox TM, Stanislawski MA, Grunwald GK *et al*. Nonobstructive coronary artery disease and risk of myocardial infarction. *JAMA*. 2014;312:1754–1763.

Maldonado N, Kelly-Arnold A, Vengrenyuk Y *et al.* A mechanistic analysis of the role of microcalcifications in atherosclerotic plaque stability: potential implications for plaque rupture. *Am J Physiol Heart Circ Physiol*. 2012;303:H619-H628.

Maile LA, Busby WH, Nichols TC *et al.* A monoclonal antibody against alphaVbeta3 integrin inhibits development of atherosclerotic lesions in diabetic pigs. *Sci Transl Med*. 2010;2:18ra11.

Mani V, Woodward M, Samber D *et al.* Predictors of change in carotid atherosclerotic plaque inflammation and burden as measured by 18F-FDG-PET and MRI, respectively, in the dal-PLAQUE study. *Int J Cardiovasc Imaging.* 2014;30:571-582.

Mann J, Davies MJ. Mechanisms of progression in native coronary artery disease: role of healed plaque disruption. *Heart*. 1999;82:265–268.

Mateo J, Izquierdo-Garcia D, Badimon JJ *et al*. Non-invasive assessment of hypoxia in rabbit advanced atherosclerosis using 18F-fluoromisonidazole positron emission tomographic imaging. *Circ Cardiovasc Imaging*. 2014;7:312-320.

Matter CM, Wyss MT, Meier P *et al.* 18F-choline images murine atherosclerotic plaques ex vivo. *Arterioscler Thromb Vasc Biol*. 2006;26:584-589.

Maurovich-Horvat P, Schlett CL, Alkadhi H *et al*. The napkin-ring sign indicates advanced atherosclerotic lesions in coronary CT angiography. *JACC Cardiovasc Imaging*. 2012;5:1243-1252.

Maroules CD, Hamilton-Craig C, Branch K *et al*. Coronary artery disease reporting and data system (CAD-RADS^{TM}): Inter-observer agreement for assessment categories and modifiers. *J Cardiovasc Comput Tomogr*. 2018;12:125–130.

McClelland RL, Chung H, Detrano R *et al*. Distribution of coronary artery calcium by race, gender, and age: results from the Multi-Ethnic Study of Atherosclerosis (MESA). *Circulation*. 2006;113:30–37.

McEvoy JW, Chen Y, Rawlings A *et al*. Diastolic blood pressure, subclinical myocardial damage, and cardiac events. Implications for blood pressure control. *J Am Coll Cardiol*. 2016;68:1713-1722.

Meijboom WB, Meijs MFL, Schujif JA *et al*. Diagnostic accuracy of 64-slice computed tomography coronary angiography: a prospective, multicentre, multivendor study. *J Am Coll Cardiol*. 2008;52:2135-44.

Meijboom WB, van Mieghem CA, Mollet NR *et al*. 64-slice computed tomography coronary angiography in patients with high, intermediate, or low pretest probability of significant coronary artery disease. *J Am Coll Cardiol*. 2007;50:1469-1475.

Meijboom WB, Van Mieghem CAG, van Pelt N *et al*. Comprehensive assessment of coronary artery stenosis: computed tomography coronary angiography versus conventional coronary angiography and correlation with fractional flow reserve in patients with stable angina. *J Am Coll Cardiol* 2008;52:636-43.

Mena E, Owenius R, Turkbey B *et al.* [18F] Fluciclatide in the in vivo evaluation of human melanoma and renal tumours expressing $\alpha v \beta 3$ and $\alpha v \beta 5$ integrins. *Eur J Nucl Med Mol Imaging.* 2014;41:1879-1888.

Miller JM, Rochitte CE, Dewey M *et al*. Diagnostic performance of coronary angiography by 64-row CT. *N Engl J Med*. 2008:359:2324-2336.

Mills NL, Churchouse AM, Lee KK *et al*. Implementation of a sensitive troponin I assay and risk of recurrent myocardial infarction and death in patients with suspected acute coronary syndrome. *JAMA*. 2011;305;1210-1216.

Minoretti P, Falcone C, Calcagnino M *et al*. Prognostic significance of plasma osteopontin levels in patients with chronic stable angina. *Eur Heart J*. 2006;27:802-807.

Mojtahedi A, Alavi A, Thamake S *et al.* Assessment of vulnerable atherosclerotic and fibrotic plaques in coronary arteries using 68Ga-DOTATATE PET/CT. *Am J Nucl Med Mol Imaging*. 2015;5:65-71.

Montalescot G, Sechtem U, Achenbach S *et al*. 2013 ESC guidelines on the management of stable coronary artery disease: the Task Force on the management of stable coronary artery disease of the European Society of Cardiology. *Eur Heart J*. 2013;34:2949-3003.

Moreno PR, Falk E, Palacios IF, *et al*. Macrophage infiltration in acute coronary syndromes. Implications for plaque rupture. *Circulation.* 1994;90:775-778.

Mori H, Torii S, Kutyna M, Sakamoto A *et al*. Coronary artery calcification and its progression: what does it really mean? *JACC Cardiovasc Imaging*. 2018;11:127-142.

Moss AJ, Adamson PD, Newby DE *et al*. Positron emission tomography imaging of coronary atherosclerosis. *Future Cardiol*. 2015;12:483-496.

Moss AJ, Doris MK, Andrews JPM *et al*. Molecular coronary plaque imaging using 18F-fluoride. *Circ Cardiovasc Imaging*. 2019;12:e008574.

Moss AJ, Dweck MR, Doris MK *et al*. Ticagrelor to reduce myocardial injury in patients with high-risk coronary artery plaque. *JACC Cardiovasc Imaging*. 2019. Doi: 10/1016/j.jcmg.2019.05.023

Moss AJ, Hutchison, Dweck MR. Gazing into smoldering volcanoes: precision cardiac imaging. *Future Sci OA*. 2018;5:FSO294.

Moss AJ, Newby DE. CT coronary angiography evaluation of suspected anginal chest pain. *Heart*. 2016;102:263-268.

Moss AJ, Williams MC, Newby DE *et al*. The updated NICE guidelines: Cardiac CT as the 1st line test for coronary artery disease. *Curr Cardiovasc Imaging Rep*. 2017;10:15.

Motoyama S, Kondo T, Anno H *et al*. Atherosclerotic plaque characterization by 0.5-mm-slice multislice computed tomographic imaging. *Circ. J*. 2007;71:363–366.

Motoyama S, Kondo T, Sarai M *et al*. Multislice computed tomographic characteristics of coronary lesions in acute coronary syndromes. *J Am Coll Cardiol*. 2007;50:319-326.

Motoyama S, Ito H, Sarai M *et al*. Plaque characterization by coronary computed tomography angiography and the likelihood of acute coronary events in mid-term follow-up. *J Am Coll Cardiol*. 2015;66:337–346.

Motoyama S, Sarai M, Harigaya H *et al*. Computed tomographic angiography characteristics of atherosclerotic plaques subsequently resulting in acute coronary syndrome. *J Am Coll Cardiol*. 2009;54:49–57.

Nakazato R, Arsanjani R, Achenbach S *et al*. Age-related risk of major adverse cardiac event risk and coronary artery disease extent and severity by coronary CT angiography: results from 15 187 patients from the International Multisite CONFIRM Study. *Eur Heart J Cardiovasc Imaging* 2014;15:586-94.

Naoum C, Berman DS, Ahmadi A *et al*. Predictive value of age- and sex-specific nomograms of global plaque burden on coronary computed tomography angiography for major cardiac events. *Circ Cardiovasc Imaging*. 2017;10:e004896.

Narula J, Nakano M, Virmani R, et al. Histopathologic characteristics of atherosclerotic coronary disease and implications of the findings for the invasive and noninvasive detection of vulnerable plaques. *J Am Coll Cardiol*. 2013;61:1041–1051.

National Institute for Health and Clinical Excellence. Chest pain of recent onset: Assessment and diagnosis of recent onset chest pain or discomfort of suspected cardiac origin (update). CG95. London: National Institute for Health and Clinical Excellence. 2016.

New SE, Goettsch C, Aikawa M *et al.* Macrophage-derived matrix vesicles: an alternative novel mechanism for microcalcification in atherosclerotic plaques. *Circ Res*. 2013;113:72-77.

Newby DE. Computed tomography or functional stress testing for the prediction of risk: can I have my cake and eat it? *Circulation*. 2017;136:2006–2008.

Newby DE, Williams MC, Flapan AD *et al*. Role of multidetector computed tomography in the diagnosis and management of patients attending the rapid access chest pain clinic, The Scottish computed tomography of the heart (SCOT-HEART) trial: study protocol for randomized controlled trial. *Trials*. 2012;13:184.

Newman CM, Bruun BC, Porter KE *et al*. Osteopontin is not a marker for proliferating human vascular smooth muscle cells. *Arterioscler Thromb*. 1995;15:2010-2018.

Nitta U, Tahara N, Tahara A *et al*. Pioglitazone decreases coronary artery inflammation in impaired glucose tolerance and diabetes mellitus: evaluation by FDG-PET/CT imaging. *JACC Cardiovasc Imaging*. 2013;6:1172-1182.

Noh TS, Moon SH, Cho YS *et al.* Relation of carotid artery 18F-FDG uptake to C-reactive protein and Framingham risk score in a large cohort of asymptomatic adults. *J Nucl Med.* 2013;54:2070-2076.

Obaid DR, Calvert PA, Brown A *et al*. Coronary CT angiography features of ruptured and high-risk atherosclerotic plaques: Correlation with intra-vascular ultrasound. *J Cardiovasc Comput Tomogr*. 2017;11:455–461.

O'Brien ER, Garvin MR, Stewart DK *et al*. Osteopontin is synthesized by macrophage, smooth muscle and endothelial cells in primary and restenotic human coronary atherosclerotic plaques. *Arterioscler Thromb*. 1994;14:1648-1656.

Oemraswingh RM, Cheng JM, Garcia-Garcia HM *et al*. High-sensitivity Troponin T in relation to coronary plaque characteristics in patients with stable coronary artery disease; results of the ATHEROREMO-IVUS study. *Atherosclerosis*. 2017;247:135-41.

Ogawa M, Nakamura S, Saito Y *et al*. What can be seen by 18F-FDG PET in atherosclerosis imaging? The effect of foam cell formation on 18F-FDG uptake to macrophages in vitro. *J Nucl Med.* 2012;53:55-58.

Owen DR, Yeo AJ, Gunn RN *et al.* An 18-kDa translocator protein (TSPO) polymorphism explains differences in binding affinity of the PET radioligand PBR28. *J Cereb Blood Flow Metab.* 2012;32:1-5.

Pan Y, Rose CE, Haber M *et al*. Assessing agreement of repeated binary measurements with an application to the CDC's anthrax vaccine clinical trial. *Int J Biostat*. 2013;9:19-32.

Park E, Gallezot JD, Delgadillo A *et al.* (11)C-PBR28 imaging in multiple sclerosis patients and healthy controls: test-retest reproducibility and focal visualization of active white matter areas. *Eur J Nucl Med Mol Imaging*. 2015;42:1081-1092.

Parker RA, Weir CJ, Rubio N *et al*. Application of mixed effects limits of agreement in the presence of multiple sources of variability: Exemplar from the comparison of several devices to measure respiratory rate in COPD patients. *PLoS One*. 2016;11:e0168321.

Patterson CM, Nair A, Ahmed N *et al*. Clinical outcomes when applying NICE guidance for investigation of recent-onset chest pain to a rapid-access chest pain clinic population. *Heart*. 2015;101:113-118.

Pawade TA, Cartlidge TR, Jenkins WS *et al*. Optimization and Reproducibility of Aortic Valve 18F-Fluoride Positron Emission Tomography in Patients With Aortic Stenosis. *Circ Cardiovasc Imaging*. 2016;9:e005131.

Pugliese F, Gaemperli O, Kinderlerer AR *et al.* Imaging of vascular inflammation with [11C]-PK11195 and positron emission tomography/computed tomography angiography. *J Am Coll Cardiol.* 2010;56:653-661.

Redberg RF, Katz MH. Statins for primary prevention: the debate is intense, but the data are weak. *JAMA Intern Med*. 2017;177:21–23.

Ridker PM, Danielson E, Fonseca FA *et al.* Rosuvastatin to prevent vascular events in men and women with elevated C-reactive protein. *N Engl J Med*. 2008;359:2195-2207.

Ripa RS, Knudsen A, Hag AM *et al.* Feasibility of simultaneous PET/MR of the carotid artery: first clinical experience and comparison to PET/CT. *Am J Nucl Med Mol Imaging.* 2013;3:361-371.

Rogers IS, Nasir K, Figueroa AL *et al.* Feasibility of FDG imaging of the coronary arteries: comparison between acute coronary syndrome and stable angina. *JACC Cardiovasc Imaging.* 2010;3:388-397.

Rominger A, Saam T, Vogl E *et al.* In vivo imaging of macrophage activity in coronary arteries using 68Ga-DOTATATE PET/CT: correlation with coronary calcium burden and risk factors. *J Nucl Med.* 2010;51:193-197.

Rubeaux M, Joshi NV, Dweck MR *et al.* Motion correction of 18F-NaF PET for imaging coronary atherosclerotic plaques. *J Nucl Med*. 2016;57:54-59.

Rudd JH, Myers KS, Bansilal S *et al*. (18)Fluorodeoxyglucose positron emission tomography imaging of atherosclerotic plaque inflammation is highly reproducible: implications for atherosclerosis therapy trials. *J Am Coll Cardiol*. 2007;50:892-896.

Rudd JH, Myers KS, Bansilal S *et al.* Atherosclerosis inflammation imaging with 18F-FDG PET: carotid, iliac, and femoral uptake reproducibility, quantification methods, and recommendations. *J Nucl Med.* 2007;49:871-878.

Rudd JH, Myers KS, Bansilal S *et al.* Relationships among regional arterial inflammation, calcification, risk factors, and biomarkers. A prospective Fluorodeoxyglucose positron-emission tomography/computed tomography imaging study. *Circ Cardiovasc Imaging.* 2009;2:107-115.

Rudd JH, Warburton EA, Fryer TD *et al.* Imaging atherosclerotic plaque inflammation with [^{18}F]-fluorodeoxyglucose positron emission tomography. *Circulation.* 2002;105:2708-2711.

Salarian M, Sadeghi MM. Hype or Hope. *Circ Cardiovasc Imaging*. 2019;12. Doi: 10/1161/circimaging.199.009591.

Satomi T, Ogawa M, Mori I *et al.* Comparison of contrast agents for atherosclerosis imaging using cultured macrophages: FDG versus ultrasmall superparamagnetic iron oxide. *J Nucl Med*. 2013;54:999-1004.

Schwartz GG, Olsson AG, Abt M *et al.* Effects of dalcetrapib in patients with a recent acute coronary syndrome. *N Engl J Med*. 2012;367:2089-2099.

Schecter G, Resar JR, McVeigh ER. Displacement and velocity of the coronary arteries: cardiac and respiratory motion. *IEEE Trans Med Imaging*. 2006;25:369-375.

Schlett CL, Maurovich-Horvat P, Ferencik M *et al*. Histogram analysis of lipid-core plaques in coronary computed tomographic angiography: ex vivo validation against histology. *Invest Radiol*. 2013;48:646–653.

Schirrmeister H, Guhlmann A, Elsner K *et al.* Sensitivity in detecting osseous lesions depends on anatomic localization: planar bone scintigraphy versus 18F PET. *J Nucl Med*. 1999;40:1623-1629.

SCOT-HEART investigators. CT coronary angiography in patients with suspected angina due to coronary artery disease (SCOT-HEART): an open-label, parallel group multicentre trial. *Lancet*. 2015;285:2383-91.

SCOT-HEART investigators. CT coronary angiography and 5 year risk of myocardial infarction. *N Engl J Med*. 2018;379:924-933.

Sekhri N, Feder GS, Juhghans C *et al*. How effective are rapid access chest pain clinics? Prognosis of incident angina and non-cardiac chest pain in 8762 consecutive patients. *Heart*. 2007;93:458-63.

Shah AS, Anand A, Sandoval Y *et al*. High-sensitivity cardiac troponin I at presentation in patients with suspected acute coronary syndrome: a cohort study. *Lancet*. 2015;386:2481-8.

Shah AS, Griffiths M, Lee KK *et al*. High sensitivity cardiac troponin and the under-diagnosis of myocardial infarction in women: prospective cohort study. *BMJ*. 2015;350:g7873.

Shah S, Bellam N, Leipsic J *et al*. Prognostic significance of calcified plaque among symptomatic patients with nonobstructive coronary artery disease. *J Nucl Cardiol*. 2014;21:453-466.

Shanahan CM, Cary NRB, Metcalfe JC *et al*.. High expression of genes for calcification-regulating proteins in human atherosclerotic plaques. *J Clin Invest*. 1994;93:2393-2402.

Singh P, Emami H, Subramanian S *et al*. Coronary plaque morphology and anti-inflammatory impact of Atorvastatin: a multicentre 18F-fluorodeoxyglucose positron emission tomographic/computed tomographic study. *Circ Cardiovasc Imaging*. 2016;9:e004195.

Sim AM, Rashdan NA, Cui L *et al*. A novel fluorescein-bisphosphonate based diagnostic tool for the detection of hydroxyapatite in both cell and tissue models. *Sci Rep*. 2018;8:17360.

Skinner JS, Smeeth L, Kendall JM *et al*. NICE guidance. Chest pain of recent onset: assessment and diagnosis of recent onset chest pain or discomfort of suspected cardiac origin. *Heart*. 2010;96:974-978.

Slomka PJ, Diaz-Zamudio M, Dey D *et al.* Automatic registration of misaligned CT attenuation correction maps in Rb-82 PET/CT improves detection of angiographically significant coronary artery disease. *J Nucl Cardiol.* 2015;22:1285-1295.

Sluimer JC, Kolodgie FD, Bijnens AP *et al.* Thin-walled microvessels in human coronary atherosclerotic plaques show incomplete endothelial junctions relevance of comprised structural integrity for intraplaque microvascular leakage. *J Am Coll Cardiol.* 2009;53:1517-1527.

Soret M, Bacharach SL, Buvat I. Partial-volume effect in PET tumor imaging. *J Nucl Med.* 2007;48:932-945.

Stone GW, Maehara A, Lansky AJ *et al*. A prospective natural-history study of coronary atherosclerosis. *N Engl J Med*. 2011;364:226-235.

Swirski FK, Pittet MJ, Kircher MF *et al*. Monocyte accumulation in mouse atherogenesis is progressive and proportional to extent of disease. *Proc Natl Acad Sci USA.* 2006;103:10340-10345.

Tahara N, Mukherjee J, de Haas HJ *et al.* 2-deoxy-2-[18F]-fluoro-D-mannose positron emission tomography imaging in atherosclerosis. *Nat Med.* 2014;20:215-219.

Takamura K, Fujimoto S, Kondo T *et al*. Incremental prognostic value of coronary computed tomography angiography: high-risk plaque characteristics in asymptomatic patients. *J Atheroscler Thromb*. 2017;24:1174-1185.

Tarkin JM, Joshi FR, Evans NR *et al*. Detection of Atherosclerotic Inflammation by 68Ga-DOTATATE PET Compared to [18F]FDG PET Imaging. *J Am Coll Cardiol*. 2017;69:1774-1791.

Tarkin JM, Joshi FR, Rudd JHF. PET imaging of inflammation in atherosclerosis. *Nat Rev Cardiol.* 2014;11:443-457.

Tavakoli S, Zamora D, Ullevig S *et al*. Bioenergetic profiles diverge during macrophage polarization: implications for the interpretation of 18F-FDG PET imaging of atherosclerosis. *J Nucl Med.* 2013;54:1661-1667.

Tawakol A, Fayad ZA, Mogg R *et al*. Intensification of statin therapy results in a rapid reduction in atherosclerotic inflammation: results of a multicenter fluorodeoxyglucose-positron emission tomography/computed tomography feasibility study. *J Am Coll Cardiol*. 2013;62:909-917.

Tawakol A, Migrino RQ, Bashian GG *et al.* In vivo 18F-fluorodeoxyglucose positron emission tomography imaging provides a noninvasive measure of carotid plaque inflammation in patients. *J Am Col Cardiol.* 2006;48:1817-1824.

Thomsen C, Abdulla J. Characteristics of high-risk coronary plaques identified by computed tomographic angiography and associated prognosis: a systematic review and meta-analysis. *Eur Heart J Cardiovasc Imaging*. 2016;17:120–129.

Van der Valk FM, Sluimer JC, Vöö SA *et al.* In vivo imaging of hypoxia in atherosclerotic plaques in humans. *JACC Cardiovasc Imaging*. 2015;8:1340-1341.

Van Lierde J, De Geest H, Verstraete M *et al*., Van de Werf F. Angiographic assessment of the infarct-related residual coronary stenosis after spontaneous or therapeutic thrombolysis. *J Am Coll Cardiol*. 1990;16:1545-1549.

Vasan RS. Biomarkers of cardiovascular disease: molecular basis and practical considerations. *Circulation*. 2006;113:2335-62.

Vesey AT, Dweck MR, Fayad ZA. Utility of Combining PET and MR Imaging of Carotid Plaque. *Neuroimaging Clin N Am.* 2016;26:55-68.

Vesey AT, Jenkins WS, Irkle A *et al*. 18F-Fluoride and 18F-Fluorodeoxyglucose Positron Emission Tomography After Transient Ischemic Attack or Minor Ischemic Stroke. *Circ Cardiovasc Imaging*. 2017;10:e004976.

Virchow R. Cellular Pathology as based upon physiological and pathological histology: twenty lectures delivered in the Pathological Institute of Berlin during the months of February, March and April, 1858. Robert M. De Witt, New York, USA. 1860.

Virmani R, Burke AP, Kolodgie FD *et al*. Pathology of the thin-cap fibroatheroma: a type of vulnerable plaque. *J Interven Cardiology*. 2003;16:267–272.

Vranckx P, Valgimigli M, Jüni P, *et al*. Ticagrelor plus aspirin for 1 month, followed by ticagrelor monotherapy for 23 months vs aspirin plus clopidogrel or ticagrelor for 12 months, followed by aspirin monotherapy for 12 months after implantation of a drug-eluting stent: a multicenter, open-label, randomised superiority trial. *Lancet*. 2018;392:940-49.

Wallentin L, Becker RC, Budaj A *et al*. Ticagrelor versus clopidogrel in patients with acute coronary syndromes. *N Engl J Med*. 2009;361:1045-57.

Welsh P, Tuckwell K, McInnes IB *et al*. Effect of IL-6 receptor blockade on high-sensitivity troponin T and NT-proBNP in rheumatoid arthritis. *Atherosclerosis*. 2016;254:167-171.

Williams MC, Golay SK, Hunter A *et al*. Observer variability in the assessment of CT coronary angiography and coronary artery calcium score: substudy of the Scottish COmputed Tomography of the HEART (SCOT-HEART) trial. *Open Heart*. 2015;2:e000234

Williams MC, Hunter A, Shah ASV *et al*. Use of coronary computed tomographic angiography to guide management of patients with coronary disease. *J Am Coll Cardiol*. 2016;67:1759-1768.

Williams MC, Moss AJ, Dweck M *et al*. Coronary artery plaque characteristics associated with adverse outcomes in the SCOT-HEART study. *J Am Coll Caridol*. 2018;73:291-301.

Williams MC, Newby DE. CT myocardial perfusion: a step towards quantification. *Heart*. 2012;98:521-2.

Williams MC. Reid JH, McKillop G *et al*. Cardiac and coronary CT comprehensive imaging approach in the assessment of coronary heart disease. *Heart*. 2011;97:1198-1205.

Woodward M, Brindle P, Tunstall-Pedoe H *et al*. Adding social deprivation and family history to cardiovascular risk assessment: the ASSIGN score from the Scottish Heart Health Extended Cohort (SHHEC). *Heart*. 2007;93:172–176.

You AYF, Bergholt MS, St-Pierre J-P *et al*. Raman spectropscopy imaging reveals interplay between atherosclerosis and medial calcification in human aorta. *Sci Adv*. 2017;3:e1701156.

Zemplenyi T, Crawford DW, Cole MA. Adaptation to arterial wall hypoxia demonstrated in vivo with oxygen microcathodes. *Atherosclerosis.* 1989;76:173-179.